FACULTAD DE CIENCIAS

Departamento de Física de Materiales

OXIDACIÓN CATALÍTICA SELECTIVA DE FURFURAL A ANHÍDRIDO Y/O ÁCIDO MALEICO

Memoria para aspirar al grado de

DOCTOR

Noelia Alonso Fagúndez

Grupo de Energía y Química Sostenible.
Instituto de Catálisis y Petroleoquímica, C.S.I.C.

Madrid, 2017

Noelia Alonso Fagúndez

OXIDACIÓN CATALÍTICA SELECTIVA DE FURFURAL A ANHÍDRIDO Y/O ÁCIDO MALEICO

Memoria para aspirar al grado de

DOCTOR

Directores:

Dr. D. Manuel López Granados

Investigador Científico

Instituto de Catálisis y Petroleoquímica (CSIC)

Dr. D. Rafael Mariscal López

Investigador Científico

Instituto de Catálisis y Petroleoquímica (CSIC)

UNIVERSIDAD AUTÓNOMA DE MADRID

FACULTAD DE CIENCIAS

Dpto. Física de Materiales

Madrid, 2017

TABLA DE CONTENIDOS

1. RESUMEN

1. RESUMEN

La creciente demanda de combustibles fósiles unida a la disminución de las reservas de petróleo traerá como consecuencia el encarecimiento de precios no sólo de los combustibles, sino de todos los productos derivados del mismo. En este panorama tiene sentido la búsqueda de materias primas alternativas que permitan obtener tanto combustibles como productos químicos. El consumo elevado de combustibles fósiles está asociado también a la emisión de gases nocivos, por lo que la tendencia es la sustitución progresiva de estos combustibles por otros sistemas más sostenibles. Se está desarrollando un concepto nuevo, el de biorrefinería, en la cual la biomasa se utiliza como materia prima para lograr los mismos objetivos que en las refinerías tradicionales. Para que este proceso sea interesante es necesario utilizar una fuente de carbohidratos que no distorsione el comercio de alimentos ni amenace la biodiversidad del planeta. La biomasa lignocelulósica, y en particular la que proviene de residuos agrícolas, se presenta como un candidato a tener en cuenta.

Los principales constituyentes de la biomasa de interés en biorrefinería son fundamentalmente la sacarosa, el almidón, los triglicéridos, los terpenos y la lignocelulosa. Este último es el componente mayoritario de los vegetales y está compuesto por tres fracciones químicas, celulosa (45 %), hemicelulosa (30 %) y lignina (25 %), que pueden separarse en un esquema de biorrefinería. Estos constituyentes por sí solos o sus derivados permiten obtener productos de mayor valor añadido, con un esquema similar al de la refinería tradicional del petróleo.

Uno de los compuestos obtenidos a partir de subproductos agrícolas, en concreto de la fracción de xilosa, es el furfural, que se utiliza como materia prima para sintetizar multitud de productos químicos, como furano, ácido furoico o alcohol furfurílico. Existen descritos numerosos procesos que permiten obtener también otros compuestos industriales que a día de hoy se sintetizan a partir de derivados fósiles. Entre ellos se encuentra el anhídrido maleico, que actualmente se obtiene de la oxidación selectiva de *n*-butano, utilizando para ello catalizadores de vanadio.

Así pues, teniendo en cuenta el elevado potencial que presenta el furfural, esta tesis se centrará en la búsqueda de catalizadores activos, selectivos y estables para la obtención de anhídrido/ácido maleico, utilizando como materia prima este

compuesto de origen sostenible. Se plantea así una alternativa a los compuestos de origen fósil que se han estado utilizando tradicionalmente. El estudio se centra en la reacción de oxidación del furfural tanto en fase gaseosa como en fase líquida.

Los dos primeros trabajos presentados, titulados "*Selective conversion of furfural to maleic anhydride and furan with VO_x/Al_2O_3 catalysts*" (N. Alonso Fagúndez, M. López Granados, R. Mariscal, M. Ojeda, ChemSusChem (2012), 5, 1984-1990) y "*Gas phase oxidation of furfural to maleic anhydride on V2O5/γ-Al2O3 catalysts: reaction conditions to slow down the deactivation*" (N. Alonso Fagúndez, M. Ojeda, R. Mariscal, J. L. G. Fierro, M. López Granados, Journal of Catalysis 348 (2017) 266-275), se centran en el estudio de la reacción de oxidación de furfural en fase gaseosa, utilizando catalizadores de óxido de vanadio preparados mediante el método de impregnación a humedad incipiente. La serie de catalizadores sintetizada cubre un rango de concentración de vanadio comprendido entre 0,5 y 25 at.V/nm^2. La reacción en fase gaseosa estudiada se lleva a cabo en un reactor de lecho fijo en un rango de temperaturas entre 473-673 K, utilizando como reactivo furfural comercial diluido en una corriente mezcla de O_2-N_2 y con tiempos de contacto cortos, de pocos segundos.

En primer lugar se realiza una exploración de la influencia de la estructura de la especies VO_x presentes en el catalizador sobre la reacción de oxidación de furfural bajo las mismas condiciones de operación. Los resultados de actividad catalítica reflejan cómo la conversión de furfural aumenta conforme aumenta el contenido de vanadio en el catalizador, presentando un máximo para el catalizador con cobertura de monocapa (8 at.V/nm^2) y vuelve a disminuir conforme aumenta el contenido de vanadio. Un comportamiento similar se observa cuando se analiza el rendimiento hacia anhídrido maleico.

Las diferentes técnicas de caracterización a las que se someten los catalizadores sintetizados reflejan que sobre los catalizadores con cargas de vanadio inferiores a la cobertura de monocapa las especies predominantes son monovadatos, siendo las especies de polivanadatos las mayoritarias en el catalizador con cobertura de monocapa; para cargas superiores de vanadio empiezan a formarse cristales de V_2O_5. Teniendo en cuenta estos resultados, junto con los análisis de la actividad catalítica de los diferentes catalizadores, se puede

concluir que las especies polivanadatos son intrínsecamente más activas que las especies monovanadatos y estas a su vez son más activas que los cristales de V_2O_5.

Considerando los resultados obtenidos en este primer trabajo, se elige como catalizador más activo aquel que presenta mayor cantidad de especies de polivanadatos sobre su superficie (8 at.V/nm^2). El segundo trabajo presentado se centra en el estudio del efecto de las variables de operación sobre la actividad catalítica de este catalizador para largos tiempos de reacción.

En una primera exploración se mide la actividad catalítica del catalizador a baja temperatura y tomándose medidas de actividad catalítica durante 10 h a intervalos de 1 h. Bajo estas condiciones se obtienen bajas conversiones de furfural y un rendimiento hacia anhídrido maleico prácticamente nulo. Las discrepancias en el balance de carbono se asocian a la formación de productos pesados no detectados por cromatografía de gases. A continuación se aumenta la temperatura de reacción en intervalos de 15 K y manteniendo cada temperatura de reacción durante 10 horas. La conversión de furfural aumenta conforme aumenta la temperatura de reacción; para el caso del rendimiento hacia anhídrido maleico se observa que éste aumenta también con la temperatura de reacción, pero para temperaturas demasiado altas y conversión total de furfural su valor comienza a disminuir, produciéndose la sobreoxidación hacia CO_2.

Se plantea una nueva serie de experimentos en la que el catalizador se pone en contacto con el medio de reacción a una temperatura elevada con conversión total de furfural. Los resultados obtenidos evidencian un rendimiento hacia anhídrido maleico notablemente superior al obtenido siguiendo el protocolo anterior. A pesar de que se observa una lenta desactivación del catalizador, su actividad puede recuperarse tras un proceso de calcinación a 773 K durante 1 h. A medida que aumenta la concentración de oxígeno en el medio de reacción se mejora el rendimiento hacia anhídrido maleico en detrimento de los productos pesados no detectados por cromatografía de gases.

La presencia de especies pesadas del tipo maleatos ha quedado evidenciada en las diferentes técnicas de caracterización a las que se han sometidos los catalizadores usados. Dichas especies están involucradas en el proceso de

desactivación del catalizador, depositándose sobre su superficie y limitando el acceso de los reactivos a los sitios activos del mismo. Cuando la reacción se realiza a bajas temperaturas (y por lo tanto a bajas conversiones de furfural) estas especies se depositan rápidamente sobre la superficie del catalizador, desactivándolo; el aumento de la temperatura de reacción apenas se traduce en una mejora en el rendimiento hacia anhídrido maleico.

En vista de estos resultados se puede concluir que en la transformación de furfural intervienen dos rutas diferentes: la resignificación de furfural hacia compuestos pesados o la oxidación de furfural hacia anhídrido maleico y CO_2. Parece razonable asumir que el parámetro clave para alcanzar un rendimiento elevado hacia anhídrido maleico es exponer al catalizador a una mezcla de reacción con alto poder oxidante, lo cual se alcanza a elevadas temperaturas de reacción y altas relaciones oxígeno/furfural. De este modo, la desactivación del catalizador por la deposición de resinas y/o maleatos no puede evitarse, pero sí puede desacelerarse de manera notable.

Los dos siguientes trabajos recogidos, titulados *"Poly-(styrene sulphonic acid): An acid catalyst from polystyrene waste for reactions of interest in biomass valorization"* (N. Alonso Fagúndez, V. Laserna, A.C. Alba Rubio, M. Mengibar, A. Heras, R. Mariscal, M. López Granados, Catalysis Today 234 (2014) 285-294) y *"Aqueous-phase catalytic oxidation of furfural with H_2O_2: high yield of maleico acid by using titanium silicalite-1"* (N. Alonso Fagúndez, I. Aguirrezabal Telleria, P. L. Arias, J. L. G. Fierro, R. Mariscal, M. López Granados, RSC Advances (2014), 4, 54960-54972) se centran en la reacción de oxidación de furfural en fase líquida, utilizando en este caso peróxido de hidrógeno como agente oxidante. Esta reacción se ha estudiado en un reactor discontinuo de vidrio de fondo redondo bajo agitación continua y sumergido en un baño de aceite termostatizado para alcanzar la temperatura deseada.

En el primero de estos trabajos se utilizan catalizadores ácidos con grupos sulfónicos tales como Amberlita 15, H_2SO_4 o ácido poliestiren-sulfónico (PSSA), este último obtenido a partir de la sulfonación de residuos de poliestireno. Con el fin de estudiar la reutilización de este último catalizador se plantea un método de

heterogeneización del mismo mediante su fijación en una matriz de sílice por un proceso sol-gel.

El principal inconveniente en la reacción de oxidación del furfural con H_2O_2 y con catalizadores ácidos es el control de la selectividad. Los principales productos son compuestos C4 diácidos, tales como ácido succínico y ácido maleico, 2-5H-furanona o 5-hidroxi-furan-2(5H)-ona, obteniéndose como subproducto de reacción ácido fórmico. Esta falta de selectividad es consecuencia de un complejo mecanismo de reacción que comienza con la oxidación Baeyer-Villiger del furfural hacia el correspondiente éster.

De la reacción sin catalizador se aprecia que tiene lugar un proceso autocatalítico, aunque a baja velocidad, debido a los ácidos formados como productos de reacción. Del estudio de las variables de operación se deduce, de manera general para todos los catalizadores probados, que el aumento de temperatura mejora la conversión de furfural y el rendimiento hacia los productos de interés. En cuanto a la relación H_2O_2/furfural en el medio de reacción, se observa una distribución de productos diferente en función de la concentración de H_2O_2 utilizada: por ejemplo, para relaciones de 4 se favorece la formación de ácido succínico, mientras que para relaciones mayores el producto mayoritario es el ácido maleico.

Se ha estudiado también la reutilización del catalizador PSSA nanocomposite sintetizado a partir de residuos. La actividad del catalizador permanece estable durante los tres primeros ciclos de reacción, se desactiva en el cuarto ciclo y después logra estabilizarse de nuevo. Esta pérdida de actividad está directamente relacionada con el lixiviado de los átomos de azufre presentes en el mismo. Se realiza una nueva serie de reutilizaciones utilizando como catalizador un nanocomposite sometido a un tratamiento hidrotermal para eliminar la mayor parte del polímero anclado débilmente. En este caso se observa una desactivación durante los tres primeros ciclos de reacción y a partir del cuarto ciclo se alcanza el estado estacionario. En las dos series de reutilizaciones estudiadas se observa que la actividad del catalizador se vuele estable cuando la concentración de azufre del catalizador permanece constante y por lo tanto no se produce su lixiviación.

En vista de los resultados obtenidos se puede deducir que para que el catalizador sea más estable y más activo durante mayor número de ciclos de reutilización es necesario mejorar la síntesis de los nanocomposites para conseguir aumentar la carga inicial de polímero en el catalizador, y consecuentemente el número de sitios ácidos, y su estabilidad hidrotermal, reduciéndose así la lixiviación del polímero.

El principal inconveniente de la utilización de catalizadores ácidos en la oxidación en fase líquida del furfural es el control de la selectividad. En el cuarto trabajo presentado se explora la actividad catalítica de la Titania Silicalita (TS-1). En este caso la distribución de productos es diferente, siendo los principales productos de reacción ácido maleico, ácido furoico y 5-hidroxi-furan-2(5H)-ona. También se detecta presencia de ácido succínico, ácido furanoico y ácido málico, pero en concentraciones muy bajas, lo que lleva a pensar que el mecanismo de reacción es diferente al que tiene lugar cuando se utilizan catalizadores ácidos.

Del estudio de la concentración de catalizador en el medio de reacción se puede deducir que la incorporación de la TS-1 acelera la velocidad de la reacción y modifica la distribución de la selectividad de los productos obtenidos con respecto a los catalizadores ácidos, siendo el ácido maleico y la hidroxifuranona los productos principales. Este efecto se ve intensificado conforme aumenta la concentración de catalizador en el medio de reacción hasta relaciones catalizador/furfural equivalentes; sin embargo, para cantidades de catalizador superiores se produce la sobreoxidación de los productos.

La temperatura aumenta la velocidad de conversión de furfural. Para tiempos cortos de reacción, el producto mayoritario es la hidroxifuranona, siendo el ácido maleico el producto principal conforme avanza la reacción; el rendimiento hacia ácido maleico no se mejora aumentando la temperatura de reacción. Relaciones H_2O_2/Furfural superiores a la estequiométrica son necesarias para alcanzar una elevada velocidad de conversión de furfural y rendimiento hacia ácido maleico; sin embargo, valores demasiado altos producen la sobreoxidación de los productos obtenidos.

Los resultados obtenidos evidencian que para tiempos cortos de reacción, en los que el principal producto es la hidroxifuranona, la selectividad del H_2O_2 es muy

elevada, pero conforme avanza la reacción se produce su desactivación de manera no selectiva debido a la presencia de la TS-1. Para optimizar la cantidad de H_2O_2 empleada se propone hacer una reacción en dos etapas y con dos catalizadores diferentes: en primer lugar se utiliza TS-1 para oxidar furfural a hidroxifuranona y en una segunda etapa se realiza la oxidación de la hidroxifuranona hacia ácido maleico, utilizando como catalizador Amberlita 70. El rendimiento final alcanzado hacia anhídrido maleico es del 90% después de 48 horas de reacción.

El estudio de la reutilización del catalizador, utilizando como reactivo furfural comercial, revela una actividad estable del mismo durante 6 ciclos de reacción; sin embargo, cuando se utiliza furfural obtenido a partir de biomasa real se observa una lenta pero progresiva desactivación del catalizador, probablemente debido a las impurezas presentes en la disolución . La caracterización de los catalizadores usados refleja que se produce una lixiviación del Ti, y en mucho menor grado del Si.

La distribución de productos registrada con el catalizador TS-1 lleva a pensar que la reacción sigue un mecanismo diferente a cuando se utilizan catalizadores ácidos y que no comienza con una etapa Baeyer-Villiger. En este caso, en primer lugar se produce la epoxidación del doble enlace del furfural con menor impedimento estérico y es sobre el grupo aldehído de este intermedio de reacción sobre el que se produce la reacción Baeyer-Villiger. El éster resultante de este proceso se hidroliza rápidamente hacia el ácido β-formilacrílico, formándose una molécula de ácido fórmico. El ácido formado se encuentra en equilibrio con la hidroxifuranona, que se oxida finalmente hacia el ácido maleico de interés.

2. INTRODUCCIÓN

INDICE

ÍNDICE DE FIGURAS

2. INTRODUCCIÓN

2.1. Aspectos generales

El **mercado energético mundial** actual se basa en el consumo de recursos fósiles, cuya demanda es cada vez mayor. Según la OPEP (Organización de Países Exportadores de Petróleo), se estima que al ritmo de consumo actual las reservas de petróleo se agoten en un plazo máximo de unos 65 años, por lo que resulta de vital importancia buscar sustitutos de este compuesto, sobre todo teniendo en cuenta que según el EIA (United States Energy Information Administration) el 86 % de las fuentes de energía primarias a nivel mundial están basadas en el petróleo o sus derivados. La disminución de las reservas de petróleo traerá como consecuencia el encarecimiento de precios no sólo de los combustibles, sino de todos los productos derivados del mismo. En este panorama tiene sentido buscar materias primas alternativas al petróleo que permitan obtener de igual modo tanto combustibles como productos químicos [1].

Este elevado consumo de combustibles fósiles tiene como consecuencia directa la **problemática medioambiental** asociada a la emisión de gases nocivos como SO_2, CO, NO_x y partículas, producidos durante su combustión, y su contribución al calentamiento global y como consecuencia al cambio climático. La preocupación a nivel internacional sobre este aspecto ha llevado a adoptar una serie de medidas y acuerdos para reducir su impacto. Entre estas actuaciones cabe destacar:

- El *Protocolo de Kioto* (1997) es el único tratado internacional en el que se fijan límites de emisión de los gases que provocan el cambio climático. En él se establece que el conjunto de los países desarrollados debe reducir, en promedio, sus emisiones de los 6 gases de efecto invernadero (GEI) en un 5,2% respecto de sus emisiones en 1990. Algunas de las principales potencia emisoras, como China, quedaron fuera de este acuerdo, y otras como Estados Unidos no lo ratificaron. Por su parte la Unión Europea propuso una reducción de GEI del 7,5%.

- El *Libro Blanco de las Energía Renovables* fue aprobado por la Unión Europea en 1998 y tenía como objetivo fundamental duplicar la aportación

de las energías renovables del momento, de manera que en 2010 fuese del 12%. España se acogió a este compromiso en la Ley del Sector Eléctrico. Las acciones a llevar a cabo tenían como objetivo la reducción de unas 400 toneladas de CO_2 mediante el uso de energías renovables como fotovoltaica, eólica, solar térmica y biomasa.

- La última acción llevada a cabo contra el cambio climático ha sido la *Cumbre de París* (2015). El texto fue aprobado por un total de 195 países y contempla la necesidad de realizar una inversión económica de los países más desarrollados para realizar una transición hacia una economía limpia. Con estas acciones se pretende que la temperatura media del planeta a finales de siglo aumente por debajo de los 2 grados. El acuerdo entrará en vigor en 2020 y se establecen mecanismos de revisión de los objetivos cada cinco años.

Además de producir un gran volumen de emisiones contaminantes, el uso del petróleo conduce a una **dependencia energética** de España de terceros países, algunos de ellos políticamente inestables, como consecuencia de una localización centralizada de las reservas petrolíferas. Es por ello por lo que se necesita fomentar el uso de fuentes de energía renovable como la biomasa, con un ciclo de vida que implica menos emisiones de CO_2 y con una distribución de recursos más homogénea a lo largo del planeta.

Los combustibles fósiles podrían ser reemplazados a largo plazo por otros sistemas más sostenibles derivados de las energías renovables; la materia prima utilizada en multitud de procesos químicos implantados se obtiene a partir de compuestos derivados del petróleo, y por lo tanto basados en el carbono. En este sentido **la biomasa es la única fuente renovable que contiene carbono en su estructura** y es por tanto el candidato idóneo para llevar a cabo su sustitución parcial o total. La sustitución de combustibles fósiles por biomasa lleva siendo objeto de investigación desde hace años. El uso de fuentes de energía renovables para la síntesis de productos químicos y la posterior transformación de éstos en polímeros, lubricantes o disolventes que actualmente se obtienen a partir de derivados del petróleo es el objetivo a alcanzar. Sin embargo, los biocombustibles

siguen sin ser económicamente competitivos frente a los combustibles tradicionales obtenidos a partir de fuentes fósiles [2].

Teniendo en cuenta este escenario energético se introduce el **concepto de biorrefinería** en paralelismo con una refinería tradicional, en la que se obtienen diversos productos utilizando como materia prima el petróleo. En una biorrefinería se obtienen, por tanto, biocombustibles y productos químicos de alto valor añadido, utilizando como materia prima cualquier tipo de biomasa, en lugar de petróleo. En este tipo de instalaciones podría obtenerse además energía en forma de calor y electricidad, e incluso en los casos más avanzados existe la posibilidad de obtener como subproductos aditivos alimentarios, para uso como pienso de animales o bien como complemento dietético en alimentación humana [3]. La obtención de calor, electricidad y bioproductos justificaría la rentabilidad de este proceso.

Desde un punto de vista funcional una biorrefinería está constituida por diversas plataformas tecnológicas, que se diferencian por el tipo de materia prima a procesar o por la estrategia tecnológica a seguir. Se puede hablar de **diferentes tipos de biorrefinerías** en función de la flexibilidad funcional de las mismas. Las biorrefinerías de *Generación I* se caracterizan por su escasa flexibilidad en lo que respecta al tipo de materias primas que pueden procesarse y los productos que se pueden obtener. Las unidades de *Generación II* son más flexibles en cuanto a los productos finales obtenidos. Finalmente, las de *Generación III* permitirían procesar materias primas de diferente naturaleza para obtener un amplio abanico de productos finales, al igual que las refinerías de petróleo actuales.

Actualmente existen varios modelos de biorrefinerías muy primarias que difieren según la fuente de biomasa que emplean y en las cuales se procesa un único tipo de biomasa (caña de azúcar, maíz, etc…) a un determinado tipo de producto (biodiesel, bioetanol, etc…). El objetivo es plantear una biorrefinería madura, es decir, una instalación muy flexible en cuanto al tipo de materia prima y a los productos obtenidos en función de la oferta y la demanda, tal como sucede en una refinería convencional petroquímica.

En función de los productos y las tecnologías que se traten en las biorrefinerías se distinguen 5 tipos de plataformas diferentes como son la termoquímica, la de biogás, la oleoquímica, la de azúcares y la de técnicas genéticas. Sin embargo, no

resulta sencillo realizar una clasificación rigurosa de los tipos de biorrefinería debido a la creciente complejidad de las mismas [4].

Muchas de las grandes empresas químicas y biotecnológicas ya establecidas (DuPont, Dow Chemicals, Nature Works), así como pequeñas empresas emergentes, están activamente involucradas en el desarrollo y comercialización de bioproductos, principalmente biocombustibles, a partir de una gran variedad de fuentes de biomasa renovable.

Sin embargo, el uso de biomasa en sustitución del petróleo está generando un importante **debate internacional** debido a los altos **costes de producción**, a la **viabilidad del proceso** y sobre todo, dependiendo de la materia prima utilizada, a la **competencia con el sector de la alimentación**. Por ello, para que este proceso sea interesante es necesario utilizar una fuente de carbohidratos que no distorsione el comercio de alimentos ni amenace la biodiversidad del planeta. Atendiendo a esto la **biomasa lignocelulósica**, y en particular la de elevada capacidad de producción, se presenta como una fuente de materia prima a tener en cuenta como consecuencia de su **abundancia, su elevada disponibilidad, bajo coste y carácter poco contaminante**, ya que proviene en su mayoría de residuos agrícolas y no introduce excesivas tensiones en la industria agroalimentaria como otros tipos de biomasa utilizadas hasta ahora, tales como el maíz, la caña de azúcar, los cereales o la remolacha azucarera.

La **biomasa forestal** está reconocida como la mayor fuente potencial de energía renovable [5-7]. Su aprovechamiento completo (y no sólo de fracciones azucaradas o amiláceas para la obtención de etanol vía fermentación, fracciones fibrosas para pasta celulósica o combustión completa) permitiría, además, la disposición de una enorme variedad de productos químicos, cuyo desarrollo tecnológico precisa de la integración de todas las etapas, desde el cultivo y recolección, hasta el fraccionamiento de la biomasa y conversión a diferentes productos [8]. La integración de etapas de producción de biocombustibles, como bioetanol o biodiesel, con las de valorización de otros productos químicos resulta fundamental, ya que pese a que éstos últimos presentan un volumen de producción mucho menor poseen un alto valor añadido que puede ayudar a rentabilizar dichas instalaciones.

La utilización directa de la biomasa vegetal como combustible para la producción de calor o de electricidad es una opción, pero su desarrollo se ve limitado principalmente por problemas de transporte, sobreexplotación de recursos y sobre todo la competencia económica de otras fuentes de energía, como combustibles fósiles.

La industria del sector de la pasta celulósica está perfectamente situada para evolucionar desde las actuales instalaciones, que en cierta forma aplican ya un esquema de biorrefinería para obtener pasta celulósica y energía, hacia instalaciones integradas de producción de energía y otros productos químicos a partir de la biomasa lignocelulósica.

2.2. Composición de la biomasa lignocelulósica y sus pretratamientos

Los principales constituyentes de la biomasa de interés en biorrefinería son fundamentalmente la sacarosa, el almidón, los triglicéridos, los terpenos y la lignocelulosa. Este último es el componente mayoritario de los vegetales, cuya función es la de proporcionar rigidez a su estructura. Se encuentra presente tanto en las raíces como en los tallos, troncos y hojas. Este material lignocelulósico está compuesto por tres fracciones químicas, celulosa (45 %), hemicelulosa (30 %) y lignina (25 %), que en teoría se pueden separar en un esquema de biorrefinería. Estos constituyentes por sí solos o sus derivados permiten obtener productos de mayor valor añadido y de aplicación en multitud de campos, con un esquema similar al de la refinería tradicional del petróleo [9].

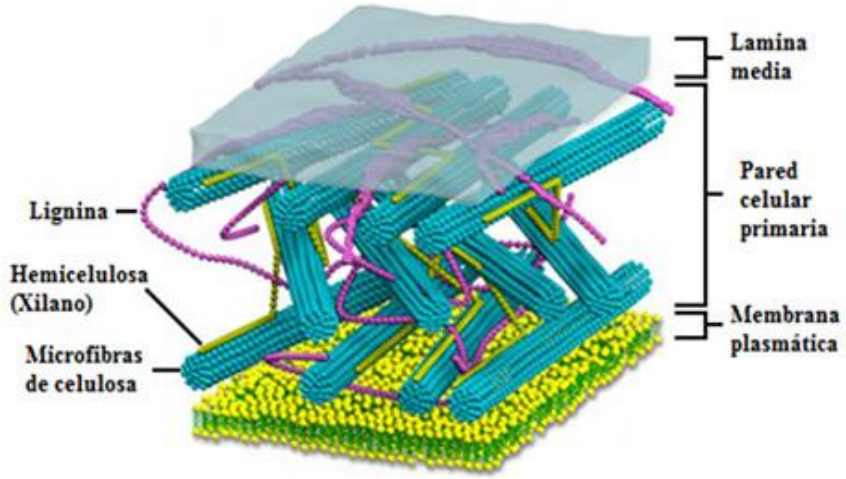

Figura 1. Estructura de la biomasa lignocelulosica

La **celulosa** es un polisacárido con enlaces β (1,4) de monómeros de D-glucopiranosa. Es un material cristalino con una conformación plana extendida de doble hélice y con puentes de hidrógeno que ayudan a mantener y reforzar la conformación en cadena.

La **hemicelulosa** es un polisacárido formado por hexosas, D-galactosa, D-glucosa y D-manosa, y pentosas, D-arabinosa y D-xilosa, siendo éste último el monosacárido más abundante. Presenta una estructura amorfa por su naturaleza ramificada por lo que, comparada con la celulosa, su sacarificación resulta relativamente fácil.

Finalmente la **lignina** es un polímero formado a base de monómeros fenilpropílicos (alcoholes cumarílico, coniferílico y sinapílico), muy ramificado y sustituido que se encuentra en las paredes celulares vegetales. La lignina se asocia normalmente con la celulosa y la hemicelulosa para formar la lignocelulosa. Dependiendo del tipo de monómeros estructurales se obtienen diferentes tipos de lignina. La lignina se encuentra recubriendo todo el conjunto anterior, y es muy inerte químicamente, por lo que otorga al material una alta resistencia a los ataques químicos y/o biológicos.

La principal barrera para el desarrollo de una biorrefinería lignocelulósica es su **resistencia a la degradación**. Resulta complicado realizar la separación de los principales componentes de la biomasa sin degradar su estructura química, ya que la elevada complejidad en composición y enlaces químicos y físicos que presenta

dificulta su separación mediante tecnologías convencionales [10, 11]. Para poder acceder a la celulosa y hemicelulosa es necesario romper el sello protector de lignina e incrementar la superficie del material. Durante varias décadas se han empleado diferentes alternativas para desarrollar **pre-tratamientos de bajo coste que eliminen de manera eficiente el sello protector de lignina y generen corrientes de azúcares derivados de la celulosa y hemicelulosa**. Estos métodos incluyen procesos biológicos, mecánicos, físicos y químicos, o una combinación de los mismos.

Entre los **pretratamientos físico-químicos** destaca el tratamiento con vapor, que es la técnica más utilizada para el pretratamiento de la lignocelulosa, la explosión de fibras por amoniaco, la explosión de CO_2 o el proceso organosolv, en el que se utilizan disolventes orgánicos [12].

También se pueden aplicar **pretratamientos físicos**, que consisten en el procesado mecánico de la biomasa lignocelulósica para reducir su tamaño. Se emplean métodos tales como la molienda, irradiación mediante rayos gamma, haz de electrones, o radiaciones microondas, y extrusión, con objeto de mejorar la hidrólisis enzimática o la biodegradabilidad de los materiales lignocelulósicos.

Por su parte, los **pretratamientos químicos** se emplean con la finalidad de romper la cubierta protectora alrededor de la celulosa y hacer la hemicelulosa más accesible a la hidrólisis, ya que ésta tiene una estructura amorfa relativamente débil que es fácilmente hidrolizable por ácidos o bases, comparada con la estructura cristalina fuerte, rígida y resistente a la hidrólisis que presenta la celulosa. Estos pretratamientos se pueden clasificar en tratamientos ácidos, tratamientos alcalinos y tratamientos con disolventes (líquidos iónicos).

Otra alternativa son los **tratamientos biológicos**, en los que se emplean microorganimos degradantes de la madera, tales como hongos y bacterias, que modifican la composición química y/o estructura de la biomasa lignocelulósica permitiendo la digestión enzimática más fácilmente.

Una vez que la lignocelulosa ha sido tratada mediante algunos de los procedimientos anteriores, se consigue un mejor acceso a los azúcares de la lignocelulosa. Existen dos estrategias principales para el procesado de la biomasa

lignocelulósica [2, 13] La primera incluye **rutas termoquímicas** que permiten procesar la lignocelulosa a altas temperaturas y/o presiones, sin necesidad de los tratamientos previos que acaban de ser citados, obteniendo como resultado la ruptura de la biomasa. Entre ellos destacan la gasificación, la pirolisis y la licuefacción.

En la gasificación se obtiene como resultado un gas de síntesis (mezcla de CO y H_2), que se emplea para la obtención de metanol o para la síntesis de Fischer-Tropsch. Por su parte la pirolisis y la licuefacción dan lugar a lo que se denomina biocrudos (bio-oils), que consiste en una mezcla líquida con más de 350 compuestos, como ácidos, aldehídos, alcoholes, azúcares, ésteres, cetonas y aromáticos que se han probado con éxito en motores, turbinas y quemadores con pequeñas modificaciones.

La segunda estrategia de procesado de la biomasa lignocelulósica es la **hidrólisis**, en la que los azúcares y la lignina se separan y se procesan selectivamente por los siguientes medios:

- *Conversión química:* consiste en la utilización de diferentes catalizadores en medio acuoso para despolimerizar los polisacáridos en los azúcares que los componen y transformarlos en productos de utilidad. Mientras que la lignina y la hemicelulosa hidrolizan rápidamente a temperaturas medias en presencia de ácidos o bases, la celulosa es más difícil de hidrolizar, ya que su estructura cristalina impide el acceso de los catalizadores a sus enlaces.

- *Rutas biológicas (fermentación)*: se trata de un procesado bioquímico en el que se utilizan microorganismos y/o reacciones enzimáticas para convertir un sustrato fermentable en productos recuperables.

Una vez separados los diferentes componentes de la biomasa mediante cualquiera de los procedimientos nombrados anteriormente, éstos **pueden procesarse en un esquema de biorrefinería** obteniéndose así diferentes compuestos de cada uno de ellos:

A partir de la **celulosa** se pueden sintetizar polímeros celulósicos, como el papel; es además susceptible de hidrolizarse hasta sus monómeros constituyentes, obteniéndose medios fermentables para la producción de etanol, un biocarburante

que se puede emplear como sustitutivo de la gasolina. Mediante transformaciones químicas se pueden obtener productos químicos como el 5-hidroximetilfurfural (HMF) y el ácido levulínico, ambos disponibles a partir de la deshidratación de hexosas catalizada por un ácido. El HMF es un compuesto versátil desde el que se pueden sintetizar otros productos químicos de interés, los cuales pueden emplearse como disolventes, lubricantes y polímeros [14-16].

De la **hemicelulosa** pueden obtenerse medios fermentables y diversos productos químicos, dada la gran variedad de monómeros constituyentes. Entre estos productos destacan aquellos con aplicaciones en cosmética o farmacia y productos para alimentación animal y humana, principalmente relacionados con alimentos dietéticos. La **xilosa**, que es la pentosa más abundante de la hemicelulosa, es barata y fácilmente accesible desde la lignocelulosa, siendo el xilitol y el **furfural** sus principales derivados. El xilitol se obtiene por hidrogenación catalítica a alta presión empleando catalizadores de Ni soportados o Ni Raney. Por su parte, el furfural se produce sometiendo a la xilosa a un medio acuoso ácido y a temperaturas y presiones relativamente elevadas (entre 423-443 K y hasta 10 bares de presión) [12].

La fracción de **lignina** se usa principalmente en el sector de materiales (tableros), aunque también en la obtención de derivados de esteroles con aplicaciones en farmacia, antioxidantes, materiales poliméricos y aditivos de betunes y asfaltos.

En la Figura 2 se representa de manera esquemática un ejemplo de algunos de los productos potenciales que pueden obtenerse en una instalación a partir de lignocelulosa mediante transformaciones químicas y biotecnológicas. En ella se puede apreciar el amplio abanico de posibles usos de los productos químicos en los que puede fraccionarse el material lignocelulósico.

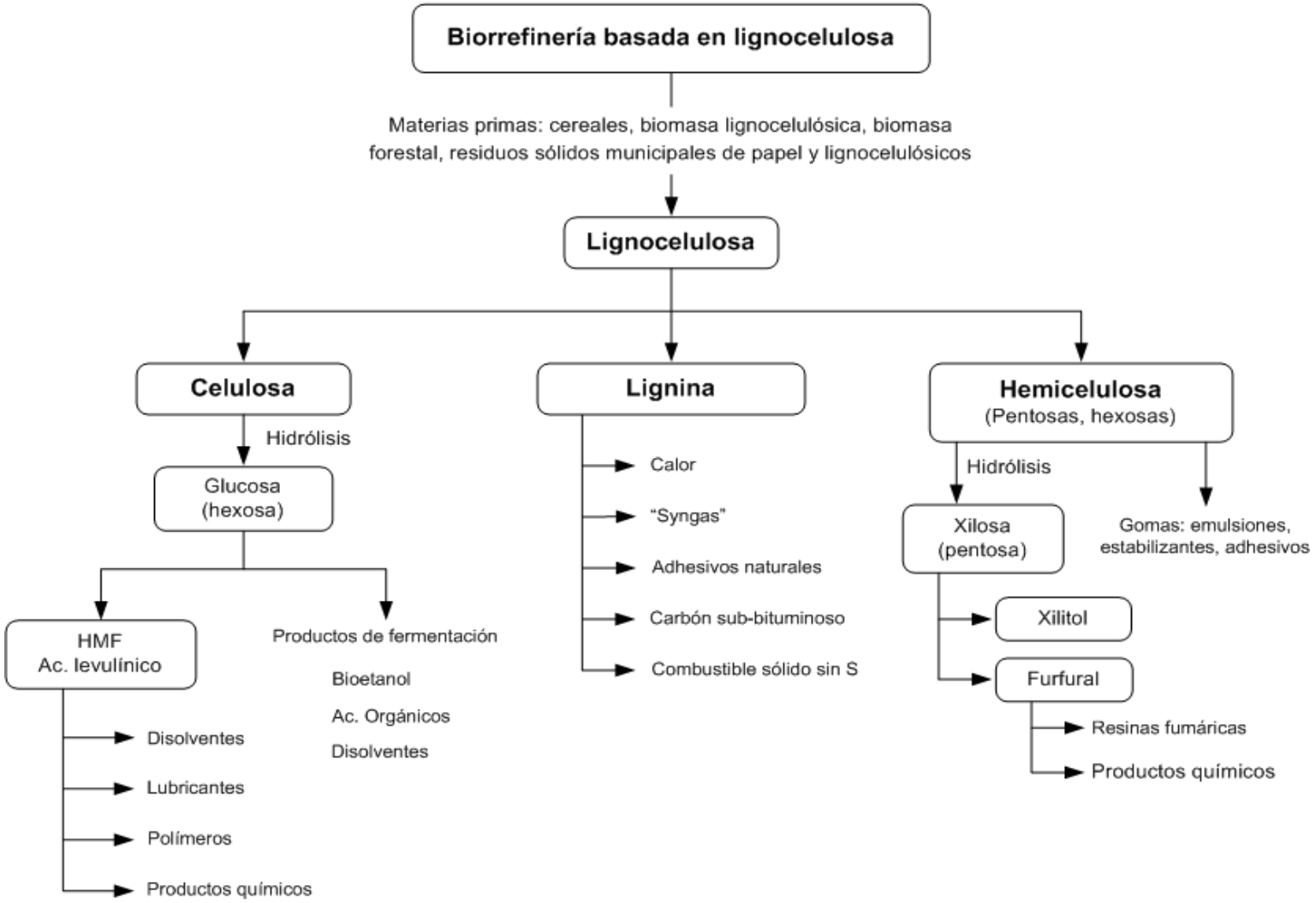

Figura 2. Productos obtenidos en una biorrefinería de material lignocelulósico

2.3. Relevancia del furfural y del anhídrido/ácido maleico

El **furfural (2-furfuraldehído)** es un compuesto orgánico obtenido a partir de subproductos agrícolas. La producción anual de furfural es superior a las 300.000 toneladas, siendo el único producto químico con elevada producción obtenido a partir de la lignocelulosa. El principal productor, con un aproximadamente un 70% de la producción mundial, es China [17].

El furfural **se obtiene comercialmente** a día de hoy directamente a partir de la biomasa lignocelulósica, derivada principalmente de residuos agrícolas o forestales. Durante dicho proceso los polisacáridos C5 presentes en el material lignocelulósico se exponen a un medio acuoso ácido, en el que se hidrolizan hacia sus monosacáridos, principalmente xilosa. Estos monosacáridos son deshidratados posteriormente hacia furfural. Se obtienen como producto disoluciones de furfural que posteriormente hay que destilar y purificar para evitar su degradación. El producto final es furfural con una pureza superior al 98% [17].

El furfural ha sido identificado como uno de los principales productos químicos de alto valor añadido derivable de la biomasa [18] debido al elevado número de productos químicos que ya se producen a partir de este compuesto, y a la amplia variedad de otros biocombustibles, materias primas y productos de química fina que también pueden obtenerse a partir de éste mediante reacciones químicas simples. Los dos grupos funcionales (grupo aldehído y anillo aromático) son los responsables de la alta reactividad química del furfural [17, 19-21].

Los principales compuestos que se obtienen a partir del furfural son furano, ácido furoico, y los alcoholes furfurílico y tetrahidrofurfurílico. Sin embargo, las aplicaciones del furfural van más allá y existen descritos numerosos procesos que permiten obtener otros compuestos industriales que a día de hoy se sintetizan a partir de fuentes petroquímicas. Entre ellos se encuentra el anhídrido maleico, que actualmente se obtiene principalmente a partir de la oxidación selectiva del *n*-butano.

En la Figura 3 se recogen algunos de los principales compuestos químicos que se pueden sintetizar a partir del furfural. A lo largo de esta tesis se estudiará la oxidación de furfural para la obtención de diferentes compuestos C4, tales como el

anhídrido maleico en su oxidación en fase gaseosa, o bien **ácido maleico** y **succínico** en su oxidación en fase líquida.

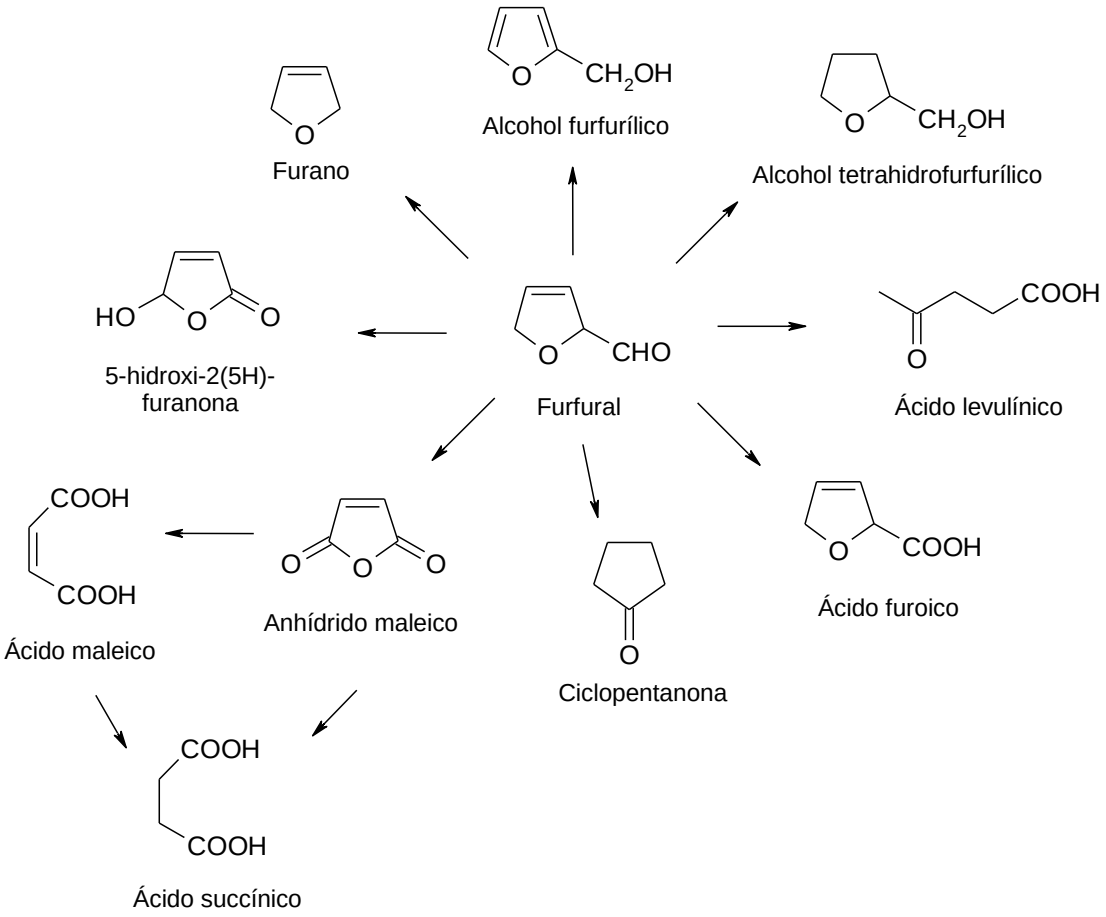

Figura 3. Principales compuestos químicos derivados del furfural

El **anhídrido maleico** es uno de los "building blocks" más empleados como precursor de una inmensa variedad de productos químicos, siendo un importante intermedio en la industria petroquímica. Se **utiliza**, por ejemplo, para la síntesis de resinas de poliéster insaturadas por medio de una reacción de esterificación, cuya aplicación se destina principalmente a la producción de resinas reforzadas de fibra de vidrio utilizadas en el sector de la construcción, y en material de navegación y automóviles. También se emplea en aditivos para aceites y productos alimentarios,

en la industria del papel y en aditivos de petróleo, barnices, celofán, detergentes, pinturas, ciertos productos farmacéuticos, plásticos, lubricantes, etc. [22, 23]

Muchos compuestos químicos comerciales, como el ácido fumárico, el ácido succínico, el ácido aspártico o el ácido tartárico, se pueden obtener a partir del anhídrido maleico. Estos derivados tienen importancia en la industria farmacéutica y textil, en la obtención de productos químicos para fotografía, agentes de bronceado y aditivos del petróleo [24].

La **producción anual de anhídrido maleico** a nivel mundial está en torno a 1800 kton. Este compuesto se ha obtenido tradicionalmente mediante la **oxidación** en fase vapor del **benceno** o de otros compuestos aromáticos, utilizando para ello catalizadores de óxidos de vanadio [24, 25]. Sin embargo, en el año 2006 quedaban ya muy pocas plantas operativas que continuaran empleando benceno como materia prima, ya que una importante subida de precios de este compuesto, así como los efectos nocivos que se le atribuyen, incentivaron la búsqueda de nuevas rutas para su obtención. Como consecuencia de este desarrollo se empezaron a construir nuevas plantas en las que el ***n*-butano** era la materia prima utilizada. Esta reacción de oxidación tiene lugar en fase vapor con **catalizadores de óxidos de vanadio y fósforo (VPO)** a elevadas temperaturas, del orden de 673-723 K. Las selectividades alcanzadas hacia anhídrido maleico son del 67-75% con una conversión de *n*-butano entre el 70-85%. Diferentes estudios acerca de esta reacción demuestran que la selectividad hacia el producto de interés está relacionada directamente con la acidez tipo Lewis que presenta el soporte, de tal manera que una elevada acidez favorece la oxidación de *n*-butano hacia el producto de interés. Por este motivo se suele emplear como soporte Al_2O_3 con elevada área superficial [26, 27].

La utilización del *n*-butano como materia prima implica una **fuerte dependencia del petróleo** para la obtención del anhídrido maleico, cuyo mercado y disponibilidad está sujeto a importantes fluctuaciones. El actual escenario inestable de precios de los combustibles fósiles y de sus derivados, junto con los problemas medioambientales ocasionadas por el consumo de éstos, hace que todos los esfuerzos se dirijan hacia el fomento de las energías alternativas o limpias.

Recientemente se han presentado también estudios acerca de la producción de anhídrido maleico en fase gaseosa utilizando diferentes productos de partida. Un ejemplo es la utilización de **bio-butanol** como materia prima, con el que se alcanza un rendimiento hacia anhídrido maleico inferior al obtenido en la oxidación de furfural [28]. Para el caso de la oxidación en fase líquida de **HMF**, el rendimiento total registrado hacia ácido y hacia anhídrido maleico es del 80%, utilizando como agente oxidante oxígeno a una presión relativamente elevada de 1 MPa [29]. Otra manera de obtener ácido maleico con un rendimiento elevado (70%) es a partir de la oxidación en fase gas y a presión atmosférica de **ácido levulínico** [30].

Ninguno de los compuestos nombrados anteriormente (bio-butanol, HMF y ácido levulínico) están disponibles comercialmente a una escala suficientemente grande como para poder reemplazar la producción de anhídrido/ácido maleico a partir de recursos fósiles. Por contra, el furfural es uno de los pocos compuestos que actualmente se producen a partir de biomasa, y su síntesis no interfiere con la producción de alimentos para humanos y animales, ya que se utilizan residuos agrícolas como materia prima [12].

Por todo ello, y teniendo en cuenta el elevado potencial que presenta, **se propone la utilización de furfural como materia prima alternativa para la síntesis de anhídrido maleico.** La posibilidad de obtener anhídrido maleico mediante la oxidación de furfural ha quedado técnicamente demostrada por diferentes grupos de investigación, tanto en fase vapor [31-35] como en fase líquida [36, 37]. La oxidación en fase gas presenta la ventaja de utilizar un agente oxidante económico, como es el aire, en lugar de oxígeno o H_2O_2 utilizados habitualmente en las reacciones de oxidación en fase líquida. Por contra, se necesitan altas temperaturas de reacción para alcanzar rendimientos notables.

2.4. Procesos catalíticos heterogéneos en la oxidación selectiva de furfural a anhídrido/ácido maleico

2.4.1. Oxidación catalítica en fase gaseosa

La reacción de **oxidación de furfural en fase gas** se lleva a cabo en un reactor de lecho ficho a temperaturas entre 473-673 K, utilizando como reactivo furfural

diluido en una corriente mezcla de O_2-N_2 (por debajo de 5% v/v) y con tiempos de contacto cortos, de apenas unos segundos. Para esta reacción se han estudiado catalizadores basados en diferentes **óxidos de vanadio** (óxido de vanadio o bien mezclas de óxidos tales como V-Mo o V-Bi), utilizando como soportes asbestos o alúmina [31, 33-35, 38, 39].

Durante esta oxidación de furfural en fase gas se obtienen además resinas que disminuyen la selectividad hacia anhídrido maleico. Estos productos pesados pueden formarse a través de la condensación del furfural con los productos de la reacción o bien a través de la resignificación del propio furfural. Los trabajos recogidos señalan que la selectividad de la reacción puede mejorarse aumentando la temperatura de reacción, la concentración de oxígeno o bien mediante la adición de agua [34].

Existen estudios en los que se ha analizado el **mecanismo y la cinética** de la reacción utilizando como catalizadores $Sn(VO_3)_4$ y catalizadores de V-Mo-P (P_2O_5, $Fe_2(MoO_4)_3$, MoO_3 y V_2O_5) [31, 34, 35, 39]. Estos estudios cinéticos, realizados en el rango de temperaturas entre 497-753 K, indican que la oxidación de furfural se produce de manera paralela en dos rutas: hacia anhídrido maleico o hacia CO_x [31, 39]. Se han propuesto en bibliografía dos mecanismos de reacción para la oxidación de furfural hacia anhídrido maleico, los cuales comparten la primera etapa de oxidación hacia ácido furoico y su posterior decarboxilación hacia furano.

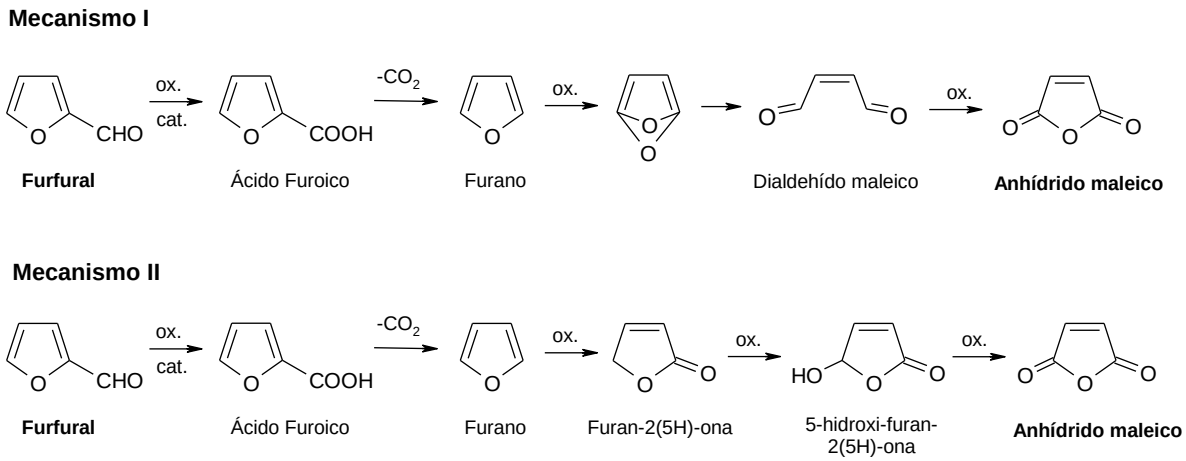

Figura 4. Mecanismo de oxidación de furfural con O_2 en fase gas

El primer mecanismo de reacción propone que una vez que se ha formado el furano se introduce un átomo de oxígeno en la posición 1,4 del anillo. A continuación se produce la apertura del anillo, dando como resultado el dialdehído maleico y tras la oxidación de este el anhídrido maleico [38].

El segundo mecanismo de reacción propone que el furano se oxida hacia 5-hidroxi-2(5H)-furanona mediante la adición de dos átomos de oxígeno en las posiciones 2 y 5 del anillo de furano. En una última etapa de oxidación se obtendría el anhídrido maleico [34].

Sin embargo, estos dos mecanismos de reacción propuestos no están soportados por ninguna evidencia experimental, y no se establece una relación clara entre la estructura de los catalizadores y su actividad, necesario para diseñar catalizadores más activos en la reacción de interés, por lo que existe un vacío en este campo.

Los **óxidos de vanadio soportados** se utilizan como catalizadores en la oxidación de *n*-butano con oxígeno para producir anhídrido maleico [26]. Existen ciertos estudios en los que se propone que especies derivadas del furano están involucradas en este mecanismo de la reacción [40]. Habitualmente los óxidos de vanadio se depositan sobre soportes con elevada área superficial para aumentar la fuerza mecánica, el número de sitios de reacción y la velocidad de reacción. La densidad del vanadio superficial y las características del soporte pueden influir de manera importante en las propiedades electrónicas y en la actividad catalítica de estas especies de vanadio soportadas [41]. Por lo tanto, es necesario llevar a cabo una investigación detallada acerca del papel que tienen las especies VO_X presentes en los catalizadores en la formación de anhídrido maleico y/o furano a partir de la oxidación catalítica selectiva de furfural.

2.4.2. Oxidación catalítica en fase líquida

Respecto a la **oxidación de furfural en fase líquida, en la que se obtiene como producto ácido maleico,** existen en bibliografía reacciones a temperaturas relativamente moderadas (383 K) en las que se utiliza oxígeno como agente oxidante a presiones elevadas (2 MPa) y **catalizadores homogéneos**, como el ácido

fosfomolíbdico. Estas reacciones se llevan a cabo en un sistema bifásico, en el que se utiliza un disolvente orgánico con elevada afinidad hacia el furfural, con el objetivo de reducir la polimerización de éste y la consecuente formación de resinas. Se han estudiado disolventes como el tetraclorometano o el tolueno, alcanzándose rendimientos de hasta el 50% hacia ácido maleico [36, 37]. El disolvente orgánico actúa como un reservorio de furfural, evitando su polimerización, mientras que la concentración del furfural en la fase acuosa, donde se encuentra el catalizador y donde ocurre la reacción de oxidación, es baja. La reutilización de estos catalizadores no ha sido probada, lo cual resulta fundamental para implementar esta reacción en un proceso industrial.

El uso de **catalizadores sólidos** en estas reacciones resulta más interesante, debido a su facilidad a la hora de recuperarlo del medio de reacción para su posterior reutilización. Además, para que el proceso sea económicamente viable para poder implantarlo a escala industrial sería interesante mejorar los rendimientos alcanzados hasta la fecha. Por ello resulta imprescindible el desarrollo de nuevos catalizadores sólidos con los que se pueda establecer una relación directa entre sus propiedades físico-químicas y su actividad catalítica.

Actualmente se han realizado también estudios de oxidación de furfural en fase líquida en los que se utiliza **H_2O_2 como agente oxidante**. En principio, la utilización de peróxido de hidrógeno como agente oxidante podría presentar ciertas ventajas con respecto a un proceso en fase gas; en primer lugar, porque no se requieren temperaturas elevadas para llevar a cabo la reacción y se realiza a presión atmosférica, y en segundo lugar porque se puede utilizar como reactivo furfural diluido en medio acuoso. La importancia de este último punto radica en que el furfural que se obtiene a partir de residuos lignocelulósicos es una disolución acuosa. Para obtener el producto con una pureza superior al 98% es necesario hacer posteriormente una doble destilación, lo cual resulta energéticamente muy costoso. El hecho de poder utilizar como materia prima una disolución acuosa de furfural permitiría prescindir de esta etapa de destilación.

Esta reacción puede ser catalizada tanto por ácidos fuertes (H_2SO_4 o HCl) como por ácidos débiles (ácido acético o ácido fórmico); incluso puede llevarse a cabo, aunque de manera más lenta, sin adición de catalizadores, ya que los ácidos que se forman durante la reacción aceleran la velocidad. También se han utilizado

como catalizadores óxidos metálicos, tales como el sulfato de vanadilo ($VOSO_4$), el vanadato de sodio ($NaVO_4$), el molibdato de sodio (Na_2MoO_4), el dicromato de potasio ($K_2Cr_2O_7$) y óxidos de niobio [42-44].

El **principal inconveniente** de realizar la oxidación del furfural con H_2O_2 y con catalizadores ácidos es el **control de la selectividad**, ya que se ha detectado un elevado número de compuestos entre los productos de reacción, tales como ácido maleico, ácido succínico, ácido fumárico, ácido β–formilacrílico o 2(5H)-furanona [42, 45]. Esta falta de selectividad es una consecuencia de un complejo mecanismo de reacción que comienza con la oxidación Baeyer-Villiger del furfural hacia el correspondiente éster [42, 45]. La identificación de un catalizador que consiga oxidar selectivamente el furfural hacia ácido maleico en una única etapa y que pueda recuperarse fácilmente del medio de reacción para sus posteriores reutilizaciones es todavía un reto.

Existen en bibliografía estudios sobre la oxidación selectiva de furano con H_2O_2 utilizando **titania silicalita TS-1** como catalizador [46, 47]. Alguno de los productos detectados durante la oxidación de furano con H_2O_2 fueron el dialdehído maleico y la 5-hidroxi-furan-2-(5H)-ona. Estos productos están directamente relacionados con el ácido maleico, ya que éste puede obtenerse a partir de su oxidación. El anillo de furano posee una estructura química similar a la del furfural, exceptuando el grupo funcional aldehído presente en este último, por lo que el estudio de la TS-1 como catalizador en la oxidación de furfural podría dar buenos resultados al respecto.

Una de las aplicaciones más habituales de la TS-1 es su utilización en la epoxidación de numerosos alquenos [48-50]. La activación del peróxido de hidrógeno por parte de la TS-1 está relacionada con el entorno particular de los cationes de Ti (IV) incorporados en la red de silicalita y localizados dentro de los poros hidrófobos de las zeolita. Esto permite una adsorción simultánea del sustrato hidrófobo y del oxidante [46, 51, 52].

Por otro lado, el **ácido poliestiren-sulfónico** comercial **(PSSA)** se ha utilizado como catalizador para la síntesis de biodiesel y para la deshidratación de xilosa a furfural [53], por lo que su utilización en la etapa posterior de obtención de ácido maleico a partir de furfural previamente obtenido resultaría muy interesante a nivel industrial.

El PSSA es una macromolécula lineal, soluble en agua y en otros disolventes polares, por lo tanto, para poder valorar la reutilización del PSSA es necesario separar el catalizador del medio de reacción mediante un proceso de ultrafiltración. Con el objetivo de simplificar este proceso de separación, se han presentado estudios en los que se propone el anclaje del polímero PSSA sobre un soporte sólido inorgánico, como el SiO_2. El resultado es un nanocomposite que se puede separar del medio de reacción mediante técnicas convencionales como filtración o centrifugación [54].

Para la síntesis de este nanocomposite se sigue una metodología sol-gel para hidrolizar y condensar los precursores sílica. Para esta reacción se utiliza tetraetil ortosilicato (TEOS) y 3-aminopropiltrietoxisilano (APTES), ya que la presencia de grupos etoxi generan un entorno favorable para la formación de etanol después de la hidrólisis, evitando así la presencia de metanol en el medio. El propio PSSA actúa como catalizador en la reacciones de hidrólisis y condensación implicada en el proceso sol-gel. Las interacciones electrostáticas que se generan entre los grupos amino y los grupos sulfónicos son las que permiten que el polímero permanezca anclado sobre las moléculas de sílica. El número de interacciones depende de las variables de síntesis, como la relación entre la concentración de polímero, TEOS y APTES.

2.5. Objetivos y metodología de esta Tesis Doctoral

Por todo lo descrito anteriormente, el **principal objetivo** de este trabajo es **identificar catalizadores sólidos que sean activos, selectivos y estables en la oxidación catalítica selectiva de furfural. Este trabajo se realizará tanto en la reacción en fase vapor como en fase líquida, para obtener anhídrido y/o ácido maleico**.

A nivel **académico** la presente tesis doctoral pretende arrojar cierta luz sobre los mecanismos de reacción y el estudio de variables de operación, ya que en los estudios realizados hasta la fecha apenas se recoge información al respecto. La identificación de especies intermedias de reacción y del mecanismo de reacción resulta fundamental para poder definir el catalizador óptimo.

Desde el punto de vista **medioambiental** hay destacar el reto que supone la utilización de la materia prima de origen renovable que se plantea como alternativa (el furfural), frente a las materias primas convencionales derivabas de combustibles fósiles que actualmente se están utilizando para la síntesis de los productos de interés. La utilización de residuos lignocelulósicos para la obtención de la materia prima permite además dar salida a estos, evitando así su acumulación. Estos residuos están distribuidos de manera homogénea por todo el planeta frente a la focalización de los combustibles de origen fósil, lo que se traduce también en una ventaja **económica** para países como España, que evitarían depender de terceros países para la síntesis de estos compuestos.

Para la síntesis de los catalizadores PSSA, tanto en su forma soluble como en su forma de nanocomposite, se propone utilizar como producto de partida residuos de poliestireno, en concreto poliestireno expandido, que serán sulfonados para formar el catalizador PSSA estudiado. Se pretende de esta manera obtener un catalizador económico aprovechando residuos de poliestireno.

Por otro lado, el desarrollo de catalizadores sólidos activos, selectivos y estables en la reacción de interés daría como resultado la optimización del proceso de producción y por lo tanto una reducción en los costes de producción.

Para poder alcanzar el objetivo principal de este trabajo se proponen los siguientes **objetivos parciales**:

- Identificación de catalizadores sólidos activos, selectivos y estables en la reacción de oxidación de furfural, tanto en fase gaseosa como en fase líquida.
- Identificación de especies intermedias de reacción para poder definir un mecanismo de reacción que conduzca a la formación de los productos de interés.
- Estudio de la estabilidad de los catalizadores mediante sucesivos ciclos de reutilización.
- Análisis de las propiedades fisicoquímicas de los catalizadores, tanto frescos como usados, para poder establecer las especies activas en la reacción y las posibles causas de desactivación de los catalizadores.

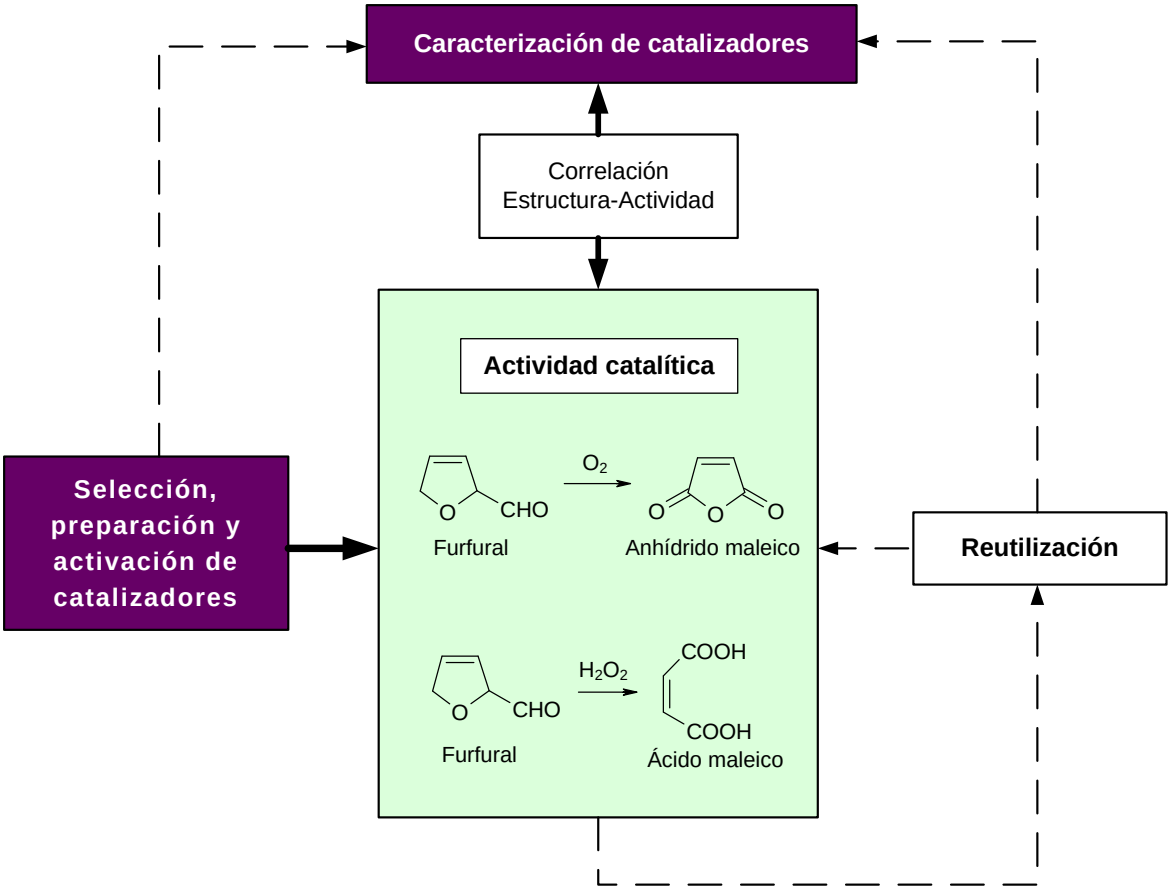

Figura 5. Esquema de la metodología utilizada para la consecución de los objetivos propuestos

En la Figura 5 se representa un esquema de la metodología experimental seguida para alcanzar los objetivos de esta tesis. Dicha metodología se puede estructurar de la siguiente manera:

- Selección de los catalizadores de estudio teniendo en cuenta las referencias bibliográficas recogidas al respecto y su posterior preparación y activación de acuerdo a la metodología seleccionada.
- Estudio de las propiedades catalíticas de los catalizadores activados, tales como conversión, selectividad y rendimiento. Se realizará también el estudio de las variables de operación (temperatura, concentración de reactivos, concentración de catalizador...) para encontrar las condiciones óptimas de máximo rendimiento hacia el producto de interés para cada catalizador.

- Caracterización de los catalizadores frescos mediante diferentes técnicas con el fin de establecer una relación entre sus propiedades fisicoquímicas y sus propiedades catalíticas.
- Estudio de la estabilidad de los catalizadores mediante la reutilización del catalizador durante sucesivos ciclos de reacción y caracterización de los catalizadores usados, para poder identificar posibles causas de desactivación catalítica.

2.6. Bibliografía

1. A. Corma, S.I., A. Velty, *Chemical Routes for the Transformation of Biomass into Chemicals.* Chemical Reviews, 2007. **107**: p. 2411-2502.
2. G. Centi, A.V.S., *Catalysis for Renewables*. From Feedstock to Energy Production. 2007.
3. Kamm, B. and M. Kamm, *Biorefineries - Multi product processes*, in *Advances in Biochemical Engineering/Biotechnology*2006. p. 175-204.
4. F. Cherubini, G.J., M. Wellisch, T. Willke, I. Skiadas, R. Van Ree, E. De Jong, *Toward a common classification approach for biorefinery systems.* Biofuels, bioproducts & biorefining, 2009. **3**: p. 534-546.
5. Clark, J.H., *Green chemistry for the second generation biorefinery - Sustainable chemical manufacturing based on biomass.* Journal of Chemical Technology and Biotechnology, 2007. **82**(7): p. 603-609.
6. Jefferson, M., *Sustainable energy development: performance and prospects.* Renewable Energy, 2006. **31**(5): p. 571-582.
7. Deswarte, F.E.I., et al., *Toward an integrated straw-based biorefi nery.* Biofuels, Bioproducts and Biorefining, 2007. **1**(4): p. 245-254.
8. Sanders, J., et al., *Bio-refinery as the bio-inspired process to bulk chemicals.* Macromolecular Bioscience, 2007. **7**(2): p. 105-117.
9. Huber, G.W., S. Iborra, and A. Corma, *Synthesis of transportation fuels from biomass: Chemistry, catalysts, and engineering.* Chemical Reviews, 2006. **106**(9): p. 4044-4098.
10. Nimz, H. and R. Casten, *Chemical processing of lignocellulosics.* European Journal of Wood and Wood Products, 1986. **44**(6): p. 207-212.
11. Zhang, Y.H.P., et al., *Fractionating recalcitrant lignocellulose at modest reaction conditions.* Biotechnology and Bioengineering, 2007. **97**(2): p. 214-223.
12. Mamman, A.S., et al., *Furfural: Hemicellulose/xylose-derived biochemical.* Biofuels, Bioproducts and Biorefining, 2008. **2**(5): p. 438-454.
13. D.M. Alonso, J.Q.B., J.A. Dumesic, *Catalytic conversion of biomass to biofuels.* Green chemistry, 2010. **12**(9): p. 1493-1513.
14. Alonso, D.M., et al., *Integrated conversion of hemicellulose and cellulose from lignocellulosic biomass.* Energy & Environmental Science, 2013. **6**(1): p. 76-80.
15. Alonso, D.M., S.G. Wettstein, and J.A. Dumesic, *Bimetallic catalysts for upgrading of biomass to fuels and chemicals.* Chemical Society Reviews, 2012. **41**(24): p. 8075-8098.
16. Alonso, D.M., S.G. Wettstein, and J.A. Dumesic, *Gamma-valerolactone, a sustainable platform molecule derived from lignocellulosic biomass.* Green Chemistry, 2013. **15**(3): p. 584-595.
17. Mariscal, R., et al., *Furfural: a renewable and versatile platform molecule for the synthesis of chemicals and fuels.* Energy & Environmental Science, 2016. **9**(4): p. 1144-1189.
18. Bozell, J.J. and G.R. Petersen, *Technology development for the production of biobased products from biorefinery carbohydrates-the US Department of Energy's "Top 10" revisited.* Green Chemistry, 2010. **12**(4): p. 539-554.
19. Zeitsch, K.J., *The Chemistry and Technology of Furfural and Its Many By-Products*. 2000.
20. Gandini, A., *The irruption of polymers from renewable resources on the scene of macromolecular science and technology.* Green Chemistry, 2011. **13**(5): p. 1061-1083.
21. B. Kamm, P.R. Gruber, and M. Kamm, *Biorefineries - Industrial Processes and Products Status Quo and Future Directions, Wiley-VCH, 2005.* 2005.

22. Lohbeck, H.H.K., W. Fuhrmann, and N. Fedtke, Ullmann´s Encyclopedia of Industrial Chemistry, 2000. **20**: p. 463-473.
23. Felthouse, T.R., et al., *Maleic Anhydride, Maleic Acid, and Fumaric Acid*, in *Kirk-Othmer Encyclopedia of Chemical Technology*. 2000, John Wiley & Sons, Inc.
24. Du, Z., et al., *Oxidation of 5-hydroxymethylfurfural to maleic anhydride with molecular oxygen.* Green Chemistry.
25. Centi, G., et al., *Mechanistic aspects of maleic anhydride synthesis from C4 hydrocarbons over phosphorus vanadium oxide.* Chemical Reviews, 1988. **88**(1): p. 55-80.
26. Wachs, I.E., et al., *Fundamental studies of butane oxidation over model-supported vanadium oxide catalysts: Molecular structure-reactivity relationships.* Journal of Catalysis, 1997. **170**(1): p. 75-88.
27. Guliants, V.V., et al., *Effect of promoters for n-butane oxidation to maleic anhydride over vanadium-phosphorus-oxide catalysts: Comparison with supported vanadia catalysts.* Catalysis Letters, 1999. **62**(2-4): p. 87-91.
28. Pavarelli, G., et al., *A New Process for Maleic Anhydride Synthesis from a Renewable Building Block: The Gas-Phase Oxidehydration of Bio-1-butanol.* ChemSusChem, 2015. **8**(13): p. 2250-2259.
29. Li, X. and Y. Zhang, *The conversion of 5-hydroxymethyl furfural (HMF) to maleic anhydride with vanadium-based heterogeneous catalysts.* Green Chemistry, 2016. **18**(3): p. 643-647.
30. Chatzidimitriou, A. and J.Q. Bond, *Oxidation of levulinic acid for the production of maleic anhydride: breathing new life into biochemicals.* Green Chemistry, 2015. **17**(8): p. 4367-4376.
31. Murthy, M.S. and K. Rajamani, *Kinetics of vapour phase oxidation of furfural on vanadium catalyst.* Chemical Engineering Science, 1974. **29**(2): p. 601-609.
32. Stepen, R.A., T.V. Barakov, and Y.I. Khol'kin, *Maleic anhydride in the products of oxidation of furfural by molecular oxygen.* Chemistry of Heterocyclic Compounds, 1975. **9**(3): p. 280-281.
33. Nielsen, E.R., *Vapor Phase Oxidation of Furfural.* Industrial & Engineering Chemistry, 1949. **41**(2): p. 365-368.
34. Slavinskaya, V.A., et al., *Incomplete catalytic oxidation of furan compounds (review).* Chemistry of Heterocyclic Compounds, 1978. **13**(7): p. 710-721.
35. Kreile, D.R., et al., *The reactivity of furan compounds in vapor-phase catalytic oxidation.* Chemistry of Heterocyclic Compounds, 1969. **5**(4): p. 429-430.
36. Guo, H. and G. Yin, *Catalytic aerobic oxidation of renewable furfural with phosphomolybdic acid catalyst: An alternative route to maleic acid.* Journal of Physical Chemistry C, 2011. **115**(35): p. 17516-17522.
37. Shi, S., H. Guo, and G. Yin, *Synthesis of maleic acid from renewable resources: Catalytic oxidation of furfural in liquid media with dioxygen.* Catalysis Communications. **12**(8): p. 731-733.
38. Milas, N.A. and W.L. Walsh, *Catalytic oxidations. I. Oxidations in the furan series.* Journal of the American Chemical Society, 1935. **57**(8): p. 1389-1393.
39. Rajamani, K., P. Subramanian, and M.S. Murthy, *Kinetics and mechanism of vapor phase oxidation of furfural over tin vanadate catalyst.* Industrial & Engineering Chemistry Process Design and Development, 1976. **15**(2): p. 232-234.
40. Zhanglin, Y., et al., *On the Mechanism of n-Butane Oxidation to Maleic Anhydride on VPO Catalysts.* Journal of Catalysis, 1994. **145**(2): p. 256-266.

41. Bond, G.C. and S.F. Tahir, *Vanadium oxide monolayer catalysts Preparation, characterization and catalytic activity.* Applied Catalysis, 1991. **71**(1): p. 1-31.
42. Choudhary, H., S. Nishimura, and K. Ebitani, *Highly efficient aqueous oxidation of furfural to succinic acid using reusable heterogeneous acid catalyst with hydrogen peroxide.* Chemistry Letters, 2012. **41**(4): p. 409-411.
43. Badovskaya, L.A., et al., *Catalytic oxidation of furan and hydrofuran compounds. 7. Production of 2(5H)-furanone by oxidation of furfural with hydrogen peroxide and some of its transformations in aqueous solutions.* Chemistry of Heterocyclic Compounds, 2002. **38**(9): p. 1040-1048.
44. Muzychenko, G.F., L.A. Badovskaya, and V.G. Kul'nevich, *Role of water in the oxidation of furfural with hydrogen peroxide.* Chemistry of Heterocyclic Compounds, 1972. **8**(11): p. 1311-1313.
45. Choudhary, H., S. Nishimura, and K. Ebitani, *Metal-free oxidative synthesis of succinic acid from biomass-derived furan compounds using a solid acid catalyst with hydrogen peroxide.* Applied Catalysis A: General, 2013. **458**: p. 55-62.
46. Wahlen, J., et al., *Titanium silicalite 1 (TS-1) catalyzed oxidative transformations of furan derivatives with hydrogen peroxide.* Advanced Synthesis and Catalysis, 2004. **346**(2-3): p. 333-338.
47. Kumar, P. and R.K. Pandey, *An efficient synthesis of 5-hydroxy-2(5H)-furanone: Using a titanium silicate molecular sieve catalyst.* Green Chemistry, 2000. **2**(1): p. 29-31.
48. Clerici, M.G., G. Bellussi, and U. Romano, *Synthesis of propylene oxide from propylene and hydrogen peroxide catalyzed by titanium silicalite.* Journal of Catalysis, 1991. **129**(1): p. 159-167.
49. Kumar, S.B., et al., *Epoxidation of Styrene over a Titanium Silicate Molecular Sieve TS1 Using Dilute H2O2 as Oxidizing Agent.* Journal of Catalysis, 1995. **156**(1): p. 163-166.
50. Uguina, M.A., et al., *Preliminary study on the TS-1 deactivation during styrene oxidation with H2O2.* Catalysis Today, 2000. **61**(1–4): p. 263-270.
51. Astorino, E., et al., *Spectroscopic Characterization of Silicalite-1 and Titanium Silicalite-1.* Journal of Catalysis, 1995. **157**(2): p. 482-500.
52. Bonino, F., et al., *Ti-Peroxo Species in the TS-1/H2O2/H2O System.* The Journal of Physical Chemistry B, 2004. **108**(11): p. 3573-3583.
53. Granados, M.L., et al., *Poly(styrenesulphonic) acid: An active and reusable acid catalyst soluble in polar solvents.* Green Chemistry, 2011. **13**(11): p. 3203-3212.
54. Sádaba, I., et al., *Silica-poly(styrenesulphonic acid) nanocomposites for the catalytic dehydration of xylose to furfural.* Applied Catalysis B: Environmental, 2014. **150–151**: p. 421-431.
55. Bajdur, W., et al., *Effective polyelectrolytes synthesised from expanded polystyrene wastes.* European Polymer Journal, 2002. **38**(2): p. 299-304.
56. Sułkowski, W.W., et al., *Preparation and properties of flocculants derived from polystyrene waste.* Polymer Degradation and Stability, 2005. **90**(2 SPEC. ISS.): p. 272-280.
57. Sułkowski, W.W., et al., *The influence of the chemical additives in polystyrene on the features of flocculants obtained during sulphonation of the polystyrene.* Macromolecular Symposia, 2006. **245-246**: p. 315-321.
58. Inagaki, Y., et al., *Reclamation of waste polystyrene by sulfonation.* Langmuir, 1999. **15**(12): p. 4171-4175.
59. Bekri-Abbes, I., S. Bayoudh, and M. Baklouti, *The removal of hardness of water using sulfonated waste plastic.* Desalination, 2008. **222**(1-3): p. 81-86.

60. Bekri-Abbes, I., S. Bayoudh, and M. Baklouti, *A technique for purifying wastewater with polymeric flocculantproduced from waste plastic.* Desalination, 2007. **204**(1-3 SPEC. ISS.): p. 198-203.
61. Bekri-Abbes, I., S. Bayoudh, and M. Baklouti, *Converting waste polystyrene into adsorbent: Potential use in the removal of lead and cadmium ions from aqueous solution.* Journal of Polymers and the Environment, 2006. **14**(3): p. 249-256.
62. De Assunção, R.M.N., et al., *Synthesis, characterization, and application of the sodium poly(styrenesulfonate) produced from waste polystyrene cups as an admixture in concrete.* Journal of Applied Polymer Science, 2005. **96**(5): p. 1534-1538.

3. PUBLICACIONES

INDICE

3. PUBLICACIONES

- Publicación 1: *"Selective Conversion of Furfural to Maleic Anhydride and Furan with VO_x/Al_2O_3 catalysts"*
- Publicación 2: *"Gas Phase Oxidation of Furfural to Maleic Anhydride on V_2O_5/γ-Al_2O_3 Catalysts: Reaction Conditions to Slow Down the Deactivation"*
- Publicación 3: *"Poly-(Styrene Sulphonic Acid): an Acid Catalyst From Polystyrene Waste for Reactions of Interest in Biomass Valorization"*
- Publicación 4: *"Aqueous-Phase Catalytic Oxidation of Furfural with H_2O_2: High Yield of Maleic Acid by Using Titanium Silicalite-1"*

PUBLICACIÓN 1:

Título: *"Selective Conversion of Furfural to Maleic Anhydride and Furan with VO_x/Al_2O_3 catalysts"*

Autores: *Noelia Alonso Fagúndez, Manuel López Granados, Rafael Mariscal, Manuel Ojeda*

Revista: *CHEMSUSCHEM*

Año: *2012*

CHEMSUSCHEM

ChemPubSoc Europe

DOI: 10.1002/cssc.201200167

Selective Conversion of Furfural to Maleic Anhydride and Furan with VO_x/Al_2O_3 Catalysts

Noelia Alonso-Fagúndez, Manuel López Granados, Rafael Mariscal, and Manuel Ojeda*[a]

Furfural can be converted into maleic anhydride (73% yield) through selective gas phase oxidation at 593 K with O_2 by using VO_x/Al_2O_3 (10 $at_V\,nm^{-2}$) as solid catalysts. The use of lower temperatures and/or O_2 pressures result in the additional formation of furan (maximum 9% yield). Mechanistically, furfural ($C_5H_4O_2$) is oxidized stepwise to furan (C_4H_4O), 2-furanone ($C_4H_4O_2$), and finally, maleic anhydride ($C_4H_2O_3$). The specific structure of the supported vanadium oxides and reaction conditions (temperature and reactants pressures) all influence furfural oxidation catalysis. We have found that Al_2O_3-supported polyvanadates are intrinsically more active (2.70 $mmol\,h^{-1}\,g\text{-}at\,V^{-1}$) than monovanadates ($VO_4$) and V_2O_5 crystals (0.89 and 0.70 $mmol\,h^{-1}\,g\text{-}at\,V^{-1}$, respectively) in maleic anhydride and furan formation rates (553 K, 1.6 kPa furfural, 2.5 kPa O_2). Our alternative approach enables the use of biomass instead of petroleum to synthesize maleic anhydride and furan from furfural. The potential variety of industrial applications is of enormous interest for the development of future biorefineries.

Introduction

Maleic anhydride (MA) and furan are important chemical intermediates used for the manufacture of unsaturated polyester resins and other industrial chemicals for use as pharmaceuticals, herbicides, stabilizers, fine chemicals, etc.[1] Furan is mainly prepared by either catalytic furfural decarbonylation or from butadiene, whereas maleic anhydride is typically obtained by selective catalytic oxidation of *n*-butane or benzene,[2] which are petroleum-derived chemicals. However, exploring new technologies to replace fossil feedstocks by lignocellulosic biomass for maleic anhydride and furan synthesis would be of great interest because of: (i) depletion of petroleum reserves; (ii) significant price increase in the last years; and (iii) environmental concerns associated with the use of petroleum (mainly CO_2 emissions). In contrast to biofuels, transition from petroleum to biomass feedstocks for the production of chemicals seems to be more feasible,[3] although this will require overcoming some significant technological challenges. In light of this context, we have developed a route to synthesize maleic anhydride and furan from furfural by utilizing vanadium oxides supported on alumina as catalysts. Furfural is a renewable resource obtained from pentoses (xylose and arabinose) present in lignocellulosic biomass through acid-catalyzed dehydration.[4,5] Therefore, furfural oxidation to maleic anhydride and furan would provide an alternative pathway for the synthesis of these two important chemicals by using biomass instead of petroleum as a renewable feedstock.

In investigations of gas phase furfural oxidation to maleic acid reported by Nielsen more than sixty years ago high catalytic yields were achieved.[6] Later, the mechanism and kinetics of maleic anhydride formation from furfural was investigated by using $Sn(VO_3)_4$ and promoted V-Mo-P (P_2O_5, $Fe_2(MoO_4)_3$, MoO_3, V_2O_5) as solid catalysts.[7–10] However, the use of these catalytic systems was not appropriately justified and appeared to be arbitrary. Furthermore, detailed kinetic results, and more importantly the establishment of structure–activity relationships necessary to rationally design more active catalysts, were missing. Recent communications have also demonstrated the use of homogeneous catalysts [$Cu(NO_3)_2$ and phosphomolybdic acid, $H_3PMo_{12}O_{40}{\cdot}x\,H_2O$] to oxidize furfural to maleic acid (383 K, 2 MPa O_2, 14 h) in liquid phase (pure water and water/tetrachloroethane biphasic batch reactors) and high O_2 pressures (2 MPa) with relatively high yields ($\approx$35–50%).[11,12] However, the use of solid catalysts in furfural oxidation reactions would be a preferable option because of their advantageous catalyst recovery, reutilization, and environmental friendliness. Moreover, the use of milder reaction conditions (atmospheric pressure) would result in less complex and inexpensive catalytic technologies. Higher yields than those reported in the literature (ca. 50%) are required for economically viable large scale operations. In this context, the use of new solid catalysts, as well as a detailed knowledge of their catalytic functionalities and chemical structures, is of outstanding interest for the scientific community.

Supported vanadium oxides are well-known to efficiently catalyze *n*-butane/O_2 reactions to yield maleic anhydride.[13] Previous reports proposed that furan-type intermediates are involved in the butane oxidation reaction mechanism.[14] Hence, supported VO_x structures have been investigated as active and selective catalysts for furfural oxidation to maleic anhydride and furan. Vanadium oxides are commonly deposited onto high-surface area support materials to increase the mechanical strength, number of active sites, and measured reaction rates.

[a] *N. Alonso-Fagúndez, Dr. M. L. Granados, Dr. R. Mariscal, Dr. M. Ojeda*
Group of Sustainable Energy and Chemistry
Institute of Catalysis and Petrochemistry (CSIC)
C/Marie Curie 2. 28049 Madrid (Spain)
Fax: (+34) 915854760
E-mail: manuel.ojeda@csic.es

However, the vanadium surface density, as well as the identity of the support, may significantly affect the electronic properties and catalytic performance of supported vanadium oxide species.[15] Therefore, we have undertaken the first detailed investigation on the effects of VO_x structures in maleic anhydride and/or furan formation rates via selective furfural oxidation reactions.

Results and Discussion

Catalyst preparation

The nomenclature, chemical composition, and measured surface areas of VO_x/Al_2O_3 solids (0.5–25 $at_V\,nm^{-2}$) prepared via incipient wetness impregnation are summarized in Table 1.

Table 1. Nomenclature, nominal chemical composition, and measured surface areas of VO_x/Al_2O_3 solids.

Nomenclature	V density [$at_V\,nm^{-2}$]	V content [wt%]	Surface area [$m^2\,g^{-1}$][a]
Al_2O_3	0.0	0.0	134
0.5 V	0.5	0.6	134
1 V	1.0	1.1	134
2.5 V	2.5	2.7	131
5 V	5.0	5.0	130
8 V	8.0	7.5	131
10 V	10	8.9	123
15 V	15	12.2	104
20 V	20	14.9	96
25 V	25	17.1	90
V_2O_5	–	–	12

[a] Determined from N_2 adsorption–desorption isotherms at 77 K.

Samples are denoted in this work as *x* V, where *x* represents the VO_x surface density ($at_V\,nm^{-2}$). Crystalline V_2O_5 was also prepared as a reference. Thermogravimetric analyses (TGA) in synthetic air of impregnated precursors clearly show two decomposition processes (Figure 1). The first one, occurring at temperatures up to 423 K, is the removal of physisorbed H_2O molecules, whereas the second weight loss at higher temperatures (473–673 K) corresponds to the combustion of vanadyl oxalate species to form CO_2 and H_2O. On the basis of the TGA data we dried the impregnated solids at 393 K for 12 h and subsequently treated these materials in a 21 vol% O_2/He flow at 723 K (heating rate of 0.167 $K\,s^{-1}$) for 3 h to thermally decompose the precursors and form the VO_x/Al_2O_3 catalytic materials.

As shown in Table 1, the incorporation of VO_x species up to 8 $at_V\,nm^{-2}$ does not noticeably modify the measured surface area, which suggests that these VO_x species are uniformly dispersed over the Al_2O_3 support surface. However, for higher VO_x densities (> 8 $at_V\,nm^{-2}$), the surface area decreases monotonically with vanadium content. This could reflect the saturation of the Al_2O_3 surface with the VO_x species (monolayer formation) and the concomitant partial blocking of the support pores, which would result in the decrease of the surface area.

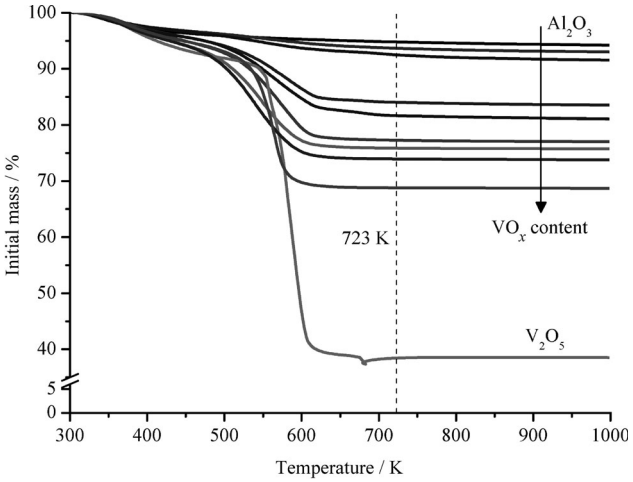

Figure 1. Thermogravimetric analysis (TGA) of VO_x/Al_2O_3 (0–25 $at_V\,nm^{-2}$) precursors in synthetic air at a heating rate of 0.167 $K\,s^{-1}$.

The observed decline suggests an increase in solid density upon addition of vanadia.

Molecular structure of VO_x/Al_2O_3 solids

The X-ray powder diffraction patterns of the VO_x/Al_2O_3 samples (0.5–25 $at_V\,nm^{-2}$), as well as those for γ-Al_2O_3 and V_2O_5 reference materials, are depicted in Figure 2. At relatively low VO_x loadings of 0.5–8 $at_V\,nm^{-2}$, only diffraction lines from the support (γ-Al_2O_3; ICDD# 00-048-0367) are detected, which indicates that well-dispersed VO_x species (monovanadates and polyvanadates, undetectable by XRD) are formed. However, diffraction peaks attributed to bulk V_2O_5 crystals (ICDD# 01-077-2418) become increasingly evident as the VO_x loading is increased. These XRD data suggest that monolayer coverage is exceeded for VO_x/Al_2O_3 solids with vanadium loadings higher than 8 $at_V\,nm^{-2}$, consistent with previous reports,[16–18] and also with the decrease of surface area described above.

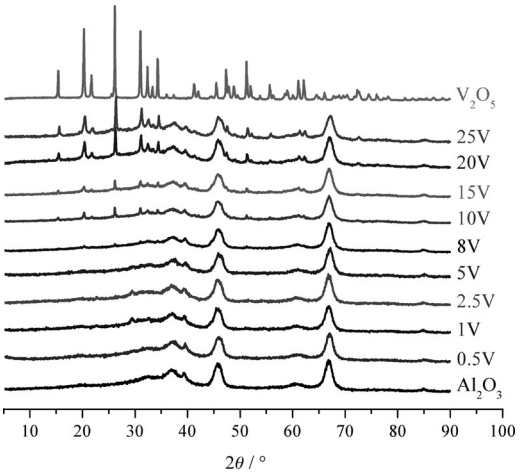

Figure 2. X-ray diffraction patterns of VO_x/Al_2O_3 solids (0–25 $at_V\,nm^{-2}$) treated in ambient air at 773 K (heating rate of 0.167 $K\,s^{-1}$) for 3 h.

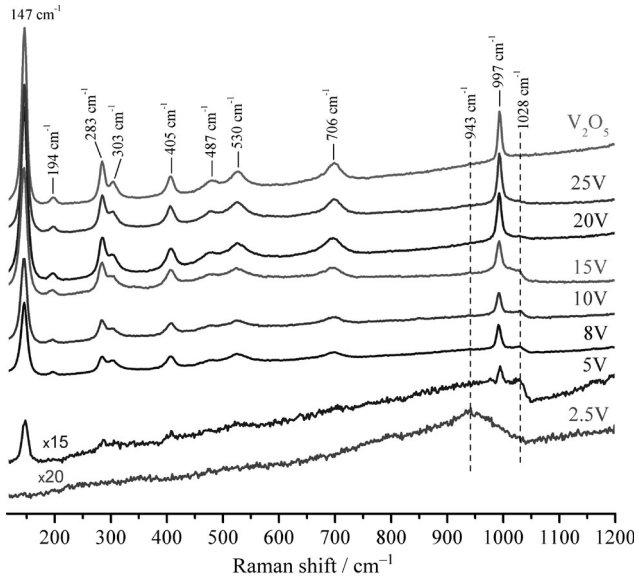

Figure 3. Visible Raman spectra of VO_x/Al_2O_3 solids previously dehydrated in a 21 vol% O_2/N_2 flow at 623 K for 0.25 h.

Raman spectra of dehydrated VO_x/Al_2O_3 samples in synthetic air (Figure 3; 21 vol% O_2/N_2, 623 K, 0.25 h) show a weak band at approximately 1028 cm^{-1} characteristic of isolated monovanadates species (terminal V=O vibrations), and a broad band at approximately 943 cm^{-1} characteristic of polyvanadates species (V–O–V and/or V–O–Al vibrations) for samples with vanadium loading lower than 5 $at_V nm^{-2}$. The presence of bulk V_2O_5 crystallites in samples with higher VO_x loadings are characterized by Raman bands at 997, 706, 530, 487, 405, 303, 283, 194, and 147 cm^{-1}.[18–24] The specific assignment of these Raman bands to V_2O_5 crystallites has been reported in detail previously.[25–27] Visible Raman spectra are more sensitive to highly polymerized VO_x species and crystalline V_2O_5, whereas UV Raman spectroscopy possesses a higher sensitivity to isolated and less polymerized VO_x species.[28] The use of a visible laser ($\lambda_{excitation} = 532$ nm) has caused the spectra of the solids with lower vanadium loadings, in which monovanadates are expected to be present, to be dominated by fluorescence phenomena from the support such that relevant Raman bands are almost indistinguishable. However, visible Raman spectroscopy allows an easier identification of the VO_x loading at which bulk V_2O_5 crystallites originate. The formation of these V_2O_5 crystallites is incipiently observed by Raman spectroscopy for the 5 V sample, whereas they are clearly detected in the 8 V sample. In contrast, only diffraction lines from the γ-Al_2O_3 support are observed in the corresponding XRD patterns (Figure 2). This is not inconsistent, but indicates that relatively small and/or amorphous V_2O_5 agglomerates, which are not detectable by XRD, are present in the 5 V and 8 V samples. Although the Raman spectra of these two samples appear to be dominated by bulk V_2O_5 species, these species exhibit a much larger Raman scattering cross section relative to dispersed monovanadate and polyvanadate structures.[29] Therefore, we conclude that 5 and 8 V samples contain V_2O_5 crystallites, whereas polymerized VO_x species predominate on the Al_2O_3 surface.

In summary we find that at low surface VO_x densities (<2.5 $at_V nm^{-2}$), highly dispersed vanadia species (monovanadates, VO_4) with one short V=O terminal bond and three anchoring V–O–Al bonds are formed. With increasing vanadium surface density (>2.5 $at_V nm^{-2}$), polyvanadates (V–O–V bonds) are expected to form gradually on the catalyst surface. Eventually, bulk V_2O_5 crystallites originate at vanadium contents exceeding monolayer coverage (>8 $at_V nm^{-2}$).

Furfural oxidation with VO_x/Al_2O_3 catalysts

Furfural conversion and selectivity values (molar basis), measured on VO_x/Al_2O_3 (10 $at_V nm^{-2}$, 553 K, 1.6 kPa furfural, 2.5 kPa O_2) with three different pellet sizes (125–300, 300–425, and 425–600 μm) and dilution ratios (SiO_2/catalyst = 10–20, mass basis), are nearly identical (42 ± 2% furfural conversion), indicating that measured rates at these conditions are unaffected by transport artifacts and temperature gradients. Undiluted beds, often used in previous catalytic oxidation studies, may have led to lower reaction rates as a result of mass and heat transfer restrictions.

VO_x/Al_2O_3 solids are active and stable catalysts in furfural oxidation in vapor phase (523–613 K, 1.6 kPa furfural, 2.5 kPa O_2); no significant deactivation is detected during at least 12 h time-on-stream. Main reaction products include maleic anhydride, furan, and CO_2. In addition, other minor compounds, such as 2-furanone, were detected in low concentrations. Based on these reaction products, we propose in Scheme 1

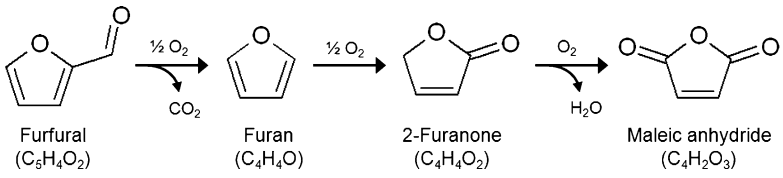

Scheme 1. Proposed reaction pathways for the selective oxidation of furfural to furan and maleic anhydride with VO_x/Al_2O_3 catalysts.

a plausible mechanism for maleic anhydride formation from furfural consistent with the experimental data. Firstly, furfural decarbonylation yields furan , which is the main reaction intermediate. Comparable maleic anhydride formation rates are measured in furfural/O_2 and furan/O_2 with 10 V catalyst at the same temperature (573 K, 6.7 and 3.7 $mmol\,h^{-1}\,g_{cat}^{-1}$ for furfural and furan, respectively). Furan has been also found in appreciable amounts in previous reports dealing with furfural oxidation.[9,10] Subsequently, furan is oxidized stepwise to form 2-furanone (highly reactive, evidenced by the low concentrations detected by gas chromatography) and maleic anhydride. CO_2 and H_2O may be formed through non selective combustion of

furfural, furan, 2-furanone and/or maleic anhydride (not shown in Scheme 1).

The effects of furfural and O_2 pressures on the rates of maleic anhydride and furan formation are reported in Figure 4. We have found that rates increase linearly with both reactant pressures. Identical effects (first-order kinetics) of both furfural and O_2 pressures on maleic anhydride formation rates are reported in literature.[7,8] Mechanistically, this suggests that neither furfural nor O_2 saturates the catalytic surface under our reaction conditions. Moreover, the fact that furfural oxidation to maleic anhydride and furan differ from zero-order kinetics in O_2 implies a different reaction pathway to the so-called Mars–van-Krevelen mechanism; otherwise, no O_2 pressure effects would have been measured (assuming that catalyst re-oxidation is significantly faster than that of furfural). Our data suggests that furfural oxidation on VO_x/Al_2O_3 most likely occurs via a Langmuir–Hinshelwood pathway.

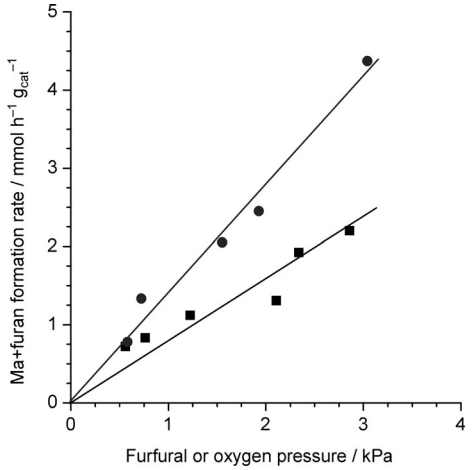

Figure 4. Influence of furfural (●, 0.6–3.1 kPa furfural, 2 kPa O_2) and O_2 (■, 0.6–2.9 kPa O_2, 2 kPa furfural) pressures on measured rates of maleic anhydride and furan formation (10 V catalyst, 553 K).

Some authors previously observed a favorable effect of added H_2O to the furfural/O_2 mixture on the selectivity to maleic anhydride with promoted V-Mo-P catalysts.[9] They claimed that H_2O is adsorbed on the catalyst surface and partially decreases the surface coverage of furfural and maleic anhydride, thereby preventing their condensation, giving much larger products (difficult to desorb and detect by gas chromatography). We have investigated the effects of H_2O addition (0–1.5 kPa) to furfural/O_2 reactants (573 K, 1.6 kPa furfural, 2.5 kPa O_2) and found that neither furfural conversion nor maleic anhydride selectivity are significantly affected. These results are consistent with the hypothesis that neither furfural nor O_2 saturates the catalytic surface under our reaction conditions suggested by the measured first-order kinetics (Figure 4).

The catalytic performance data obtained in furfural oxidation with VO_x/Al_2O_3 catalysts (553 K, 1.6 kPa furfural, 2.5 kPa O_2) is summarized in Figure 5. Results from the bare support and bulk V_2O_5 crystallites are also included for reference. The yield data of CO_2 account exclusively for reactant and product combustion pathways, that is, CO_2 molecules formed via furfural decarbonylation, are not considered in these calculations. Furfural conversion increases gradually with VO_x content, reaches a maximum at 8–10 $at_V nm^{-2}$, and then decreases monotonically. A similar behavior is found for the measured yields of maleic anhydride and furan, which reach values close to 12.5 and 6.5%, respectively, under these non-optimized preliminary reaction conditions. The main side reaction under the oxidative conditions is the polymerization of furfural to generate resins.[12] On heating, furfural undergoes self-condensation reactions to form black cross-linked polymers. The complexity of this polymerization causes key intermediates with high molecular weights and/or low volatilities to be undetectable by gas chromatography (GC). In addition, furfural and furan undergo the Diels–Alder reaction with maleic anhydride to form the corresponding adducts, which are also difficult to be detected by GC.[30] Significant furfural resinification in O_2 atmospheres leading to undetected products (ca. 50%) has also been reported by other researchers.[11,12]

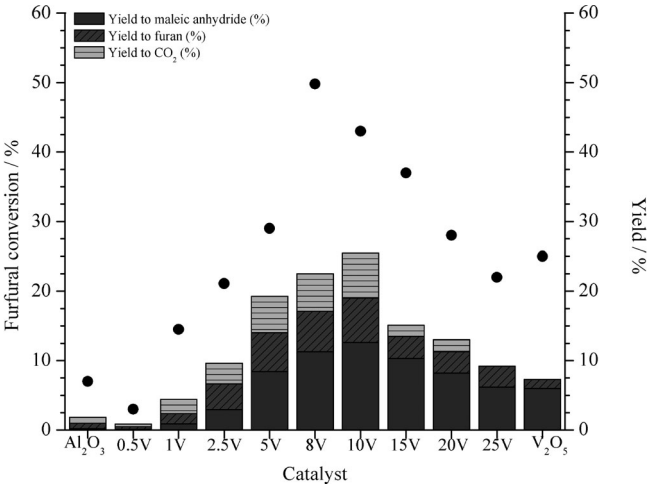

Figure 5. Furfural conversion (●) and yields to maleic anhydride, furan, and CO_2 measured with VO_x/Al_2O_3 catalysts (553 K, 1.6 kPa furfural, 2.5 kPa O_2)

Normalized rates (per vanadium content) of maleic anhydride and furan formation (553 and 573 K, 1.6 kPa furfural, 2.5 kPa O_2) are shown in Figure 6. These normalized rates increase rapidly with vanadium content if VO_x is < 5 $at_V nm^{-2}$; higher contents lead to decreased rates. These data unequivocally suggest that polyvanadate species are intrinsically more active than isolated monovanadates and bulk V_2O_5 crystals in the selective oxidation of furfural to maleic anhydride and furan, as reflected by the highest yields to maleic anhydride and furan found at intermediate vanadium densities (ca. 5 $at_V nm^{-2}$).

Assuming that monovanadates, polyvanadates, and V_2O_5 domains exist exclusively on samples 0.5 V, 2.5 V, and 15 V respectively, the intrinsic activity of these species can be ranked. Thus, polyvanadates exhibit the highest normalized rate (2.70 mmol h^{-1} g-at V^{-1}), whereas monovanadates and V_2O_5 show similar activities (0.89 and 0.70 mmol h^{-1} g-at V^{-1}, respectively).

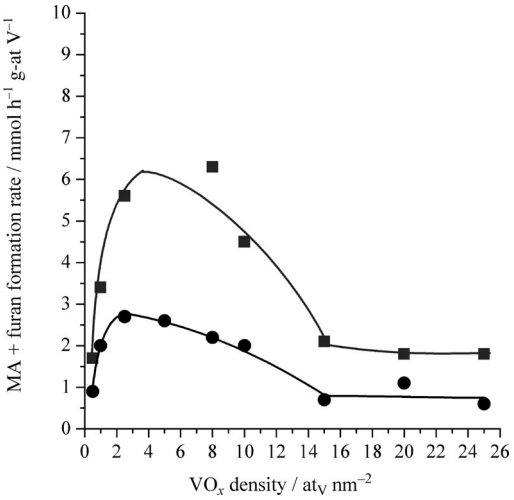

Figure 6. Normalized rates of maleic anhydride (MA) and furan formation (1.6 kPa furfural, 2.5 kPa O_2) at 553 (●) and 573 K (■)

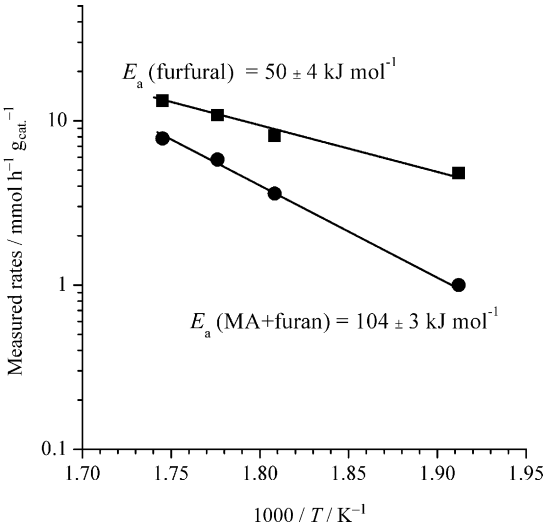

Figure 7. Arrhenius plots for furfural conversion (■) and furan/maleic anhydride (●) formation rates (10 V catalyst, 523–583 K, 1.6 kPa furfural, 2.5 kPa O_2).

The influence of reaction conditions on the rates of maleic anhydride and furan formation have been explored with the catalyst containing 10 at$_V$ nm^{-2} (10 V). This sample has been selected to investigate temperature and O_2 concentration effects on the furfural/O_2 catalytic performance because it has the highest yield (Figure 5). First, the effect of reaction temperature is considered (Table 2). As expected, furfural conversion increases significantly with reaction temperature in the range 523–593 K; higher temperatures do not result in higher furfural conversion values because O_2 is depleted. More importantly, the yield of maleic anhydride and furan reaches a maximum (ca. 56%) at these temperatures and then decreases the maximum selectivity to furan and CO_2 are observed at lower temperatures (553 K); however, the temperature effect on the two latter compounds (furan and CO_2) seems to be less significant than that of maleic anhydride.

Table 2. Effects of reaction temperature on furfural conversion, selectivity, and yield of maleic anhydride, furan, and CO_2 (10 V catalyst, 523–613 K, 1.6 kPa furfural, 2.5 kPa O_2).

T [K]	Conversion [%] furfural	O_2	Selectivity [%] MA	furan	CO_2	Yield[a] [%]
523	26	40	11	8	10	5.5
553	43	46	29	15	15	19
563	58	62	39	14	13	31
573	71	80	48	12	12	43
593	82	99	58	10	10	56
603	87	100	60	6	3	57
613	84	100	52	7	4	50

[a] Maleic anhydride and furan.

Furthermore, we observe that undesired reactions of furfural to undetected products (mainly by resinification) are favored at low temperatures. This is more clearly shown in the corresponding Arrhenius plots (Figure 7) for the rates of furfural conversion and formation of desired products (maleic anhydride and furan). We find a relatively low activation energy for furfural conversion (50 ± 4 kJ mol^{-1}), whereas for the formation of maleic anhydride and furan it is higher (104 ± 3 kJ mol^{-1}), in agreement with previous literature.[8] Thus, the differences in furfural reactivity to degradation products (resinification) or to maleic anhydride/furan are minimized as the reaction temperature is increased. Interestingly, we find that the degradation of furfural to CO_2 is not significantly affected by the reaction temperature.

The effects of O_2 concentration on the catalytic performance of the 10 V catalyst in furfural/O_2 reactions are summarized in Table 3. Increased O_2 pressure exhibits a positive effect on furfural conversion. Moreover, a maximum in maleic anhydride selectivity (ca. 73%) is found at an intermediate O_2 pressure (5.7 kPa) while maintaining 100% furfural conversion. Higher O_2 concentrations lead, however, to less selective furfural oxidations. Therefore, we find here that an appropriate choice of furfural/O_2 reaction conditions (temperature and O_2 concentration) is required to maximize the formation of maleic anhydride. In particular, we have observed that high yields (ca. 73%) are obtained at 593 K and 5.7 kPa O_2 pressure.

Table 3. Effects of O_2 pressure on furfural conversion, selectivity, and yield of maleic anhydride, furan, and CO_2 (10 V catalyst, 593 K, 1.6 kPa furfural, 2.5–7.5 kPa O_2).

P_{O_2} [kPa]	Conversion [%] furfural	O_2	Selectivity [%] MA	furan	CO_2	Yield[a] [%]
2.5	82	99	58	10	10	56
4.4	99	57	70	0	8	69
5.7	100	45	73	0	4	73
6.3	100	32	70	0	5	70
7.5	100	31	58	0	6	58

[a] Maleic anhydride and furan.

Conclusions

We report here a promising route to convert renewable furfural to maleic anhydride (73% yield) by selective gas phase oxidation at 593 K with O_2 (5.7 kPa) by using VO_x/Al_2O_3 (10 $at_V nm^{-2}$) as solid catalyst. Furfural is first oxidized to give furan and 2-furanone as reaction intermediates, which are rapidly transformed into maleic anhydride. The use of lower temperatures and/or O_2 pressures results in the additional formation of furan (maximum 9% yield). The specific structure of the supported vanadium oxides and reaction conditions (temperature and reactants pressures) have an influence on furfural oxidation catalysis. Thus, we have found that Al_2O_3-supported polyvanadates are intrinsically more active than monovanadates (VO_4) and V_2O_5 crystals. This alternative approach to obtain maleic anhydride as well as furan from furfural allows the use of biomass instead of petroleum to synthesize these important chemicals with a variety of industrial applications.

Experimental Section

Catalyst preparation

Supported VO_x/Al_2O_3 solids (0.5–25 $at_V nm^{-2}$) were prepared by incipient wetness impregnation of γ-Al_2O_3 (134 $m^2 g^{-1}$) with aqueous solutions of ammonium metavanadate (NH_4VO_3, Alfa Aesar, 99.0%) at 298 K. Oxalic acid ($C_2H_2O_4$, Alfa Aesar, 99.5%) was added (NH_4VO_3/oxalic acid equal to 0.5 molar ratio) to ensure the complete dissolution of NH_4VO_3 in H_2O. The impregnated solids were dried in ambient air at 393 K for 12 h and subsequently treated in ambient air at 773 K (heating rate of 0.167 $K s^{-1}$). Samples are denoted here as *x*V, where *x* represents the vanadium surface density ($at_V nm^{-2}$; Table 1). Crystalline V_2O_5 was also prepared as a reference following similar synthetic protocols.

Measurement of catalytic activity

Furfural oxidation was performed in a tubular fixed-bed stainless steel reactor. The catalytic bed was prepared by mixing the catalyst ($\approx$0.2 g, 300–425 μm pellet size) with low surface area SiO_2 ($\approx$2 g, $<$1 $m^2 g^{-1}$, 300–425 μm pellet size). First, the catalysts were pretreated in a 21 vol% O_2/He flow (250 $cm^3 min^{-1} g_{cat}^{-1}$) at 623 K for 1 h. The temperature was then decreased to the desired value (523–613 K) and the furfural/O_2 mixture was passed through the catalytic bed. The concentration of furfural (Aldrich, 99%) in the gas phase was controlled by using a double saturator submerged in a thermostatized oil bath and using He as a carrier gas. All transfer lines were kept at 393 K to prevent condensation. Concentrations in the inlet and effluent stream were measured on-line by gas chromatography (Agilent 6820). A capillary column (HP-5, 30 m$\times$0.32 mm$\times$0.25 μm) connected to a flame ionization detector was used to analyze furfural, maleic anhydride, and furan. An HP-PLOT Q (30 m$\times$0.32 mm$\times$0.20 μm) and a molecular sieve (30 m$\times$0.32 mm$\times$0.25 μm) capillary column connected to a thermal conductivity detector was used to determine O_2, N_2 (internal standard), CO, and CO_2 concentrations. Furfural conversion and product selectivity values were calculated by using Equations (1) and (2):

$$\text{Furfural conversion}: \; X_F = \frac{(F)_{in} - (F)_{out}}{(F)_{in}} \qquad (1)$$

where $(F)_{in}$ and $(F)_{out}$ are, respectively, the inlet and outlet furfural molar flowrates.

$$\text{Selectivity of product } i: \; S_i = \frac{(i)_{out}}{(F)_{in} - (F)_{out}} \qquad (2)$$

where $(i)_{out}$ is the outlet molar flow rate of product *i*. CO_2 selectivity calculations do not include furfural decarbonylation pathways.

Furan oxidation rates to maleic anhydride were also determined using similar experimental and analytical protocols.

Characterization techniques

Thermogravimetric analysis (TGA) under controlled atmosphere (synthetic air) was performed by using Mettler Toledo TGA/SDTA 851e equipment at a heating rate of 0.167 $K s^{-1}$ in the 300–1000 K range.

N_2 adsorption–desorption isotherms were recorded at the temperature of liquid nitrogen (77 K) using a Micromeritics TRISTAR 3000 apparatus. Samples were degassed at 393 K for 12 h prior the measurement of the adsorption–desorption isotherms. Surface area values were calculated by using the Brunauer–Emmett–Teller (BET) equation to portions of the isotherms within the $0.05 < P/P_0 < 0.30$ relative pressure range.

Powder X-ray diffraction (XRD) patterns were recorded in $2\theta = 5$–90° range in scan mode (0.02°, 1 s) using an X'Pert Pro PANalytical diffractometer with $CuK_{\alpha 1}$ ($\lambda = 0.154046$ nm) radiation. XRD peak identification was performed by comparison with reference patterns from the International Center for Diffraction Data (ICDD).

Raman spectra (1 cm^{-1} resolution) of dehydrated samples (21 vol% O_2/N_2, 623 K, 0.25 h) were recorded at room temperature with a Renishaw in Via Raman Microscope spectrometer (equipped with a laser beam emitting 532 nm at 100 mW output power).

Acknowledgements

The Spanish Ministry of Science and Innovation (MICINN, ENE-2009-12743-C04-01) and the Autonomous Government of Madrid (CARDENER-CM, S2009/ENE-1660, "Fondo Social Europeo") are gratefully acknowledged for their financial support. M.O. also expresses gratitude to MICINN for the contract within the "Ramón y Cajal" programme (RYC-2010-06067).

Keywords: anhydrides · biomass · gas-phase reactions · oxidation · vanadates

[1] V. V. Guliants, M. A. Carreon in *Catalysis, Vol. 18* (Ed.: J. J. Spivey), The Royal Society of Chemistry, **2005**, pp. 1–45.
[2] G. Centi, F. Trifiro, J. R. Ebner, V. M. Franchetti, *Chem. Rev.* **1988**, *88*, 55–80.
[3] P. N. R. Vennestrøm, C. M. Osmundsen, C. M. Christensen, E. Taarning, *Angew. Chem.* **2011**, *123*, 10686–10694; *Angew. Chem. Int. Ed.* **2011**, *50*, 10502–10509.
[4] A. S. Mamman, J. M. Lee, Y. C. Kim, I. T. Hwang, N. J. Park, Y. K. Hwang, J. S. Chang, J. S. Hwang, *Biofuels Bioprod. Biorefin.* **2008**, *2*, 438–454.
[5] J. P. Lange, *Biofuels Bioprod. Biorefin.* **2007**, *1*, 39–48.
[6] E. R. Nielsen, *Ind. Eng. Chem.* **1949**, *41*, 365–368.
[7] M. S. Murthy, K. Rajamani, *Chem. Eng. Sci.* **1974**, *29*, 601–609.
[8] K. Rajamani, P. Subramanian, M. S. Murthy, *Ind. Eng. Chem. Process Des. Dev.* **1976**, *15*, 232–234.

[9] V. A. Slavinskaya, D. R. Kreile, E. Dzilyuma, D. Sile, *Chem. Heterocycl. Compd.* **1977**, *13*, 710 – 721.
[10] D. R. Kreile, V. A. Slavinskaya, M. V. Shimanskaya, E. Y. Lukevits, *Chem. Heterocycl. Compd.* **1972**, *5*, 429 – 430.
[11] H. Guo, G. Yin, *J. Phys. Chem. C* **2011**, *115*, 17516 – 17522.
[12] S. Shi, H. Guo, G. Yin, *Catal. Commun.* **2011**, *12*, 731 – 733.
[13] I. E. Wachs, J. M. Jehng, G. Deo, B. M. Weckhuysen, V. V. Guliants, J. B. Benziger, S. Sundaresan, *J. Catal.* **1997**, *170*, 75 – 88.
[14] Y. Zhanglin, M. Forissier, R. P. Sneeden, J. C. Vedrine, J. C. Volta, *J. Catal.* **1994**, *145*, 256 – 266.
[15] G. C. Bond, S. F. Tahir, *Appl. Catal.* **1991**, *71*, 1 – 31.
[16] A. Khodakov, B. Olthof, A. T. Bell, E. Iglesia, *J. Catal.* **1999**, *181*, 205 – 216.
[17] M. V. Martínez-Huerta, X. Gao, H. Tian, I. E. Wachs, J. L. G. Fierro, M. A. Bañares, *Catal. Today* **2006**, *118*, 279 – 287.
[18] I. E. Wachs, *Catal. Today* **1996**, *27*, 437 – 455.
[19] M. D. Argyle, K. Chen, E. Iglesia, A. T. Bell, *J. Catal.* **2002**, *208*, 139.
[20] A. Christodoulakis, M. Machli, A. A. Lemonidou, S. Boghosian, *J. Catal.* **2004**, *222*, 293 – 306.
[21] H. Dai, A. T. Bell, E. Iglesia, *J. Catal.* **2004**, *221*, 491 – 499.
[22] D. E. Keller, T. Visser, F. Soulimani, D. C. Koningsberger, B. M. Weckhuysen, *Vib. Spectrosc.* **2007**, *43*, 140 – 151.
[23] C. Zhao, I. E. Wachs, *J. Catal.* **2008**, *257*, 181 – 189.
[24] B. M. Weckhuysen, D. E. Keller, *Catal. Today* **2003**, *78*, 25 – 46.
[25] W. Chen, L. Mai, J. Peng, Q. Xu, Q. Zhu, *J. Solid State Chem.* **2004**, *177*, 377 – 379.
[26] S. H. Lee, H. M. Cheong, M. Seong, P. Liu, C. E. Tracy, A. Mascarenhas, J. R. Pitts, S. K. Deb, *Solid State Ionics* **2003**, *165*, 111 – 116.
[27] G. T. Went, S. T. Oyama, A. T. Bell, *J. Phys. Chem.* **1990**, *94*, 4240 – 4246.
[28] Z. Wu, P. C. Stair, S. Rugmini, S. D. Jackson, *J. Phys. Chem. C* **2007**, *111*, 16460 – 16469.
[29] S. Xie, E. Iglesia, A. T. Bell, *J. Phys. Chem. B* **2001**, *105*, 5144.
[30] H. E. Hoydonckx, W. M. van Rhijn, W. van Rhijn, D. E. de Vos, P. A. Jacobs in *Ullmann's Encyclopedia of Industrial Chemistry*, Wiley-VCH, **2007**.

Received: March 9, 2012
Published online on July 30, 2012

PUBLICACIÓN 2:

Título: *"Gas Phase Oxidation of Furfural to Maleic Anhydride on V_2O_5/γ-Al_2O_3 Catalysts: Reaction Conditions to Slow Down the Deactivation"*

Autores: *Noelia Alonso Fagúndez, Manuel Ojeda, Rafael Mariscal, Jose Luis García Fierro, Manuel López Granados*

Revista: *Journal of Catalysis*

Año: *2017*

Journal of Catalysis 348 (2017) 265–275

Contents lists available at ScienceDirect

Journal of Catalysis

journal homepage: www.elsevier.com/locate/jcat

Gas phase oxidation of furfural to maleic anhydride on V_2O_5/γ-Al_2O_3 catalysts: Reaction conditions to slow down the deactivation

N. Alonso-Fagúndez, M. Ojeda, R. Mariscal, J.L.G. Fierro, M. López Granados *

Institute of Catalysis and Petrochemistry (CSIC), C/Marie Curie, 2, Campus de Cantoblanco, 28049 Madrid, Spain

ARTICLE INFO

Article history:
Received 6 October 2016
Revised 7 December 2016
Accepted 8 December 2016

Keywords:
Furfural
Gas phase oxidation
Maleic anhydride
Vanadium oxide

ABSTRACT

An alumina-supported vanadium oxide catalyst (13.9 wt.% vanadium oxide) has been characterized by different techniques and tested in the gas phase oxidation of furfural. These studies have shown that the catalyst unavoidably deactivates by deposition of maleates and resins over the surface. Full regeneration is accomplished by burning off these deposits at 773 K. The studies have also demonstrated that if the primary contact occurs at temperatures at which furfural conversion is low and then the temperature is increased in a low- to high-temperature mode, intense deposition of maleates and resins takes place and the catalyst is rapidly deactivated. The increase of the temperature does not result in removal of deposits but accelerates the deposition. Under this protocol, the yield of maleic anhydride never exceeded 30%, irrespective of the reaction conditions (temperature and O_2/furfural mole ratio). In contrast, if the catalyst first contacts the reaction mixture at high oxidizing potential, then the rate of maleate and resin deposition is much slower, and so is the deactivation rate, and the catalyst can display a higher yield of maleic anhydride for a longer period of time. A high oxidizing potential can be attained at a high reaction temperature (close to full conversion). A higher oxidizing potential at a given high temperature can be accomplished by increasing the O_2/furfural mole ratio. Thus, for example, first contacting the catalyst at 593 K (full conversion), 1 vol.% of furfural, and O_2/furfural mole ratio = 10, obtained an initial maleic anhydride yield of 68%, and the yield was still greater than 50% after 15 h on stream. On contacting at 573 K with 1 vol.% furfural and 20 vol.% O_2, the maleic anhydride yield was initially close to 75% and was above 60% after 15 h.

1. Introduction

Maleic anhydride (MA) is a commodity chemical with multiple applications: production of unsaturated polyester resins, 1,4-butanediol, vinyl copolymers, curing agents for epoxy resins, lubricant additives, pharmaceuticals, and agrochemicals [1,2]. MA is a petrochemical with market volume currently above 1800 kton/year and is produced primarily by selective oxidation of *n*-butane (the benzene route became obsolete for environmental reasons) [1,2].

Renewable routes based on the oxidation of furfural (FUR) in either gas [3–5] or liquid phase [6–8] have been demonstrated technically by different research groups. Gas phase oxidation offers the advantage of using low-cost air at atmospheric pressure instead of either high-pressure O_2 [6,7] or more expensive H_2O_2 [8,9] required for liquid phase oxidation of furfural.

Recently, other renewable chemical platforms have also been reported to yield MA via oxidation, such as gas phase oxidation of biobutanol, 5-hydromethylfurfural (HMF), and levulinic acid. Thus far, the yield of MA from biobutanol is lower than that obtained from furfural [10]. From HMF an overall yield of MA and maleic acid of 80% has been reported for liquid phase oxidation and at relatively high O_2 pressure (1 MPa) [11]. A high yield of MA (ca. 70%) has also been demonstrated for gas phase oxidation of levulinic acid conducted at atmospheric pressure [12].

However, biobutanol, HMF, and levulinic acid are not yet commercially available on the scale required for replacement of MA production from oil. In contrast, FUR is one of the few commodities currently produced on a large scale from biomass and is perfectly coupled with the production of human food and animal feed, because it is produced from agricultural residues [13]. FUR has been identified as one of the top value-added chemicals derivable from biomass [14] because a number of chemicals are already produced from furfural, and a wide variety of other biofuels, commodities, and fine chemicals can also be derived from it [15,16]. This makes the gas phase oxidation of furfural highly attractive.

* Corresponding author.
E-mail address: mlgranados@icp.csic.es (M. López Granados).

http://dx.doi.org/10.1016/j.jcat.2016.12.005
0021-9517/

Gas phase oxidation of furfural is conducted using catalytic fixed-bed reactors at temperatures ranging from 473 to 673 K and using dilute furfural fed in O_2–N_2 mixtures (below 5 vol.%) and notably short contact times (a few seconds). In addition, different vanadium oxide-based catalysts (V oxide and V–Mo and V–Bi mixed oxides) on a variety of supports (pumice, asbestos, and alumina) have been tested [3–5,17–20]. Unfortunately, most of the reports lack experimental and technical details, and a few of them date back to the first half of the 20th century. Fundamental insight into the reaction mechanism, the effect of different operational variables, and the deactivation processes is still needed.

This work shows that the catalytic properties of V_2O_5/ γ-Al_2O_3 depend on the thermal protocol to which the catalyst has been subjected. Moreover, it has been shown that the effect can be used efficiently to obtain a greater yield of MA. A frequent practice in conducting a reaction is to contact the catalyst with the reaction mixture at an initial temperature at which conversion is low, and eventually increase the temperature to achieve greater conversion and higher yields of the targeted products. The results reported in this work demonstrate that the catalytic properties depend on the thermal history. Substantially higher yields of MA can be attained at full conversion if the catalyst initially contacts the gas reaction mixture at the temperature required for full furfural conversion. In contrast, if the more frequent protocol is adopted, namely, the catalyst first contacts the gas reaction mixture at temperatures giving rise to low conversion (less than 40%) and then the temperature is increased to achieve full conversion, a much lower yield of MA is obtained. A characterization study of the fresh and used catalyst by thermogravimetric analysis (TGA), diffuse reflectance infrared Fourier transform (DRIFT), and X-ray photoelectron spectra (XPS) techniques was conducted, aiming at finding an explanation for this effect.

2. Experimental methods

2.1. Catalyst preparation

In vanadium oxide catalysts supported on Al_2O_3, surface V_2O_5 crystallites have been identified as intrinsically less active for this reaction than well-dispersed VO_x species [5]. The best alumina-supported vanadium oxide catalyst is that with the largest amount of well-dispersed vanadium oxide species. The maximum surface concentration of well-dispersed vanadium oxide species is attained in the range of 8–10 atoms of V per nm^2 of alumina support.

Al_2O_3-supported vanadium oxide with a surface V loading of 8 V atoms nm^{-2} (equivalent to a V_2O_5 loading equivalent of 13.9 wt.%) was prepared via incipient wetness impregnation of γ-Al_2O_3 (134 $m^2\ g^{-1}$) at 298 K using an aqueous solution of ammonium metavanadate (NH_4VO_3, Alfa Aesar, 99.0%). Oxalic acid ($C_2H_2O_4$, Alfa Aesar, 99.5%) was added (NH_4VO_3/oxalic acid molar ratio = 0.5) to ensure the complete dissolution of NH_4VO_3 in H_2O. The impregnated solids were dried in ambient air at 393 K for 12 h and subsequently treated in ambient air at 773 K (heating rate of 0.167 K s^{-1}). This V loading is representative of the range at which the surface concentration of well-dispersed V oxide species is maximized [5]. The catalyst is referred to as 8VA.

2.2. Measurement of catalytic activity

Furfural oxidation was performed in a tubular fixed-bed stainless steel reactor. The catalytic bed (1.5 mL) was prepared by mixing the catalyst (0.2 g, pellet size 300–425 μm) with low surface area SiO_2 (2 g, <1 $m^2\ g^{-1}$, pellet size 300–425 μm). First, the catalysts were pretreated in a 21 vol.% O_2/He flow (250 mL min^{-1} g_{cat}^{-1}) at 623 K for 1 h. Then the temperature was set to the desired value, and the furfural/O_2/N_2 mixture was passed through the catalytic bed (approximately 43 mL/min was always fed, which is equivalent to an overall contact time of 2.1 s or GHSV = 1720 h^{-1}). The concentration of furfural in the gas phase was controlled using a double saturator submerged in a thermostated silicone oil bath at the required temperature. N_2 was used as a carrier gas by bubbling it through the furfural present in the saturators. Heavy oligomers (brownish-colored) are unavoidably present dissolved in furfural due to oligomerization reactions [15]. The feeding of these much less volatile heavy products may cause plugging and deactivation issues, which are prevented by using this bubbling feeding system. The O_2 required to set the gas phase concentration was incorporated into the feed line downstream of the saturator and prior to the reactor. The N_2 and O_2 flows were controlled by mass flow controllers. Furfural was purchased from Aldrich (99%). Concentrations of organics in the inlet and effluent streams were measured online via gas chromatography (Agilent 6820). A capillary column (HP-5, 30 m × 0.32 mm × 0.25 μm) connected to a flame ionization detector was used to analyze furfural and maleic anhydride, and HP-PLOT Q (30 m × 0.32 mm × 0.20 μm) and molecular sieve (30 m × 0.32 mm × 0.25 μm) capillary columns connected to a thermal conductivity detector were used to determine the O_2, N_2 (internal standard), CO, and CO_2 concentrations. All transfer lines were held at 393 K to prevent condensation of water and MA. Furfural conversion is calculated as

$$X_F = \frac{(F)_{in} - (F)_{out}}{(F)_{in}} \quad (1)$$

where $(F)_{in}$ and $(F)_{out}$ are the inlet and outlet furfural molar flow rates, respectively, and MA yield as

$$Y_{MA} = \frac{MA_{out}}{(F)_{in}} \quad (2)$$

where MA_{out} is the outlet molar flow rate of MA.

The CO_2 yield formed by total oxidation of furfural was calculated on a furfural molar basis as

$$Y_{CO_2} = \frac{(CO_2)_{out} - MA_{out}}{5 \times (F)_{in}} \quad (3)$$

where $(CO_2)_{out}$ is the outlet molar flow rate of CO_2 and MA_{out} accounts for the CO_2 released to form MA (formation of a MA molecule implies release of a CO_2 molecule by decarboxylation of furoic acid)

2.3. Catalyst characterization techniques

TGA under a controlled atmosphere (synthetic air) was performed on a Mettler Toledo TGA/SDTA 851e unit at a rate of 0.167 K s^{-1} in the range 300–1000 K.

XPS were acquired with a VG Escalab 200 R spectrometer equipped with a hemispherical electron analyzer and a Mg$K\alpha$ (1253.6 eV) X-ray source. The solids were outgassed at 393 K for 1 h at 10^{-5} mbar to remove water before transfer to the ion-pumped analysis chamber. The O1*s*, V2$p_{3/2}$, C1*s*, and Al2*p* core levels were scanned a sufficient number of times to obtain high signal-to-noise ratios. The static charge of the samples was corrected by referencing the binding energies (BEs) to that of the Al2*p* peak in Al_2O_3 (74.4 eV). The accuracy of the BE was ±0.1 eV. The areas of the peaks were computed by fitting the experimental spectra to Gaussian/Lorentzian curves after background removal (using the Shirley function). Surface atom ratios were calculated from peak area ratios normalized by the corresponding atomic sensitivity factors [21].

DRIFT spectra were obtained with a Nicolet 5700 FT spectrophotometer equipped with an in situ reaction chamber, a dif-

fuse mirror system (Praying Mantis), and a high-sensitivity Hg–Cd–Te cryodetector. Spectra were obtained at a resolution of 4 cm^{-1} with an accumulation of 128 scans. Typically, the finely ground samples (ca. 50 mg) were placed in the cup of the in situ DRIFT reaction chamber, and different gas flows were passed through the catalytic bed in an attempt to mimic the situation in the real fixed-bed catalytic reactor. Furfural (Aldrich, 99%) was fed by flowing N_2 through a saturator at room temperature. The O_2 required to set the gas phase concentration was incorporated into the feed line upstream of the saturator and prior to the DRIFT cell. Mass flow controllers were used to set the N_2 and O_2 flows. The DRIFT spectrum at room temperature for KBr loaded into the cell was used as a background spectrum.

3. Results and discussion

3.1. Catalytic activity

Fig. 1 represents the catalytic behavior of the 8VA catalyst in the temperature range 513–633 K. The catalyst is first contacted with 1% furfural/5% O_2/N_2 mixtures (O_2/furfural molar ratio 5:1) at 513 K, and the reaction temperature is increased stepwise (15 K at each step). At the initial temperature (513 K), the early MA yield is close to 10%, but in less than 2 h, the yield decreases to nearly zero. The furfural conversion is initially close to 50%, but also rapidly decreases to ca. 20%. The carbon dioxide yield remains close to nil throughout the period in which the catalyst is held at 513 K. The lack of carbon balance is ascribed to the formation of heavy organics that cannot be analyzed by GC. It is well known that furfural is highly prone to polymerization, forming furanic resins [15,16]. Most of these products are condensed and stack in/downstream the catalytic bed as a consequence of its high boiling point. As a matter of fact, when the catalyst is under stream for an extended period, both the volume and the weight of the discharged catalytic bed are visibly greater than those initially loaded, indicating that certain products have been formed and retained in the catalytic bed during the course of the reaction. A minor fraction of these heavy products end up retained by the solid catalyst deposited at its surface (as will be shown later by TGA of the used catalyst). The lack of carbon balance is hereafter accounted for by the term "resins." At 513 K, initially the resin yield is close to 35%, but once steady state is reached, it accounts for nearly the entire conversion. A hypothesis as to the chemical nature of these heavy products will be given later, based on the DRIFT results discussed below.

When the temperature was increased, the conversion increased as expected. No deactivation could be observed at the different temperatures. Between 528 and 588 K, the rate of formation of MA and CO_2 increased faster than that of the resins, and consequently, the increase in the yields of MA and CO_2 accounts for a large fraction of the increase in furfural conversion. Beyond 588 K, the yield of resins still increases, but the yield of MA decreases remarkably, because MA becomes overoxidized to CO_2; at 633 K, it is almost fully oxidized to CO_2. Summarizing, there are basically two routes of furfural transformation: furfural resinification and furfural oxidation to form either MA or CO_2. The highest yield of MA (close to 30%) is attained between 588 and 603 K; beyond these temperatures MA is overoxidized.

3.1.1. Effect of O_2/furfural mole ratio

The same procedure was followed with different O_2/furfural molar ratios for two different furfural concentrations (1 and 0.5 vol.% furfural); see Fig. 2 for the 1 vol.% results. (Those from of 0.5 vol.% experiments are in Fig. S1 of the Supplementary Content). Temperature was increased from low to high temperature and kept constant for 10 h. Each datum represents the average for 10 h on stream. Initial transient data were not considered for calculating the average value because the catalyst deactivated rapidly during the first hours. No treatment was carried out between temperature steps, but for each new O_2/furfural ratio the catalyst was calcined under air flow at 773 K for 1 h prior to measurement of the catalytic behavior at the new O_2/furfural mole ratio. It has previously been verified that this calcination step completely regenerated the catalyst.

For experiments conducted with 1 vol.% furfural and for the stoichiometric O_2/furfural mole ratio required to obtain MA (2 mol oxygen per 1 mol furfural), the highest MA yield is 17.3% at 618 K, equivalent to a TOF number of 0.19×10^{-3} s^{-1}. When the O_2 concentration becomes higher, the maximum achieved MA yield is increased. Thus, for the experiment conducted at 1 vol.% furfural and 10 vol.% O_2, the maximum yield of MA was 30.8% at 583 K, equivalent to a TOF number of 0.33×10^{-3} s^{-1}. On the other hand, for all the experiments conducted at 0.5 vol.% furfural (see Fig. S1), the yield of MA is around 22–24%. For this series of experiments, the maximum MA yield was 24% (equivalent to a TOF number of

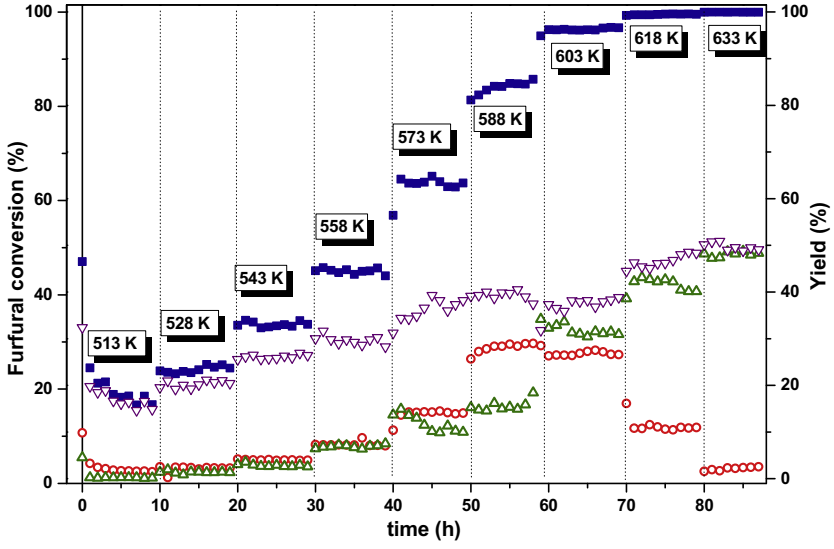

Fig. 1. Catalytic behavior of the 8VA catalyst with increase of the reaction temperature. Reaction conditions: 1 vol.% furfural and 5 vol.% O_2 (O_2/furfural molar ratio = 5), balance N_2. Symbols: (■) furfural conversion; (○) maleic anhydride yield; (△) CO_2 yield; (▽) resin yield.

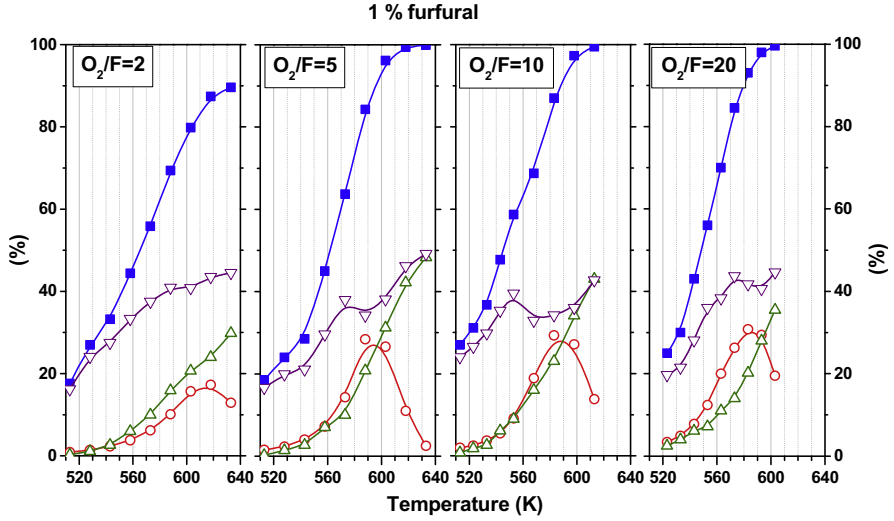

Fig. 2. Catalytic behavior of 8VA catalyst under different O_2/furfural mole ratios and with increasing reaction temperature. Furfural concentration: 1 vol.%. Symbols: (■) furfural conversion; (○) maleic anhydride yield; (△) CO_2 yield; (▽) resin yield.

0.13×10^{-3} s^{-1}) obtained at 588 K and 10 vol.% O_2. A simple inspection of the complete set of results also indicates that the temperatures at which the maximum yields are achieved become smaller with increasing the O_2/furfural mol ratio (618, 588, 583, and 583 K for 1 vol.% furfural and O_2/furfural mol ratio of 2, 5, 10, and 20, respectively) but no remarkable differences in the MA yield exist between the different reaction conditions. The same behavior can be observed for experiments conducted with 0.5 vol.% furfural.

3.1.2. Exploring the effect of O_2/furfural mol ratio and of furfural concentration when the reaction is started at temperatures with complete furfural conversion

A new protocol was adopted to conduct the reaction. Rather than starting at 513 K, the catalyst was directly contacted with the gas reaction mixture at the lowest temperature required to be practically at full conversion (the latter was selected based on the results of the previous protocol used in Figs. 1 and 2). This procedure was applied in practice by flowing only oxygen through the reactor for 1 h at 573 K, and the temperature was subsequently set to the selected value and then the reaction mixture was let through the reactor.

Fig. 3 shows the time evolution of the product yield for three different O_2/furfural molar ratios with a constant concentration of furfural (1 vol.%). The catalyst was regenerated by calcination at 773 K in air for 1 h before proceeding with each new O_2/furfural mol ratio. It was previously verified that the catalyst is completely regenerated by this reactivation protocol.

Throughout the period of time investigated and for all the experiments, the conversion was always above 99.5% (the conversion is therefore not included in the figure) and the CO_2 yield was in the range 10–15%. In contrast, the yield of MA smoothly but continuously diminished, and consequently, the lack of carbon balance indicates that the yield of resins increased. Initially, the MA yield was 60, 70, and 75% for O_2/furfural mol ratios of 5, 10, and 20, respectively, and became 45, 50, and 60% after 15 h on stream. Yield of CO_2 did not change substantially with time on stream, and consequently the yield of resins behaves in the opposite manner to MA and increases with time on stream. It is worth noticing that, no matter what the reaction conditions and the time of reaction, the MA yield was higher than the best MA yield found for the low- to high-temperature protocol experiments shown in Fig. 2 (initiating the reaction at 513 K and then raising the temperature close to full conversion). This demonstrates that when the gas mixture initially contacts the catalyst at full conversion, substantially higher MA yields are obtained. Finally, it must also be borne in mind that when the protocol of Figs. 1 and 2 is used, intense deactivation takes place during the first hour. In contrast, when this high-temperature protocol is used, the deactivation is less severe.

The highest yield of MA is obtained at higher O_2 concentrations and consequently, because the CO_2 yield is not greatly affected by the O_2/furfural ratio, the yield of resins is lower. At an O_2/furfural mol ratio of 20, the MA yield is always greater than 60% throughout the time on stream investigated (the yield of resins is less than 20%). For the last time on stream investigated (14 h), the MA yield was 63.7%, equivalent to a TOF number of 0.69×10^{-3} s^{-1}. The latter values were double those obtained in a low- to high-temperature protocol (30.8% and 0.33×10^{-3} s^{-1}, respectively). It is likely that even higher MA yields could have been obtained at an O_2/furfural ratio higher than 20, although in a hypothetical industrial application, this would have implied the use of air enriched in O_2. It is quite remarkable that increasing the O_2/furfural ratios results in depletion of the resin formation. It is well known that furfural is slowly oligomerized in the presence of O_2 at room temperature [15], and extensive formation of resins would be expected at higher O_2/furfural ratios. This observation indicates that under these conditions, the formation of resins is not thermally driven but catalyzed by surface sites. Formation of resins cannot be prevented, but it can be remarkably minimized at complete conversion using an O_2/furfural ratio $\geq$20 and the protocol used for this set of experiments.

In a new group of experiments (Fig. 4), we explored the effect of changing the O_2/furfural mol ratio but holding the O_2 concentration constant and changing the furfural concentration. In this case, an O_2/furfural mol ratio as high as 40 could be explored without using an O_2 concentration >20 vol.%. The temperatures were again initially set to reach (close to) 100% furfural conversion. The catalyst was calcined at 773 K in air for 1 h prior to every new reaction condition. Similarly to the experiments described in Fig. 3, very high MA yields were obtained for all the experiments and higher O_2/furfural ratios resulted in notably high MA yield and low resin yield. Remarkably, negligible formation of resins was observed for several hours when O_2/furfural = 40 (furfural concentration = 0.25 vol.%). The possibility that the lower formation of resins is due to a dilution effect of furfural when going from high to low furfural conversion can be discarded because this dilution effect was not observed in Fig. 2 or Fig. S1 (no significant differences in the resin yield was observed in the figure when changing from 1 to 0.5 vol.%).

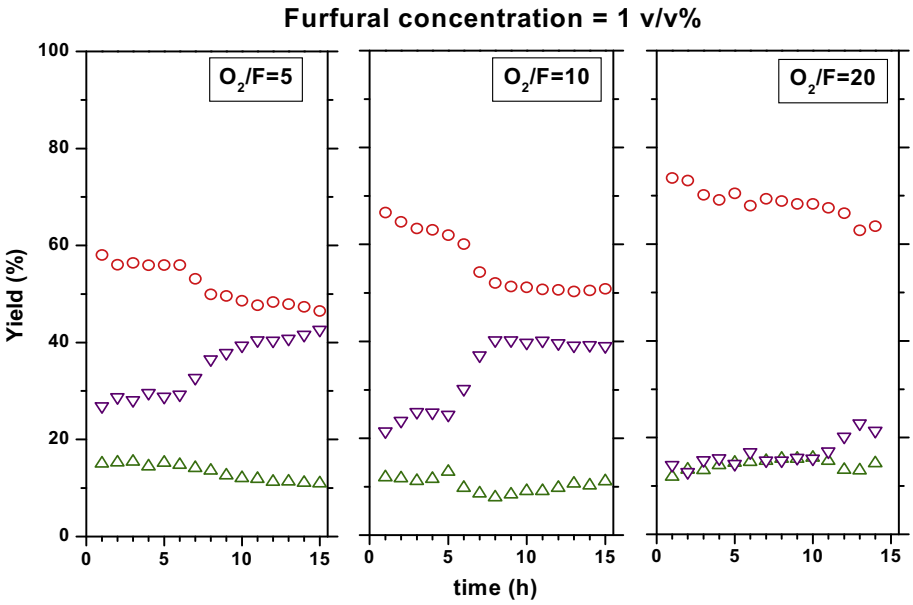

Fig. 3. Time evolution of the catalytic properties when the 8VA catalyst first contacts the reaction mixture at temperatures at which furfural conversion is complete. Constant reaction conditions: furfural concentration = 1 vol.%. Variable reaction conditions: O_2 concentration = 5, 10, and 20 vol.% and reaction temperatures set at 603, 593, and 573 K, respectively. Symbols: (○) maleic anhydride yield; (△) CO_2 yield; (▽) resin yield.

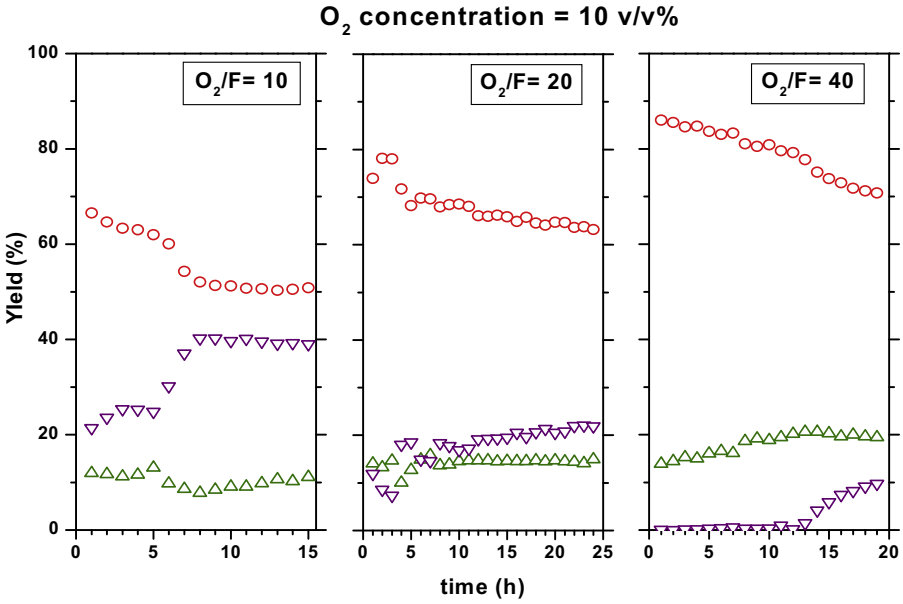

Fig. 4. Time evolution of the catalytic properties when the 8VA catalyst first contacts the reaction mixture at temperatures at which furfural conversion is complete. Constant reaction conditions: O_2 concentration = 10 vol.%. Variable reaction conditions: furfural concentration = 1, 0.5, and 0.25 vol.% and reaction temperatures set at 593, 593, and 583 K, respectively. Symbols: (○) maleic anhydride yield; (△) CO_2 yield; (▽) resin yield.

Deactivation was again evident in all experiments, but the MA yield remained well above that observed in Figs. 1 and 2. Thus, for the experiment conducted at 0.5 vol.% of FUR, 10 vol.% of O_2, and 593 K, the MA yield and TOF number were, respectively, 63.2% and 0.34×10^{-3} s^{-1}, almost three times higher than the maximum MA yield achieved with the same O_2 and FUR concentration but under the low- to high-temperature protocol (which were 24% and 0.13×10^{-3} s^{-1}, respectively). And for the experiment conducted at 0.25 vol.% of FUR, 10 vol.% of O_2, and 583 K, the MA yield was initially close to 86.0% (TOF = 0.23×10^{-3} s^{-1}) and after 20 h on stream it was 70.2% (TOF = 0.19×10^{-3} s^{-1}).

The reason for the improvement of the MA yield when a higher O_2/furfural ratio was used is not clear. The possibility that it is just a thermal effect and due to the lower temperatures needed to conduct the reaction at higher O_2/furfural ratios cannot be fully ruled out. But it seems that this is a secondary effect and that other mechanistic aspects must be involved. Thus, in Fig. 4, it is clearly observed that the same temperature (593 K) was used for O_2/furfural of both 10 and 20 and the highest yield of MA was obtained with O_2/furfural of 20 (for the whole time on stream investigated). We will come back to this point at the end of the Discussion section.

Summarizing, a notably higher yield of MA can be achieved at full furfural conversion if the fresh catalyst is initially contacted with the gas phase reaction mixture at temperatures required for complete furfural conversion. In contrast, a much lower MA yield

is obtained if the low- to high-temperature protocol of increasing the temperature from low to high conversion is followed.

3.2. Characterization of the used catalyst

Fig. 5 shows the TGA and DTG (differential thermal analysis) analysis obtained after the catalyst was in contact with a reaction mixture consisting of 0.5 vol.% furfural and 2.5 vol.% O_2 (balance N_2) at 633 K for 10 h. The catalyst was initially in contact with the reaction mixture at 513 K and temperature increased in the stepwise manner described in Fig. 2. The catalytic bed was downloaded and the grains of the used catalysts (grayish) were easily picked out from the inert silica (white) and from resin particles (black). Two weight loss processes can be observed. The first one, identified in the DTG as peaking at 370 K, is assigned to the removal of physisorbed water. Another weight loss process peaking at 720 K, representing near 5 wt.% of the weight of the used catalyst, corresponds to the burning off of C-containing products. These products are compatible with the formation of heavy hydrocarbons (resins) described when the activity data are discussed. TGA results evidence that part of these resin-like products remain deposited over the catalyst and, moreover, that they can be removed by calcination at 773 K.

Fig. 6 shows the relevant core levels obtained by XPS analysis of fresh and used 8VA catalyst. The used sample corresponds to that studied by TGA. XPS studies were also extended to the effect that calcination at 773 K (regenerated catalyst) has on the chemical surface properties. Table 1 summarizes the XPS data obtained for the different core levels. The Al2*p* core level for Al_2O_3 was chosen as a reference (74.4 eV) to compensate for the charge effects and accurately determine the BEs of the different XPS signals.

Comparison of the intensities of the C1*s* signals of fresh and used catalysts (the adventitious carbon signal in the fresh catalyst arises from ubiquitous organic chemicals contamination present in ambient air) indicates that a remarkable deposition of hydrocarbonaceous species took place over the surface of the catalyst as a consequence of the reaction environment (the XPS C/Al at. ratio went from 0.12 to 1.09, ca. 10 times greater). This observation is in agreement with the conclusions of the TGA results. Besides a very intense peak at 284.8 eV from hydrocarbon-like species, the presence of oxygenated species in the used catalyst is clear in the C1*s* signals at 286.2 and 288.5 eV (C—O and C=O species) [22]. The latter peaks are almost absent in the fresh catalyst, and the signals are so weak that a single peak at an average position of around 287.5 eV was used for a correct simulation of C1*s* in the fresh sample. The presence of these oxygenated hydrocarbons in the used catalyst is also evident in the O1*s* peak at 533.1 eV accompanying the contribution at 531.2 ± 0.1 eV from oxygen in alumina. The former O1*s* core level was not present in the fresh sample and confirms the presence of oxygenated hydrocarbon species [23]. Moreover, the XPS O/V at. ratio of the used catalyst is higher than that of the fresh catalyst (2.39 and 2.10, respectively) as a consequence of the deposition of such oxygenated hydrocarbons. The calcination of the used catalyst at 773 K results in a remarkable decrease in the XPS C/Al and O/Al at. ratios (from 1.09 to 0.17 and from 2.39 to 2.10, respectively) and the disappearance of the O1s signal at 533.1 eV. All previous results prove the substantial removal of these resinlike deposits.

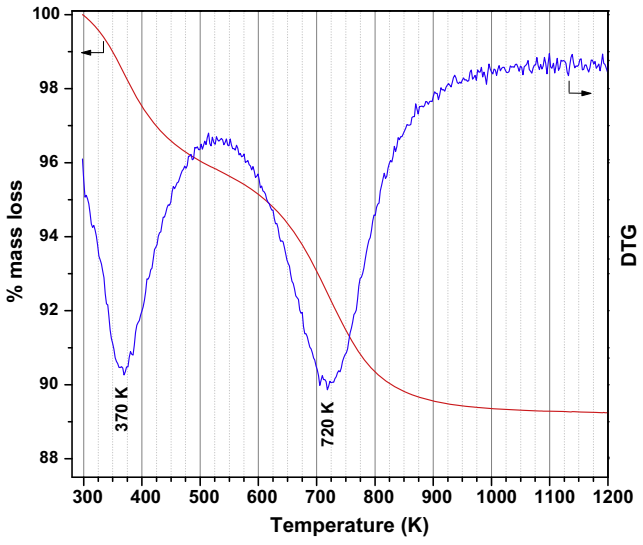

Fig. 5. TGA of the used 8VA catalyst under a 20 vol.% O_2/N_2 flow and a heating ramp of 10 K^{-1} min. (see text for a description of the aging conditions).

For the V analysis, the V2$p_{3/2}$ core level was selected to monitor the vanadium species because the highly intense O1*s* peak overshadows the V2$p_{1/2}$ contribution. In this region of the spectrum, two O1*s* satellite lines from Mg$K\alpha_3$ and Mg$K\alpha_4$ emission lines appear (because a monochromator was not used), which interferes with straightforward analysis of the V2$p_{1/2}$ line [24]. These two satellite lines occurred at 8.4 and 10.2 eV lower BE than the main O1*s* core level (from the Mg$K\alpha_{1,2}$ line) and possessed relative intensities of 0.08 and 0.041, respectively. The deconvolution of this region was accomplished by considering all of the above signals and considering that the area and BE of the V2$p_{1/2}$ core level are one-half and at 7.4 eV higher BE than those of V2$p_{3/2}$.

The BE of the V2$p_{3/2}$ core level for all the samples investigated here is at 517.6 ± 0.1 eV, indicating that V(V) species predominate. The presence of V(IV) or V(III) species cannot be rejected, especially in the used catalyst, but the presence of such reduced V species could not be confirmed. When the overall deconvolution of the O1*s* and V2*p* core levels in this region was conducted, the presence of those species was not required for a statistically good deconvolution, indicating that if they are present, they must be at much lower concentrations than V(V) species. What is more relevant is that the V/Al at. ratios in all samples are above the nominal value, in agreement with the presence of well-dispersed polyvanadate species covering the surface of the support [5]. These ratios for the fresh and used catalysts are very much alike, but the reaction environment and the further calcination of the catalyst at 773 K might affect this dispersion. because the XPS V/Al at. ratio of the calcined used catalyst is slightly less than that of the fresh catalyst (0.17 vs. 0.13).

In situ DRIFT studies conducted under relevant reaction conditions are quite helpful in identifying the hydrocarbonaceous species present over the surface of the catalyst under those conditions [25] and, as shown below, will offer clues to understanding why the thermal protocol is critical for defining the potential yield of MA. Two different experiments were conducted by flowing a reaction mixture containing furfural and O_2 at of 0.25 and 10 vol.%, respectively (O_2/furfural mol ratio = 40), through the catalyst bed placed in the in situ DRIFT cell (these conditions are those used in the last graph of Fig. 4). In a first set of experiments, the catalyst was contacted directly with the gas mixture at 573 K, aiming at simulating a very high furfural conversion. DRIFT spectra were recorded after different times on stream (Fig. 7). Although the contact mode used in the DRIFT cell (flowing through the catalyst bed) is not exactly that taking place in the fixed bed reactor, it is still valid to identify species at the catalyst surface and to draw relevant conclusions. In a second set of experiments, the catalyst initially contacted the gas mixture at 523 K (representative of a situation in which the conversion is low and after 120 min on stream, the temperature is increased to 573 K). All these latter results are collected in Fig. 8. These two experiments are representative of two different reaction mixtures. The

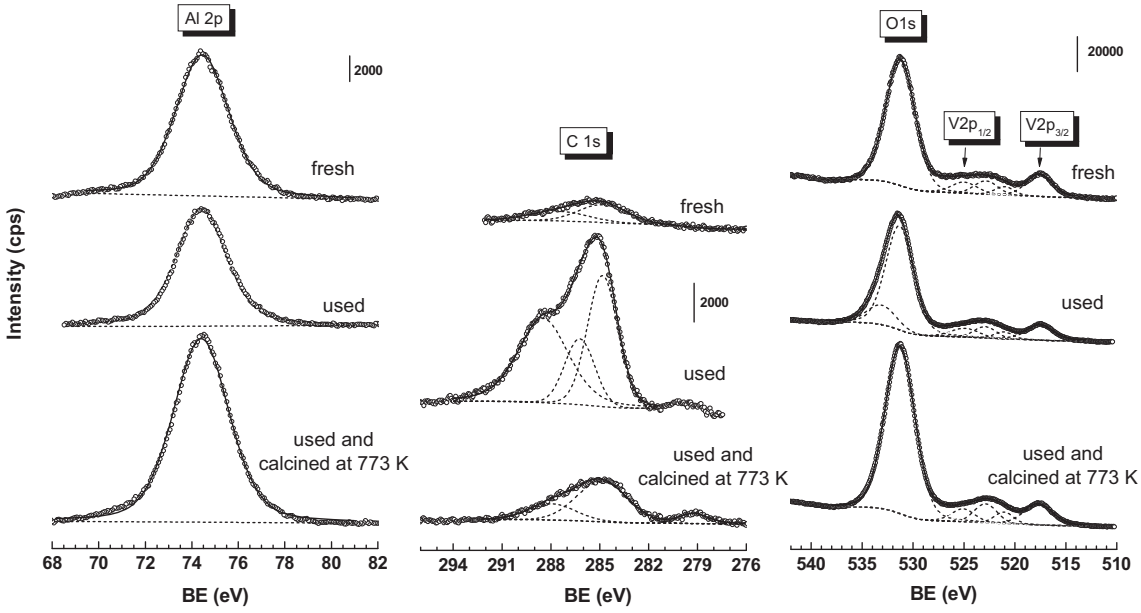

Fig. 6. Al2*p*, C1*s*, O1*s*, and V2*p* core levels of fresh 8VA catalyst, used 8VA catalyst, and used 8VA catalyst after calcination under air at 773 K (regenerated).

Table 1
Summary of XPS results obtained with fresh, used, and fresh and calcined 8VA catalyst.

	BE (eV)[a]				XPS at. ratios[a]		
	$V2p_{3/2}$	Al2p	O1s	C1s	V/Al	O/Al	C/Al
Fresh	517.6	74.4	531.2	284.8 (61%) 287.5 (39%)	0.17 (0.09)[b]	2.10	0.12
Used	517.5	74.4	531.3 (86%) 533.1 (15%)	284.8 (37%) 286.2 (18%) 288.5 (45%)	0.16 (0.09)[b]	2.39	1.09
Used and calcined at 773 K	517.7	74.4	531.3	284.8 (72%) 287.8 (28%)	0.13 (0.09)[b]	2.10	0.17

[a] Value between brackets corresponds to area percentage.
[b] Nominal V/Al at. ratio deduced from the V loading incorporated during the synthesis.

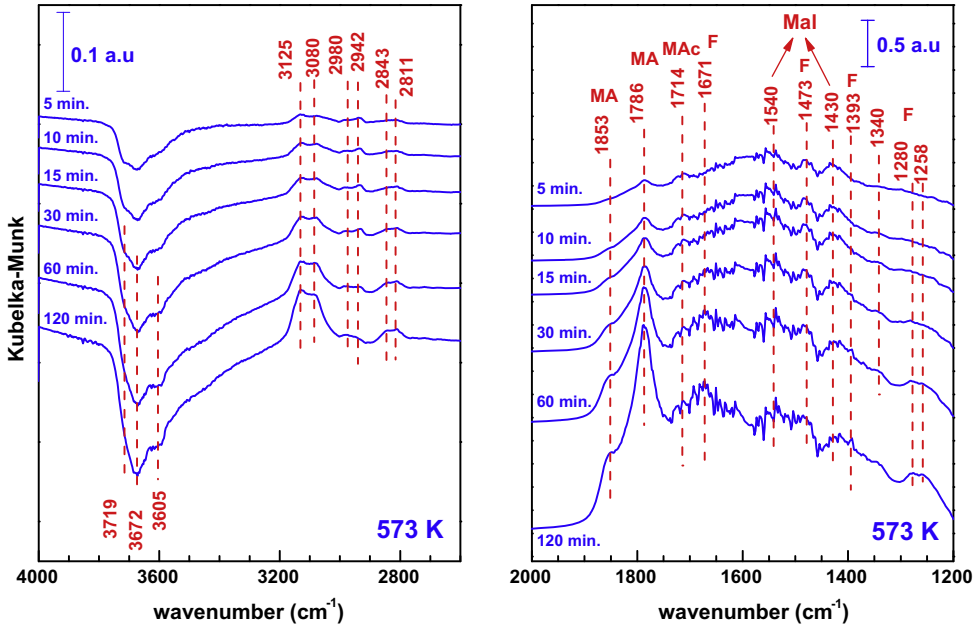

Fig.7. DRIFT spectra obtained under a flow of the furfural/O_2/N_2 mixture (0.25 vol.% furfural, 10 vol.% oxygen, and balance N_2) at 573 K. Fresh 8VA catalyst is contacted directly at 573 K for different times on stream (from top to bottom, t = 5, 10, 15, 30, 60, and 120 min). F, Mal, and MAc stand for furfural, maleates, and malic acid, respectively.

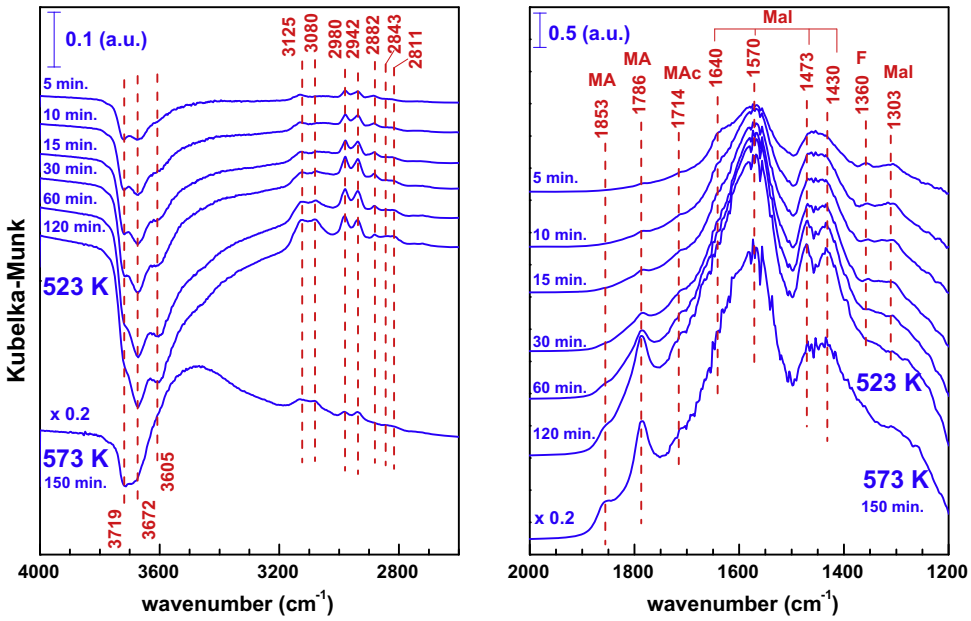

Fig. 8. DRIFT spectra obtained under flow of the furfural/O_2/N_2 mixture with 0.25 vol.% furfural and 10 vol.% oxygen (balance N_2) at 523 and 573 K. Fresh 8VA catalyst is first contacted with the reaction mixture at 523 K for different times on stream, the temperature is subsequently raised at 573 K, and a new spectrum is recorded after 150 min on stream. F, Mal, and MAc stand for furfural, maleates, and malic acid, respectively.

first experiments obviously correspond to those that produce the maximum MA yield, whereas the second series illustrate those used under the protocol of initially contacting the catalyst with reaction conditions at low temperature and then increasing the temperature to get higher conversion. Finally, in both cases, after remaining on stream for a given period of time, the feed was switched to pure N_2 (Figs. S2 and S3). The spectra collected at different times after the switching convey information on the surface species involved in the reaction.

Fig. 7 represents the spectra collected by contacting the fresh catalyst with the reaction mixture directly at 573 K. Each spectrum represented in Fig. 7 is the average obtained during the period of spectrum collection (approximately 4 min) and is the result of subtracting the spectrum of the catalyst before contact with the reaction mixture from that obtained at a given time on stream. Fortunately, IR techniques have been extensively used for the study of the chemisorption of furfural on different metal oxides and for MA production from butane on different vanadium catalysts [26–34]. Those studies are very helpful in identifying the different species present in our DRIFT studies. Table 2 summarizes the assignments of the DRIFT bands and the corresponding references on which the assignment of the band has been previously done.

The DRIFT features in the region 2000–1200 cm^{-1} are first discussed. In this region, relevant C=O, C—H, C=C, and C—C functionalities are IR active. If none of the bands prevail over the rest, the overall spectrum is quite featureless. Indeed, in the first spectrum recorded after 5 min on stream, bands at 1786, 1714, 1473 and 1430 cm^{-1} are observed and superimposed over a notably wide feature that peaks near 1540 cm^{-1}. As time on stream increases, other bands at 1853, 1671, 1393, 1340, 1280- and 1258 cm^{-1} are revealed. The bands at 1540 and 1430 cm^{-1} have been assigned previously to the formation of carboxylate (maleate) species in a bidentate configuration [30,31,34]. The consensus is that the separation between these bands ($\Delta\nu$) (asymmetric and symmetric C—O stretching bands) depends on the type of carboxylate. Thus $\Delta\nu$ of 350–500 cm^{-1} is expected for unidentate carboxylate and 150–180 and 60–100 cm^{-1} for bridging and chelating bidentate carboxylates, respectively [31]. In this case, $\Delta\nu$ is around 110 cm^{-1}, which suggests a chelating bidentate carboxylate, although the bridging configuration cannot be ruled out. The bands at 1853 and 1786 cm^{-1} have been assigned to the presence of maleic anhydride species [30,34]. The remaining bands at 1714, 1671, 1473, 1393, 1340, 1280, and 1258 cm^{-1} can be better assigned by investigating the spectra that appear when furfural and O_2 are removed and only N_2 flushes the catalyst at 573 K. These results are explained and discussed in more details in Supplementary Content (Fig. S2), but summarizing this experiment, we conclude that the bands not assigned in Fig. 7 at 1671, 1473, 1393, and 1280 cm^{-1} arise from furfural and that at 1714 cm^{-1} from maleic acid.

Table 2
Assignments of the DRIFT bands of spectra represented in Figs. 7 and 8.

Wavenumbers (cm^{-1})	Assignment	Reference
3133	C—H stretching in C=C in furfural, MA, MAc and maleate	[26–29]
3125 and 3080	C—H stretching in C=C in furfural, MA, MAc and maleate	This work
2980, 2942, and 2882	C—H stretching in strongly chemisorbed C—C containing species	This work
2843 and 2811	C—H stretching in aldehyde group of furfural	[27,28,35]
1853	C=O symmetric str. in MA	[30,34]
1786	C=O asymmetric stretching in MA	
1724 and 1714	C=O str. in maleic acid	[30]
1693 and 1671	C=O stretching in furfural	[26–28]
1640–1650	C=C stretching in maleic acid or in maleate	[31]
1568	Furfural ring stretching mode	[26–28,32,33]
1540 or 1570	C=O asymmetric stretching in maleate	[30,31,34]
1430 or 1473	C=O symmetric stretching in maleate	
1473 and 1464	Furfural ring stretching modes	[26–28,32,33]
1393 and 1367	Furfural ring stretching modes	[26–28,32,33]
1340 and 1258	Stretching C—C and/or bending C—H vibrations of strongly chemisorbed species	This work
1303	Bending C—H in maleate	[31]
1280 and 1241	In-plane C—H deformation modes in furfural ring	[26–28,32,33]

Fig. S2 also demonstrates that furfural, MA, and maleic acid, which were present at the surface of the catalyst when contacted with the furfural–O_2–N_2 stream, are desorbed by switching to N_2. This indicates that these adsorbed species are involved in the reaction mechanism. In contrast, the bands arising from maleate species (1540 and 1430 cm^{-1}) were absent in the spectra of Fig. S2, and this means that maleate species remain adsorbed at the surface of the catalyst after switching to N_2. Therefore, they are not directly participating in the reaction mechanism. As we will see below, these species are very likely involved in the deactivation of the catalyst.

The bands at 1340 and 1258 cm^{-1} remain elusive. Stretching C—C and bending C—H vibrations frequently appear in this region of the spectrum, and they must arise from other species than MA, maleic acid and furfural, because they remain deposited over surface after switching to N_2.

Returning to Fig. 7, the 4000–2600 cm^{-1} region displays C—H stretching vibrations at 3125, 3080, 2980, 2942, 2843, and 2811 cm^{-1}. The negative peaks at 3719, 3672, and 3605 cm^{-1} indicate that the OH groups of the alumina support are involved in the adsorption of different species. The bands at 3125 and 3080 cm^{-1} arise from H—C stretching vibrations in C=C bonds, and therefore they are compatible with the presence of furfural, MA, and MAc and maleate species. The bands at 2843 and 2811 cm^{-1} are C—H stretching vibrations of the aldehyde group of furfural [27,28,35]. The bands at 2980 and 2942 cm^{-1} are typical of H—C stretching vibrations in saturated C—C bonds, and therefore they indicate the presence of other species different from any of those mentioned thus far, because none of these species possess single C—C bonds. We revisit these two bands later when discussing Fig. 8.

Summarizing the DRIFT studies conducted by contacting the fresh catalyst with the reaction mixture at 573 K, it can be said that maleate species, furfural, MA, and maleic acid are present at the surface of the catalyst. The latter three species are desorbed once furfural and O_2 are removed from the feed. In contrast, the maleate species and other spectator species do not desorb and remain extensively over the surface sites after switching to N_2.

Fig. 8 represents the spectra recorded by contacting the fresh catalyst with the reaction mixture first at 523 K. After 120 min on stream, the temperature was increased to 573 K. The presence of maleic anhydride is evident from the bands at 1853 and 1786 cm^{-1} [30,34] and that of maleic acid from the shoulder at 1714 cm^{-1} [30]. A simple comparison of the intensity of the bands arising from maleate species (now at 1570 and 1430 cm^{-1}) in Figs. 7 and 8 (both at quite the same scale) reveals that these bands in Fig. 8 are much more intense than those in Fig. 7. The different position of the bands with respect to the carboxylate species of Fig. 7 suggests that the new reaction conditions in Fig. 8 have changed the exact nature of the carboxylate species. The maleate bands experience a continuous and intense growth with time on stream, which means that these species are rapidly built up over the surface of the catalyst at 523 K. In contrast, those at 1853 and 1786 cm^{-1} from MA are less intense. The C=C stretching vibration at 1640 cm^{-1} and the C—H bending mode of maleate and maleic anhydride at 1303 cm^{-1} [31], which are difficult to detect in Fig. 7, are now more clearly observed.

Another intense band at 1473 cm^{-1} is clearly detected. Assignment of this band to one of the stretching modes of the furfural ring, although reasonable (in fact earlier assigned in Fig. 7), must be ruled out in this case, because the most intense band from furfural at 1673 cm^{-1} could not be observed. Therefore, this band at 1473 cm^{-1} must be due now to a different species than furfural. As mentioned above, the position of carboxylate bands derived from dicarboxylic acids depends strongly on the type of carboxylate (unidentate, bridging bidentate, and chelating bidentate), but also on the metal oxide on which the carboxylate is adsorbed (for instance on V oxide or alumina) and on the geometry (length and angle defined by the C—O—metal bonds) [31,36]. We tentatively assigned this band to the symmetric stretching band of another carboxylate species; the antisymmetric counterpart should be now overshadowed by the most intense peak at 1570 cm^{-1}. Again, this carboxylate species is very likely a chelating bidentate carboxylate because $\Delta\nu$ is around 100 cm^{-1}. Another assignment is also possible for this 1473 cm^{-1} band, but it will be proposed later when the 4000–2600 cm^{-1} region is discussed. Finally, the weak band at 1360 cm^{-1} that appears only at shorter times on stream (from 0 to 15 min) and is subsequently overshadowed by the most intense bands is assigned to furfural; the remaining bands of furfural were overshadowed by the bands from maleates, MA, and maleic acid.

After 120 min on stream at 523 K, the temperature was increased to 573 K, and the spectrum after 150 min at this temperature is included in Fig. 8. This spectrum is similar to those previously described at 523 K, except that the bands are now much more intense (the intensity was divided by 5 for inclusion in the figure). This result indicates that MA and maleate species are also present at the surface of the catalyst, but with a concentration nearly five times higher than those at 523 K. At this point it is also very important to notice by a simple comparison of the scales of the figures that when the fresh catalyst was directly contacted with furfural/O_2/N_2 mixture at 573 K (Fig. 7), the bands from maleate and MA were much less intense than when it was contacted previously at 523 K and then temperature was raised to 573 K. This indicates that maleates do not decompose on reaching higher temperatures but, on the contrary, the rate of deposition increases.

Examining the region of C—H stretching vibrations, bands at 3125, 3080, 2980, 2942, 2882, 2843, and 2811 cm^{-1} are observed, and their intensity increases with time on stream. The features at 3125 and 3080 cm^{-1} are characteristic of C—H stretching vibrations in C=C bonds and are in principle assigned to furfural. Maleic anhydride or maleic acid cannot be ruled out, either. The presence of furfural also explains the bands at 2843 and 2811 cm^{-1} assigned to the C—H bond of the aldehyde group of furfural [27,28,35]. The negative peaks at 3719, 3672, and 3605 cm^{-1} denote the perturbation of OH groups at the surface of the alumina by the chemisorption of different species.

The features at 2980, 2942, and 2882 cm^{-1} arise from stretching C—H vibrations in saturated C—C bonds. The first two bands were previously observed in Fig. 7, but now they are much more intense (it is likely that the band at 2880 cm^{-1} was too weak to be observed in Fig. 7). As indicated in the discussion of Fig. 7, none of the species so far detected by DRIFT (furfural, maleic anhydride/acid, or maleate) have saturated C—C bonds, and consequently, new species with saturated C—C bonds must be present. It is reasonable to assign these bands to the resin-like products that are produced in the course of the reaction. These bands are more intense in the spectra of Fig. 8 collected at 523 K because, as demonstrated in the catalytic experiments, at this temperature, the production of resins is much faster than under the conditions of Fig. 7, and therefore, the bands from these resin species must also be more intense. In principle, saturated C—C bonds are not present in furfural resins, but in Supplementary Content, a route that explains its formation is proposed. In this context, the presence of CH_2 units in the resin deposits is compatible with the assignment of the band at 1473 cm^{-1} to the C—H scissoring bending mode of CH_2 [37]. The band was attributed above to chelating bidentate carboxylate species. Irrespective of what the real assignment is (both assignments can be correct), the outcome is always the same: maleate and resin deposition.

The spectra after switching to N_2 flow at 573 K were also collected (Fig. S3). The results indicate (a more detailed discussion is given in Supplementary Content) that MA, maleic acid, and furfural are desorbed. No negative band indicating maleate desorption

was detected, even if a much higher concentration of surface maleates had been built up during the time on furfural/O_2/N_2 stream.

Summarizing all the results of the DRIFT figures, it can be concluded that when the fresh catalyst is initially contacted with the reaction mixture at 523 K (a representative temperature for very low conversion), surface maleates and resin-like products are deposited at a considerably higher rate than if contacted directly at 573 K (a representative temperature for close to full conversion). If after being at 523 K the temperature is increased to 573 K, this effect is even more remarkable. In contrast, if the fresh catalyst initially contacts the reaction mixture at a high temperature at which the conversion is close to completion, the deposition rates of maleates and resins significantly decreased.

Maleates and resins must be involved in the deactivation of the route of formation of MA, either by poisoning the active sites or by restricting the access of the reactants (fouling). If the reaction is initiated at low temperature, these species are rapidly deposited and they quickly deactivate the catalyst. Actually, less than 1 h is needed to deeply deactivate the catalyst, as stressed earlier when Fig. 1 was discussed: the conversion at 513 K was initially 50% and the MA yield was 10%, but they decrease rapidly, and after 1 h these values were 20% and 3%, respectively. The increase in the temperature reinforces the deactivation because, as shown by DRIFT, the deposition rate of those species accelerates. Once these products have been deposited, the only way to regain a fresh surface and remove these species is to burn them off under air at 773 K.

An estimation of the activation energy for MA and resin formation conducted using 1 vol.% furfural and 10 vol.% O_2 shows that the value for MA formation is significantly higher than that for resins (98.3 ± 9.9 kJ mol^{-1} vs. 16.2 ± 0.5 kJ mol^{-1}). Similar values were found for other reaction conditions. The difference in the activation energy for MA and resin formation implies that as the temperature increases, the rate of MA formation is enhanced over that of resins. Very likely, this is also the situation for maleates. Consequently, the rapid accumulation of heavy resins and/or maleates over the surface is relatively retarded if the catalyst is contacted with the reaction mixture at high temperatures (at which conversion is full). Then the deactivation rate is less intense and the catalyst can display its full potential to selectively oxidize furfural to MA for a longer time.

In an attempt to gain more evidence of the importance of initially contacting the catalyst with the reaction mixture at either high temperature (close to full conversion) or low temperature (below 40%), an additional experiment was conducted. Instead of using the low- to high-temperature protocol depicted in Figs. 1 and 2 (increasing the temperature from low to high conversion), the catalyst was directly contacted with the gas reaction mixture initially at 593 K. Under these conditions the conversion was close to 100%. Then the temperature was decreased in 20 K steps down to 473 K (low conversion) and then back again to 593 K (full conversion).

In practice, only oxygen was flowed through the reactor for 1 h at 573 K, and then temperature was increased to 593 K. Subsequently, the furfural/N_2 stream was incorporated into the O_2 stream to have 1 vol.% furfural and 10 vol.% O_2 (balance N_2). After 10 h on stream, the temperature was decreased to 493 K in 20 K steps and increased again back to 593 K. The catalyst was on stream 10 h at each temperature. The points represented in the figure are the average catalytic activity for 10 h (steady state), except for the first measurement, conducted at 593 K, during which continuous deactivation was observed. For this result, the value represented was the average for the last 5 h. In the remainder of the results, no sign of deactivation was noted and the values were averaged for the complete 10 h period. Fig. 9 represents the catalytic properties obtained.

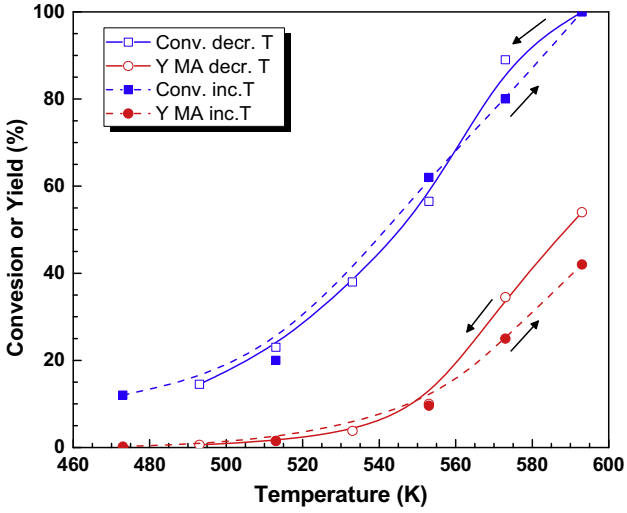

Fig. 9. Hysteresis behavior of the 8VA catalyst evidenced by cycling the temperature from high to low temperatures and back to high temperatures in the range 593–493 K. Reaction conditions: 1 vol.% furfural and 10 vol.% O_2 (balance N_2). Symbols: ■ and □, furfural conversion; ● and ○, maleic anhydride yield; open symbols: decreasing temperature; closed symbols: increasing temperature.

Although the values for conversion of furfural are quite similar for the cooling and heating ramps, the yield of MA shows clear hysteresis behavior and depends on the manner in which the temperature was set. Thus, an average MA yield close to 54% was reached when the catalyst was first contacted with the reaction mixture at 593 K (more precisely, as reported in Fig. 3, an initial yield of 67% MA was obtained at the beginning, but as stated above, the catalyst suffered from progressive deactivation and was near 50% yield after 10 h on stream; the value represented in the figure was an average for the last 5 h). In contrast, when 593 K was reached in the low- to high-temperature mode once the catalyst had been at low temperatures (closed symbol), the MA yield was only ca. 42%. This value is still higher than that presented in Fig. 2, close to 30%, but this again stresses the importance of the selection of the initial temperature of contact with the reaction mixture to define the effective MA yield. The same can be concluded for the yield of MA at 573 K, although the differences in MA yield between the down and up ramps are smaller at this temperature. At 553 K and below, the cooling and heating MA curves overlap. Therefore, the thermal protocol is of paramount importance for higher performance, especially for MA yield and catalyst stability: contacting the fresh catalyst directly with the reaction mixture at temperatures high enough to have furfural conversion close to 100% results in promotion of selective conversion of furfural to MA. Besides, it is worth noticing that once the catalyst contacts the reaction mixture at lower temperatures, it gets deactivated in terms of MA yield. Under the conditions of Fig. 9, this temperature threshold is that giving rise to conversions below 80%, but at other furfural and O_2 concentrations, this threshold may change.

It seems reasonable to assume that contacting at high temperature (full conversion) is not the key parameter for reaching high MA yields, but that the catalyst is subjected to a reaction mixture with high oxidizing potential. A high oxidizing potential can be accomplished at high temperatures, but also by working at high O_2/furfural ratios. A Mars–van Krevelen mechanism is operative in this reaction [19,20]. Consequently, O atoms from the surface vanadium oxide species are involved in the selective oxidation. In the course of the reaction, the V(V) sites are reduced, providing the O atoms to furfural and/or to an intermediate. The capacity of oxidizing the reduced vanadium back to V(V) is essential to heal the O vacancy. The oxidation of the reduced catalyst by gaseous

O_2 is the rate-determining step. In this context, a high oxidizing potential of the reaction mixture means a rapid and efficient restoration of the V(V) sites, the promotion of the selective route to MA, and, consequently, the lessening of the unselective formation of resins and maleates. Deactivation by resin and/or maleate deposition, although unavoidable, is substantially slowed down at high oxidizing potential of the reaction mixture.

4. Conclusions

When V_2O_5/γ-Al_2O_3 catalysts are used in the gas phase oxidation of furfural to MA, the catalyst is unavoidably deactivated by deposition of maleates and/or resinlike products. The regeneration of the catalyst is entirely achieved by burning off these deposits at 773 K.

When the fresh catalyst initially contacts the reaction mixture at low temperature, an intense deposition of maleates and resins takes place and the catalyst is rapidly and deeply deactivated. The increase of the temperature from low to high (from low to full conversion) does not result in removal of deposits, but accelerates their deposition. Consequently, the catalyst remains in a deactivated state, and in practice the yield of MA never exceeds 30%, irrespective of the reaction conditions.

In contrast, when the fresh catalyst initially contacts the reaction mixture at high temperature (close to full conversion), the rate of deposition of maleates and resins is severely slowed down. Consequently, the yield of MA is remarkably enhanced and the deactivation rate is greatly diminished. Under this high-temperature contact protocol, the MA yield can also be further improved by increasing the O_2/furfural mole ratio. Therefore, the high oxidizing potential of the reaction mixture seems in practice the key parameter to favor the selective transformation to MA and to prevent resin and maleate formation and subsequent deactivation.

Acknowledgment

Financial support from the Spanish Ministry of Economy and Competitiveness is gratefully acknowledged Project (CTQ2015-64226-C3-1-R).

Appendix A. Supplementary material

Supplementary data associated with this article can be found, in the online version, at http://dx.doi.org/10.1016/j.jcat.2016.12.005.

References

[1] H.H.K. Lohbeck, W. Fuhrmann, N. Fedtke, Maleic and fumaric acids, in: Ullmann's Encyclopedia of Industrial Chemistry, Weinheim, Germany, 2000, pp. 463–473.
[2] T.R. Felthouse, J.C. Burnett, B. Horrell, M.J. Mummey, Yeong-Jen Kuo, Maleic anhydride, maleic acid and fumaric acid, in: Kirk-Othmer Encyclopedia of Chemical Technology Online, 2001.
[3] D.R. Kreile, V.A. Slavinskaya, M.V. Shimanskaya, E.Y. Lukevits, The reactivity of furan compounds in vapor-phase catalytic oxidation, Chem. Heterocyl. Compd. 5 (1972) 429–430.
[4] V.A. Slavinskaya, D.R. Kreile, É.E. Dzilyuma, D.É. Sile, Incomplete catalytic oxidation of furan compounds (review), Chem. Heterocyl. Compd. 13 (1978) 710–721.
[5] N. Alonso-Fagúndez, M. López Granados, R. Mariscal, M. Ojeda, Selective conversion of furfural to maleic anhydride and furan with VO_x/Al_2O_3 catalysts, ChemSusChem 5 (2012) 1984–1990.
[6] H. Guo, G. Yin, Catalytic aerobic oxidation of renewable furfural with phosphomolybdic acid catalyst: an alternative route to maleic acid, J. Phys. Chem. C 115 (2011) 17516–17522.
[7] S. Shi, H. Guo, G. Yin, Synthesis of maleic acid from renewable resources: Catalytic oxidation of furfural in liquid media with dioxygen, Catal. Commun. 12 (2011) 731–733.
[8] N. Alonso-Fagúndez, V. Laserna, A.C. Alba-Rubio, M. Mengibar, A. Heras, R. Mariscal, M. López, Granados, poly-(styrene sulphonic acid): an acid catalyst from polystyrene waste for reactions of interest in biomass valorization, Catal. Today 34 (2014) 285–294.
[9] N. Alonso-Fagundez, I. Agirrezabal-Telleria, P.L. Arias, J.L.G. Fierro, R. Mariscal, M. López, Granados, Aqueous-phase catalytic oxidation of furfural with H_2O_2: high yield of maleic acid by using titanium silicalite-1, RSC, Adv. 4 (2014) 54960–54972.
[10] G. Pavarelli, J. Velasquez Ochoa, A. Caldarelli, F. Puzzo, F. Cavani, J.L. Dubois, A new process for maleic anhydride synthesis from a renewable building block: the gas-phase oxidehydration of bio-1-butanol, ChemSusChem 8 (2015) 2250–2259.
[11] X. Li, Y. Zhang, The conversion of 5-hydroxymethyl furfural (HMF) to maleic anhydride with vanadium-based heterogeneous catalysts, Green Chem. 18 (2016) 643–647.
[12] A. Chatzidimitriou, J.Q. Bond, Oxidation of levulinic acid for the production of maleic anhydride: breathing new life into biochemicals, Green Chem. 17 (2015) 4367–4376.
[13] A.S. Mamman, J.M. Lee, Y.C. Kim, I.T. Hwang, N.J. Park, Y.K. Hwang, J.S. Chang, J. S. Hwang, Furfural: hemicellulose/xylose-derived biochemical, Biofuels, Bioprod. Biorefin. 2 (2008) 438–454.
[14] J.J. Bozell, G.R. Petersen, Technology development for the production of biobased products from biorefinery carbohydrates – the US Department of Energy's "top 10" revisited, Green Chem. 12 (2010) 539–554.
[15] K.J. Zeitsch, The Chemistry and Technology of Furfural and Its Many By-Products, Sugar Series, vol. 13, Elsevier, The Netherlands, 2000.
[16] R. Mariscal, P. Maireles-Torres, M. Ojeda, I. Sádaba, M. López, Granados, furfural: a renewable and versatile platform molecule for the synthesis of chemicals and fuels, Energy Environ. Sci. 9 (2016) 1144–1189.
[17] E.R. Nielsen, Vapor phase oxidation of furfural, Ind. Eng. Chem. 41 (1949) 365–368.
[18] N.A. Milas, W.L. Walsh, Catalytic oxidations. I. Oxidations in the furan series, J. Am. Chem. Soc. 57 (1935) 1389–1393.
[19] K. Rajamani, P. Subramanian, M.S. Murthy, Kinetics and mechanism of vapor phase oxidation of furfural over tin vanadate catalyst, Ind. Eng. Chem. Prod. Res. Dev. 15 (1976) 232–234.
[20] M.S. Murthy, K. Rajamani, Kinetics of vapour phase oxidation of furfural on vanadium catalyst, Chem. Eng. Sci. 29 (1974) 601–609.
[21] C.D. Wagner, Sensitivity factors for XPS analysis of surface atoms, J. Electron Spectrosc. Relat. Phenom. 32 (1983) 99–102.
[22] S. Biniak, G. Szymański, J. Siedlewski, A. Światkoski, The characterization of activated carbons with oxygen and nitrogen surface groups, Carbon 35 (1997) 1799–1810.
[23] J.L. Figueiredo, M.F.R. Pereira, M.M.A. Freitas, J.J.M. Órfão, Modification of the surface chemistry of activated carbons, Carbon 37 (1999) 1379–1389.
[24] C.L. Pieck, S. Del Val, M. López Granados, M.A. Bañares, J.L.G. Fierro, Bulk and surface structures of V_2O_5/ZrO_2 systems and their relevance for o-xylene oxidation, Langmuir 18 (2002) 2642–2648.
[25] J.V. Ochoa, C. Trevisanut, J.M.M. Millet, G. Busca, F. Cavani, In situ DRIFTS-MS study of the anaerobic oxidation of ethanol over spinel mixed oxides, J. Phys. Chem. C 117 (2013) 23908–23918.
[26] G. Allen, H.J. Bernstein, Internal rotation: VIII. The infrared and Raman spectra of furfural, Can. J. Chem. 3 (1955) 1055–1061.
[27] M. Rogojerov, G. Keresztury, B. Jordanov, Vibrational spectra of partially oriented molecules having two conformers in nematic and isotropic solutions: furfural and 2-chlorobenzaldehyde, Spectrochim. Acta Part A 61 (2005) 1661–1670.
[28] P. Adámek, K. Volka, Z. Ksandr, I. Stibor, Vibrational spectra of 2-furaldehyde, J. Mol. Spectrosc. 47 (1973) 252–267.
[29] P. Mirone, P. Chiorboli, Infrared and Raman spectra and vibrational assignment of maleic anhydride, Spectrochim. Acta 18 (1962) 1425–1432.
[30] Z.Y. Xue, G.L. Schrader, Transient FTIR studies of the reaction pathway for n-butane selective oxidiation over vanadyl pyrophosphate, J. Catal. 184 (1999) 87–104.
[31] K.D. Dobson, A.J. McQuillan, In situ infrared spectroscopic analysis of the adsorption of aliphatic carboxylic acids to TiO_2, ZrO_2, Al_2O_3, and Ta_2O_5 from aqueous solutions, Spectrochim. Acta Part A 55 (1999) 1395–1405.
[32] A.R. Katritzky, J.M. Lagowski, Infrared absorption of heteroaromatic, five-membered, monocyclic nuclei. Part I. 2-monosubstituted furans, J. Chem. Soc. (1959) 657–660.
[33] R. Grigg, J.A. Knight, M.V. Sargent, 1131. Studies in furan chemistry. Part I. The infrared spectra of 2,5-disubstituted furans, J. Chem. Soc. (1965) 6057–6060.
[34] G. Busca, G. Ramis, V. Lorenzelli, On the mechanism of the selective oxidation of C_4 linear hydrocarbons to maleic anhydride: An FT-IR study of the adsorption and oxidation of 1,3-butadiene on vanadia-titania, J. Mol. Catal. 55 (1989) 1–11.
[35] L. Ballester, C. Carrió, J.F. Bertran, Fermi resonance in rotational isomers of furfural, Spectrochim. Acta Part A 28 (1972) 2103–2112.
[36] S.J. Hug, D. Bahnemann, Infrared spectra of oxalate, malonate and succinate adsorbed on the aqueous surface of rutile, anatase and lepidocrocite measured with in situ ATR-FTIR, J. Electron Spectrosc. Relat. Phenom. 150 (2006) 208–219.
[37] P. Taheri, T. Hauffman, J.M.C. Mol, J.R. Flores, F. Hannour, J.H.W. de Wit, H. Terryn, Molecular interactions of electroadsorbed carboxylic acid and succinic anhydride monomers on zinc surfaces, J. Phys. Chem. C 115 (2011) 17054–17067.

Supplementary content of

Gas phase oxidation of furfural to maleic anhydride on V_2O_5/γ-Al_2O_3 catalysts: reaction conditions to slow down the deactivation

N. Alonso-Fagúndez, M. Ojeda, R. Mariscal, J.L.G. Fierro and M. López Granados[1]

Institute of Catalysis and Petrochemistry (CSIC), C/Marie Curie, 2, Campus de Cantoblanco, 28049 Madrid (Spain)

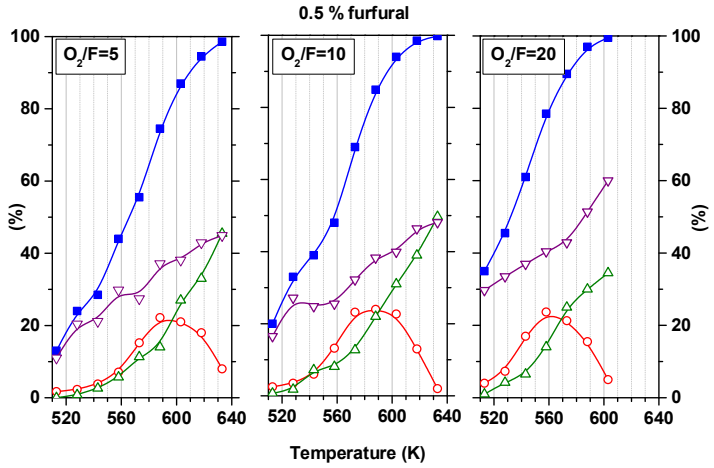

Figure S1. *Catalytic behavior of 8VA catalyst under different O_2/furfural mol ratio and upon increasing the reaction temperature. Furfural conc.: 0.5 vol. %. Symbols: (■) furfural conversion; (○) maleic anhydride yield; (△) CO_2 yield; (▽) resin yield.*

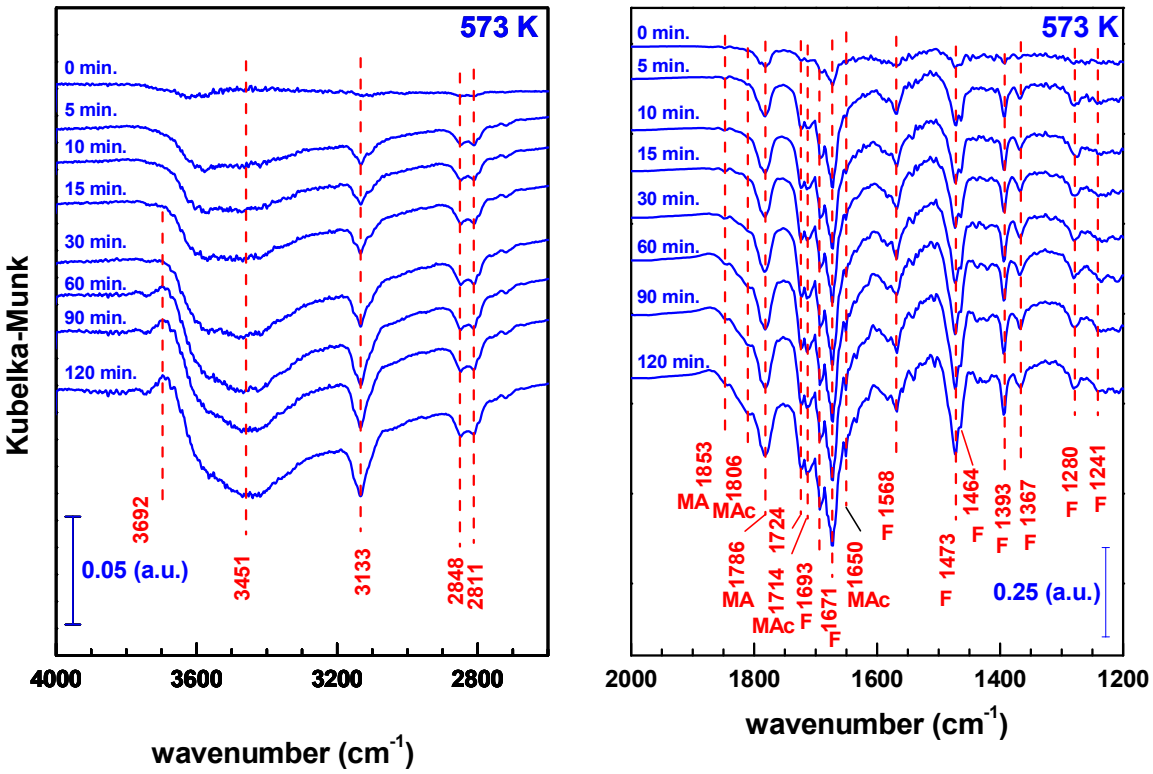

Figure S2. *DRIFT spectra region collected on the 8VA catalyst at 573 K after switching the feed from a 0.25 vol. % furfural/10 vol. % O_2/N_2 stream to only N_2 (from top to bottom: 0, 5, 10, 15, 30, 60, 90 and, 120 min after switching). F and MAc stands for furfural and malic acid, respectively.*

The Figure S2 represents the spectra collected after removing furfural and O_2 from the feed after conducting the experiments of Fig. 7. Each spectrum is the difference between the spectrum at a given time and the last spectrum recorded before switching to only N_2. In practice, Figure S2 shows the bands that disappear upon flushing with N_2 stream, and therefore, this figure conveys information on the species that are desorbed (the bands appear as negative peaks). Starting with the 2000-1200 cm^{-1} region, the bands at 1693 (shoulder), 1671, 1568, 1473, 1464 (shoulder), 1393, 1367, 1280 and 1241 cm^{-1} have been previously assigned to furfural (see Table 2 describing their assignments) whereas those at 1724, 1714 and 1650 cm^{-1} are assigned to maleic acid [30, 31]. The possibility of fumaric acid cannot be ruled out, and hereafter, fumaric acid

is not further mentioned although its presence cannot be discarded when detecting these bands. The bands at 1853 and 1786 cm^{-1} have been previously assigned to maleic anhydride [30, 34]. A weak band (shoulder) at 1806 cm^{-1} indicates the presence of other carbonyl containing species, likely carboxylic acid species.

Therefore, Figure S2 demonstrates that furfural, maleic anhydride and maleic acid were present at the surface of the catalyst when contacted with the furfural-O_2-N_2 stream at 573 K and that they are desorbed when furfural and O_2 are removed from the feed. Consequently, the bands near 1671, 1473, 1393 and 1280 cm^{-1} that were not assigned in Figure 7 arise from furfural and that at 1714 cm^{-1} from maleic acid.

It is worth stressing that although the DRIFT features of furfural, maleic anhydride and maleic acid disappear, those arising from maleate species (1540 and 1430 cm^{-1}) are absent. This observation means that maleate species remain adsorbed at the surface. These species are highly likely to be involved in deactivation of the catalyst

Regarding the 4000-2600 cm^{-1} region, the negative peaks at 3133, 2848 and 2811 cm^{-1} evidence the desorption of products with C=C bonds and aldehydic functions (this desorption also comes with the disappearance of H-bonded OH groups (band at ca. 3451 cm^{-1}) at the expense of formation of isolated OH groups (band near 3692 cm^{-1}). This is in agreement with desorption of furfural, MA and maleic acid mentioned above. Other species with C=C bonds must remain at the surface because no negative band at 3080 cm^{-1} can be observed and because the negative peak at 3133 cm^{-1} does not fully cancel the peak at 3125 cm^{-1} observed in Figure 7 (this can be easily deduced from the intensity bar inserted in Figures 7 and S2).

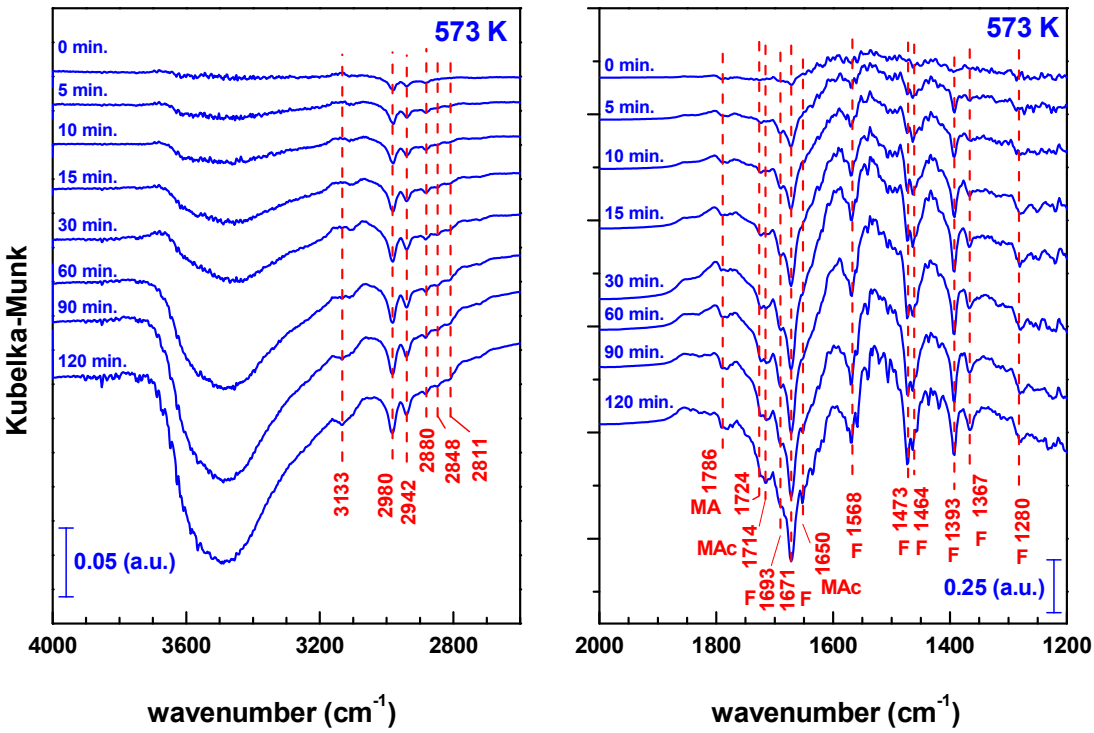

Figure S3. *DRIFT spectra region collected at 573 K after switching the feed from a 0.25 % furfural/10 % O_2/N_2 stream to a N_2 only stream. The fresh 8VA catalyst was contacted with the reaction mixture at 523 K for 120 min and subsequently at 573 K for 150 min. From top to bottom: 0, 5, 10, 15, 30, 60, 90 and 120 min after switching. F and MAc stands for furfural and malic acid, respectively.*

Figure S3 displays the spectra collected after switching to N_2 flow at 573 K, after conducting the experiments of Fig. 8. The spectra are the result of subtracting the spectrum obtained immediately after switching from that obtained at a given time on the N_2 stream. For the 4000-2600 cm^{-1} region, negative peaks at 3133, 2848 and 2811 cm^{-1} are evident as a result of the desorption of furfural (as in the spectra of Figure 8). Moreover, three additional negative features now appear at 2980, 2942 and 2880 cm^{-1}. These bands have been assigned to resin-like species, and therefore, they indicate that resins are partially desorbed or gasified at this temperature after switching to pure N_2. A simple comparison of the intensity of these bands in Figure 8 and S3 demonstrates that

most of the resin-like species remain over the surface after switching to N_2 indicating that resins are very stable at 573 K and that they do not rapidly decompose. Concerning the 2000-1200 cm^{-1} region, the negative features are again compatible with the desorption of maleic anhydride, maleic acid and furfural and again, no negative features from maleate desorption are observed even if a much higher concentration of surface maleates have been built up during the time on furfural/O_2/N_2 stream.

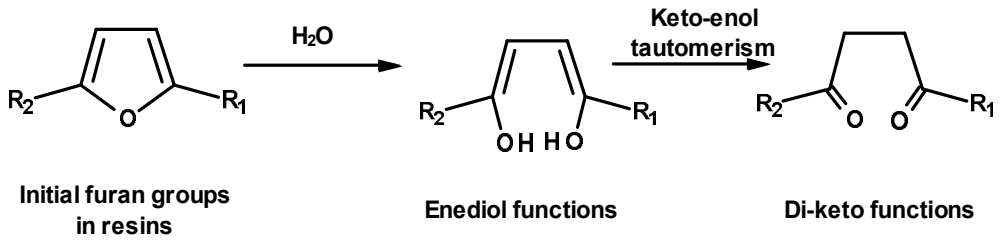

Scheme 1. *Schematic description of the formation of alkyl C-H groups from initial furan resins deposits*

Scheme 1 proposes a sound mechanism that explains the formation of saturated C-C bonds. The high temperatures and the existence of water results in the opening of the furan rings present in the furan resins. The so-formed enediol groups are rapidly converted to the corresponding keto groups by ketoenol tautomerism. The final product exhibits CH_2 groups that account for the DRIFT C-H bands.

PUBLICACIÓN 3:

Título: *"Poly-(Styrene Sulphonic Acid): an Acid Catalyst From Polystyrene Waste for Reactions of Interest in Biomass Valorization"*

Autores: *N. Alonso Fagúndez, V. Laserna, A.C. Alba Rubio, M. Mengibar, A. Heras, R. Mariscal, M. López Granados*

Revista: *Catalysis Today*

Año: *2014*

Catalysis Today 234 (2014) 285–294

Contents lists available at ScienceDirect

Catalysis Today

journal homepage: www.elsevier.com/locate/cattod

Poly-(styrene sulphonic acid): An acid catalyst from polystyrene waste for reactions of interest in biomass valorization

N. Alonso-Fagúndez[a], V. Laserna[a], A.C. Alba-Rubio[a,1], M. Mengibar[b], A. Heras[b], R. Mariscal[a], M. López Granados[a,*]

[a] Institute of Catalysis and Petrochemistry (CSIC), C/Marie Curie, 2, Campus de Cantoblanco, 28049 Madrid, Spain
[b] Department of Physical Chemistry II, Faculty of Pharmacy, Institute of Biofunctional Studies, Complutense University, Po Juan XXIII no. 1, 28040 Madrid, Spain

ARTICLE INFO

Article history:
Received 15 November 2013
Received in revised form
14 December 2013
Accepted 26 January 2014
Available online 7 March 2014

Keywords:
Biodiesel
Xylose
Furfural
Maleic acid
Succinic acid

ABSTRACT

This article reports on the use of poly-(styrene sulphonic acid) (PSSA) prepared by sulphonation of polystryrene waste as catalyst in reactions demanding acid sites. Two different waste derived catalysts (waste to catalyst, WTC) were studied: soluble PSSA (WTC-PSSA) and solid SiO_2-PSSA nanocomposite (WTC-SiO_2-PSSA). The catalytic properties of these waste derived acid catalysts have been explored in three different reactions of interest in biomass valorization: biodiesel synthesis, xylose dehydration to furfural and furfural oxidation to maleic and succinic acids. The results show that both soluble and nanocomposite WTC catalysts present promising catalytic properties. The WTC-PSSA requires ultrafiltration for reutilization whereas the WTC-SiO_2-PSSA can be separated from the reaction mixtures by more usual techniques (centrifugation or conventional filtration). Further research is required for improving the hydrothermal stability of WTC-SiO_2-PSSA in order to substantially reduce the leaching of polymer that takes place during the catalytic runs.

1. Introduction

Important achievements have been already accomplished in the catalytic processing of biomass to biofuels and biobased products. Many breakthroughs are still to come but there is a consensus that many of the processes are being or will be conducted in liquid phase at relatively high reaction temperature and by utilizing polar solvents (like water and/or oxygenated organic solvents). This implies that the catalysts must withstand phenomena like leaching of active species, thermal and chemical deterioration and fouling by deposition of heavy products. Another relevant property of the catalyst must be its low price.

We have demonstrated that commercial poly-(styrene sulphonic acid) (PSSA) can be used as an effective catalyst for biodiesel synthesis and xylose to furfural dehydration [1]. PSSA is essentially not crosslinked (it is a linear macromolecule) and it is soluble in water and in other polar organic solvents. Therefore the transport restrictions of the reactants to (or products from) all the active sites are diminished with respect to other solid porous catalysts. Leaching, thermal degradation and fouling phenomena were not detected during utilization in the reaction mixture and PSSA could be reused for a number of runs in both reactions.

However reutilization of PSSA requires the separation from the reaction medium by ultrafiltration which is not a conventional procedure [1]. To circumvent the ultrafiltration, we have proposed to retain the PSSA polymer by anchoring it on an inorganic solid: SiO_2. Thus the so formed solid organic–inorganic nanocomposite can be separated from the reaction medium by more conventional procedures like filtration or centrifugation. Part of the PSSA polymer chains are still exposed to the liquid phase, solvated by the solvent molecules and in good contact with reactants and products. A sol–gel methodology to hydrolyse and condensate SiO_2 organosilane precursors (TEOS) was used. Organosilane with aminopropyl functionalities (APTES) is also involved (see Scheme 1). Acid PSSA itself catalyzes the hydrolysis and condensation reactions implicated in the sol–gel process. Electrostatic interactions between the amine groups and part of the sulphonic functionalities are responsible of retaining the polymer molecules on SiO_2. The solid catalyst displayed satisfactory hydrothermal stability and could be reutilized in the xylose to furfural reaction [2].

The objective of this article is to explore if PS waste can be effectively sulphonated to form PSSA catalysts and therefore be

* Corresponding author at: Institute of Catalysis and Petrochemsitry (CSIC), Marie Curie, 2, Campus de Cantoblanco, 28049 Madrid, Spain. Tel.: +34 91 585 4937; fax: +34 91 585 47 60.
E-mail address: mlgranados@icp.csic.es (M.L. Granados).
[1] Current address: Department of Chemical and Biological Engineering, University of Wisconsin-Madison, 1415 Engineering Drive, Madison, WI 53706, USA.

0920-5861/$ – see front matter © 2014 Elsevier B.V. All rights reserved.
http://dx.doi.org/10.1016/j.cattod.2014.01.041

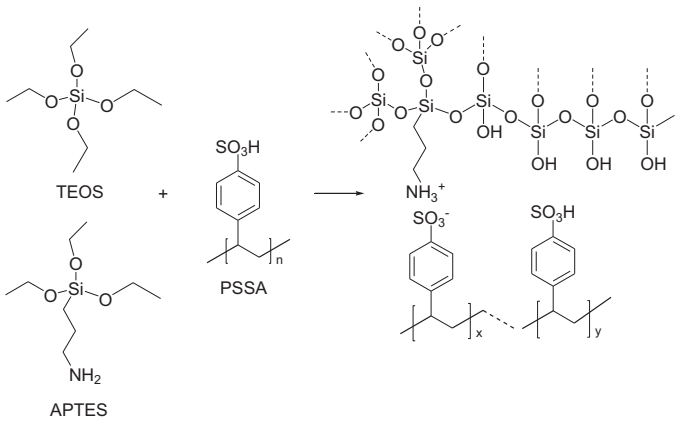

Scheme 1.

reutilized as an acid catalyst (either as soluble catalyst or as a nanocomposite). This reclamation approach represents a cheaper and more environmental friendly route to synthesize acid sulphonic catalysts than preparing catalyst by polymerization of fresh monomers. PS waste is widely accessible as it is present for example in CD covers, yogurt packaging and expanded polystyrene. Reclamation of PS waste by sulphonation has been demonstrated for many different applications [3–10]. To our knowledge PS waste has been never recycled as a catalyst (Waste To Catalyst strategy, WTC). We have to take into account that specific additives (antioxidants, UV stabilizers, fillers, pigments, lubes for processing, rubbers, antistats and flame retardants) are incorporated during the manufacture to render a given end PS product. So we have to verify if these additives may interfere in the sulphonation route or in the usage as catalyst.

In this article, it will be shown that PSSA from PS waste, either as soluble WTC-PSSA or as WTC-SiO_2-nanocomposite, presents promising properties in biodiesel reaction, xylose dehydration to furfural and in the oxidation of furfural with H_2O_2 to obtain succinic (SAc) and maleic acids (MAc). These three reactions cover a wide range of reaction conditions: from mild to relatively high reaction temperatures and both polar solvents or aqueous solutions.

This work is a preliminary exploration and it is not intended to find the best PSSA waste based catalyst but to demonstrate that the concept of preparing acid catalysts from polystyrene waste is possible. Further research must be conducted to find the best synthesis conditions to prepare the optimum catalyst for any of the biomass valorization reaction here tested.

2. Material and methods

2.1. Methodologies to prepare the catalysts

2.1.1. Conditioning of PSSA

Commercial soluble PSSA was supplied by Sigma-Aldrich as aqueous solutions. Raw PSSA (as supplied) was conditioned by using ultrafiltration membranes prior utilization as catalyst. The fraction of PSSA molecules with sizes larger than 5kDa were retained by the ultrafiltration membranes and used for catalytic studies. Further details are given elsewhere [1]. The same ultrafiltration conditioning was applied to the PSSA derived from waste.

.

2.1.2. WTC catalysts by sulphonation of waste PS

With respect to sulphonation of waste polystyrene to obtain waste derived poly-(styrene sulphonic acid) (WTC-PSSA), different sources of waste PS were employed in this work: yoghurt packaging (Y), compact disc covers (CD) and expanded polystyrene (EPS). Two well-known solid–liquid methods of sulphonation were used by changing the sulphonating agents: H_2SO_4 and acetyl sulphate. Both methods are homogeneous routes that require first the dissolution of PS waste in an organic solvent, then the sulphonation of the polymer and finally the recovery of the resulting WTC-PSSA. It was verified that the variables of synthesis selected resulted in sulphonation of the polystyrene chains close to completion. Additives are frequently incorporated to PS to achieve the characteristic properties required for a given end use. The dissolution–precipitation steps involved in the methods here utilized are expected to facilitating the removal of additives since they are organic in nature. Other gas–solid methodologies using gas phase sulphonating agents do not ensure the removal of additives.

The first sulfonation procedure is a modification of the Vink's method [11] that involves concentrated sulphuric acid as sulfonating agent. It will be referred as SUL method (SUL) and, with respect to the other sulphonating method here investigated, it requires a relative larger volume of sulphuric acid (33.3 mL per gram of waste PS). The second method is a modification of the Makowski's method developed by Williams and col. [12] and involves in-situ prepared acetyl sulphate as sulphonating agent. This method can be considered a milder method than previous SUL route since it requires a lower amount of sulphuric acid (2.25 mL per gram of waste PS) to obtain the milder sulphonating acetyl sulfate agent. It will be referred to as ACET method. More details of the procedures are given in the Supplementary Data section. The catalysts were labeled according with the nomenclature (Y or CD or EPS)-(SUL or ACET). Thus, Y-SUL means sulphonation of PS waste from yoghurt packaging by using SUL method.

2.1.3. Sol–gel route to prepare SiO_2-PSSA nanocomposites

The preparation of the sol–gel WTC-SiO_2-PSSA nanocomposites was done as follows. An aqueous mixture of 18 wt% of EPS-ACET prepared as described above, tetraethylorthosilicate (TEOS, Aldrich, 99%) and 3-aminopropyltriethoxysilane (APTES, Fluka, 96%) were introduced in a round-bottom flask as to get at. Si/N = 11 and S/N = 4. A reflux condenser was connected, and the flask was immersed in an oil bath at 348 K with magnetic stirring for 17 h. The solid was centrifuged thereafter. To remove the residual polymer not retained by the SiO_2 particles, the collected solid was washed with H_2O (ca. 200 mL) under stirring, centrifuged again and washed until neutral pH. Next, the collected solid was dried at 383 K overnight. It has been previously verified that these synthesis variables resulted in nanocomposites with improved polymer loading and relative better hydrothermal stability [2]. The nanocomposite so obtained was labeled as WTC-SiO_2-PSSA.

2.2. Characterization of the catalysts

The elemental analysis of the solids was performed on a LECO CHNS-932 analyser. Typically, 1 mg of solid was placed in an Ag crucible and combusted at 1333 K under a pure O_2 atmosphere. The CO_2, H_2O and SO_2 gases were quantified by Fourier transform infrared (FT-IR) spectroscopy while N_2 was determined by differential thermal conductivity.

The amount of sulfonic acid sites of the different catalysts were determined by acid–base titration. A known amount of catalyst (100 mg), previously dried, was put in contact with an aqueous dissolution containing 1 g of NaCl under stirring at 323 K overnight. The aim was to produce the exchange between protons from free sulfonic groups and sodium ions. After that, the solution was filtered by a Varian Captiva™ column (0.45 μm of pore diameter) and the filtrate titrated with a 0.005 M KOH solution (previously standardized with dry potassium acid phthalate). A few drops of an ethanolic solution of phenolphthalein were used to determine the end point.

Thermogravimetric (TGA) analysis of the different solids were conducted with a Mettler Toledo TGA/SDTA 851e instrument upon heating the samples in synthetic air from room temperature to 1073 K at a heating rate of 5 K min^{-1}.

The ^{1}H and ^{13}C NMR spectra were recorded in a AV-400-WB Bruker spectrometer equipped with a triple channel probe. Powder samples were finely grounded and dried for several days at 373 K in an oven and then rapidly transferred to ZrO_2 rotors (4 mm) and capped with Kel-F caps to prevent the hydration of the polymer. Frequencies used were 400.13 and 100.32 MHz for ^{1}H and ^{13}C nuclei, respectively. Samples were spun at 10 kHz. ^{1}H MAS-NMR spectra were obtained after direct irradiation at a spectral width of 35 kHz, a relaxation delay of 5 s and pulses of $\pi/3$ at 40 kHz. The CP-MAS ^{1}H–^{13}C spectra were recorded by using a spectral width of 35 kHz, excitation pulse for ^{1}H of 3.4 μs, contact time of 3.5 ms and a relaxation time of 4 s, with ^{1}H tppm15 decoupling at 80 kHz. The number of scans was 1024 for ^{13}C spectra and 256 for ^{1}H. ^{13}C chemical shift is referred to the adamantane CH2 signal (29.5 ppm) as secondary reference relative to the TMS as a primary reference. ^{1}H is referred to H_2O as a secondary reference (4.77 ppm) relative to TMS as primary reference.

Viscosities were measured at 25 ± 0.05 °C using an Ubbelohde viscometer (purchased from Schott-Gerate, Germany) with the diameter of their capillary of 1.03 mm (Nm. 525.20II). Aqueous solutions of PSSA samples in 0.1 M CH_3COOH/0.2 M NaCl were prepared at concentration about 2.4 g dL^{-1}. All solutions were filtered to 0.45 μm using a cellulose type filter prior to use. Six dilutions with corresponding pure solvent were used, the flow time measurements were repeated three times, and the average values were used to calculate the intrinsic viscosity [η] for that solution.

2.3. Measurements of the catalytic activity

2.3.1. Conversion of vegetable oil to biodiesel

To evaluate the catalytic activity in the production of biodiesel, a pressure glass tube reactor with a capacity of 15 mL from Ace Glass, Inc. was used. A given amount of catalyst (the resulting amount after drying 200 mg at 373 K overnight, aprox. 4 wt% referred to oil mass) was dissolved in 3.5 g of methanol (Scharlau, >99.8% GC, H_2O <0.005%) previously incorporated in the reactor. Once dissolved, 4 g of *Cynara cardunculus oil* (with an acidity index of 9.7%) was added (methanol/oil mol ratio = 24). Then, the reaction started when the reactor was introduced into an oil bath maintained at the selected reaction temperature (403 K). Both the oil in the bath and the reaction mixture were vigorous stirred at 1000 rpm by magnetic stirrers. The reaction was halted by stopping the agitation taking the reactor out the oil bath. The analysis of the reaction mixture was conducted by HPLC (tri, di and monoglycerides (TG, DG, MG), free fatty acids (FFA), fatty acid methyl esters and methanol) and GC for glycerol. Further details of the chromatographic analysis are given in Supplementary data section.

2.3.2. Dehydration of xylose to furfural

To evaluate the catalytic activity in the dehydration of xylose to furfural, 150 mg of D-xylose (SigmaUltra, >99%), a known amount of catalysts, deionised water (1.35 mL) and 3.5 g of organic solvent (cyclopentyl methyl ether (CPME)) (Sigma-Aldrich ≥99.9%), were poured into an Ace Glass pressure glass tube reactor (capacity of 15 mL). The reaction started when the reactor was introduced into an oil bath maintained at the selected reaction temperature (443 K). Both the oil in the bath and the reaction mixture were vigorous stirred at 1000 rpm by a magnetic stirrer. The reaction was halted by stopping the agitation taking the reactor out the oil bath. The concentrations of xylose and furfural in both aqueous and organic phase were determined by HPLC and GC analyses, respectively. Further details of the chromatographic analysis are given in Supplementary data section.

2.3.3. Selective oxidation with H_2O_2 of furfural to C_4 diacids

The reaction was carried out in batchwise mode in a glass flask reactor (50 mL) with three necks for the thermocouple, for a condenser and for sampling through a septum. The second neck was also used for addition of reactants. The required amounts of catalyst and of a 30% H_2O_2/H_2O solution (Sigma-Aldrich) were incorporated into the reactor that was heated to the reaction temperature by immersion in an oil bath. The reaction started when a known amount of a furfural dissolved in water, previously heated at the reaction temperature, was poured into the reactor. This mixture was vigorously agitated at 800 rpm. Different aliquots were sampled at different reaction time to determine the concentration of organic compounds by HPLC and the H_2O_2 concentration by iodometry. Further details of the analyses are given in Supplementary data section.

3. Results and discussion

3.1. WTC-PSSA prepared by sulphonation of polystyrene waste

Two different liquid phase routes to sulphonate PS waste were selected as they are frequently used procedures in sulphonation of commercial PS [11,12]. Gas phase sulphonation is not very effective in extensive sulphonation. Moreover liquid phase routes involve the dissolution and re-precipitation of the polymer molecules that can help in removing additives present in waste PS that may interfere in the final product. Three different types waste PS were selected: CD covers (CD) and yoghurt (Y) and expanded polystyrene packaging (EPS).

The sulphur content of different WTC-PSSA catalysts determined by elemental analysis and the amount of acid sites determined by acid–base titration are summarized in Table 1. Sulphur content and the amount of acid sites are not exactly the same in the different samples. Sulfone bridges and acidic groups other than $–SO_3H$ groups (e.g. –COOH) might have been created by oxidation of the polymer backbone during the sulfonation process and may explain the misfit between these two magnitudes. In the first case the acid content should be smaller than the S content, whereas in the second case acid content should be larger. However we have to consider that the differences between these two parameters are close to experimental error so we can assume that the presence of sulfones and other acidic groups are not very relevant, regardless the type of PS waste and the method of sulfonation

The degree of sulfonation (DS), or the percentage of aromatic rings that are substituted by sulphonic groups, was very high in all the catalysts (Table 1). The values are equivalent to the substitution of ca. 90% of the aromatic rings, which indicates that almost all of the aromatic rings were substituted. The high degree of sulphonation reached for all samples was an objective of the preparation

Table 1
Sulphur content, number of acidic sites and sulfonation degree, referred to g of dry catalyst for different WTC-PSSA catalysts.

	S content [mmol S g_{cat}^{-1}]	Acid sites [mmol H^+ g_{cat}^{-1}]	Degree of sulfonation[a]
Y-SUL	5.2	4.9	93.4
CD-SUL	4.9	4.3	84.5
EPS-SUL	5.0	5.4	87.4
Y-ACET	5.2	5.4	93.4
CD-ACET	5.0	5.4	87.4
EPS-ACET	5.0	5.4	87.4

[a] Calculated from the *S* content determined by chemical analysis according with the equation proposed by Bekri-Abbes [8].

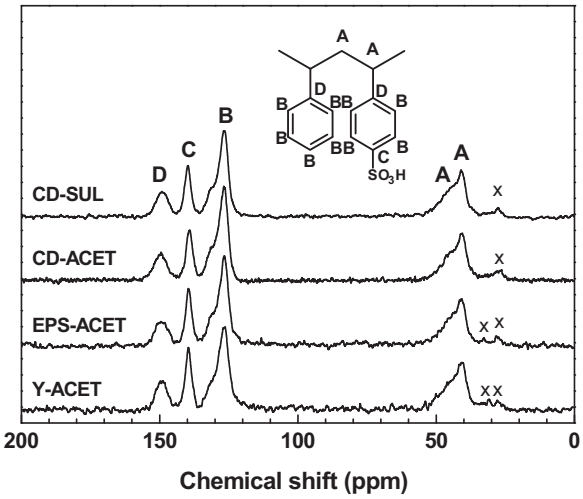

Fig. 1. ^{13}C CP MAS-NMR spectra of different PSSA catalyst prepared from waste PS.

protocols. It is worthy to stress that the ACET method which uses a much lower amount of sulphuric acid results in PSSA catalysts with similar DS than those obtained by SUL method. This indicates that the ACET method should be the preferred option to sulphonate waste polystyrene as it implies the use of less corrosive solutions.

^{13}C CP MAS-NMR spectra for representative waste polystyrene polymers are shown in Fig. 1. All the catalysts showed very similar spectra regardless of the waste or the method of sulfonation. ^{13}C NMR spectra consist of four components; A corresponds to aliphatic carbons and the remaining three signals to aromatic carbons (B, C and D). The assignments of these signals to carbons in the structure of PSSA catalysts are indicated in the inset of the figure and are based on assignment done elsewhere [13–16]. The high intensity of the C signal at ca. 140 ppm in all the ^{13}C spectra, assigned to the C-SO_3 group, confirmed the very high DS of all the catalysts. This in agreement with the DS calculated from the chemical analysis showed in Table 1. Much weaker signals marked with "x" were assigned to side bands of B, C, D signals. No signal from Carbon-containing impurities like additives and/or other copolymers were detected; if they are present must be in minute amounts. Summarizing all the NMR data, it can be concluded that the solids basically consist of sulfonated polystyrene with a quite large degree of sulfonation, in agreement with the chemical analysis.

In the next sections it will be demonstrated that PSSA readily prepared from PS residues (WTC-PSSA catalysts) by using two different sulphonating procedures can be used in biodiesel synthesis, xylose to furfural dehydration and oxidation of furfural to C_4 diacids (maleic and succinic acids). Commercial soluble PSSA (1000 kDa) has been already tested both in the biodiesel reaction and in the dehydration of xylose to furfural [1]. In that work it was demonstrated that PSSA catalyst displayed larger catalytic activity than other non-soluble sulphonic solid catalysts studied (Amberlyst 36, Amberlyst 70 and Nafion-SAC13). The ultrafiltration of the used PSSA catalyst allowed retention and reutilisation of the catalyst for several runs. No significant decay in catalytic activity was observed for the reaction repeats investigated. It was also verified that the S content of the polymer did not substantially decrease when subjected to reaction conditions. These previous results demonstrated that PSSA polyelectrolite is a promising catalyst for biodiesel and xylose to furfural reactions. The catalytic properties of PSSA prepared from PS waste, WTC-PSSA, in biodiesel and xylose to furfural reactions will be reported below.

No previous investigation with commercial PSSA has been conducted yet in the oxidation of furfural, consequently a preliminary study with commercial PSSA aiming at exploring the effect of reaction conditions on catalytic properties is required and is presented in this article beneath. The activity of WTC-PSSA will be also studied and compared with that of commercial PSSA.

3.1.1. *Biodiesel reaction and xylose to furfural reaction*

The kinetics of the reaction of transesterification by using CD-ACET is shown in Fig. 2. No FFA was detected from the very beginning of the reaction indicating that the esterification reaction is very fast under these reaction conditions. Consequently, this study was concentrated on the TG methanolysis. Fig. 1a displays the mol% of the different glycerides (triglycerides (TG), diglycerides (DG), monoglycerides (MG) and glycerol) as a function of time and shows that the catalyst is active. After 400 min almost 80% of the TG has been converted at the reaction conditions indicated in the caption of the figure, mainly to glycerol. Less than 10% of glycerides are still as DG and only traces of MG are detected. The FAME wt% present in the oil phase is displayed in Fig. 2b. We have also represented which fraction of this total FAME wt% arises from TG methanolysis which can be calculated by substraction of the FAME produced by direct esterification of the FFA present in the oil (ca. 10 wt%). Figure clearly demonstrates that a large fraction of oil has been converted to FAME. The activity of the CD-ACET catalyst is similar to that of the commercial PSSA studied elsewhere [1] in that case the FAME wt% released by TG methanolysis after 300 min. was ca. 55%, a conversion very close to that reported in Fig. 2b for CD-ACET (ca. 60%).

The intrinsic activity (per acid sites) (TOF numbers) of the PSSA catalysts prepared from waste polystyrene after 2 h of reaction were calculated. The results (see Fig. SD1 in Supplementary data section) show that the catalysts prepared by the mild sulphonation method (Y-ACET, CD-ACET and EPS-ACET) present a higher intrinsic activity than those prepared by the SUL procedure. Therefore the preferred sulfonation route is ACET method (besides the higher intrinsic activity obtained with this method, a smaller volume of sulphuric acid is required for sulphonating).

The formation of sulphones bridges by condensation of two sulphonic groups may have a considerably impact on the molecular topology of the sulfonated PS backbone. Sulphonation may create intra or intermolecular sulphone linkages that, even at very low concentration, remarkably modify the topology of the resulting PSSA molecule: intercrosslinked molecules result in looped chains and intracrosslinked molecules in associated chains [17]. We hypothesized that the cause behind this difference in activity may be the different conformation or topology of the molecules. In an attempt to see whether ACET samples present different tridimensional conformation than SUL samples, intrinsic viscosities of two representative samples were determined. Intrinsic viscosity of polymers conveys information of the hydrodynamic shape of a polymer and consequently about the topology. The intrinsic viscosity values of CD-ACET and CD-SUL samples were found to be different (0.4781 ± 0.01 and 0.2951 ± 0.01 dL g^{-1}, respectively, see Table SD1 in Supplementary data section). These samples were prepared from the same polymer waste batch, and therefore have the same molecular weight, but by using different sulphonation methodologies. The difference in intrinsic viscosity indicates that hydrodynamic properties (conformational properties) are affected by the procedure of sulphonation. We hypothesized that the formation of sulphones bridges creates different conformation of the ACET samples that are in the origin of their superior catalytic performance.

The catalytic properties in the dehydration of xylose to furfural have been also studied. Fig. 3 shows the conversion of xylose to furfural of two catalysts representative of the synthesis routes: CD-ACET and CD-SUL. In these experiments CPME solvent was used because this solvent presents excellent properties as solvent to improve the selectivity to furfural and it is considered a green

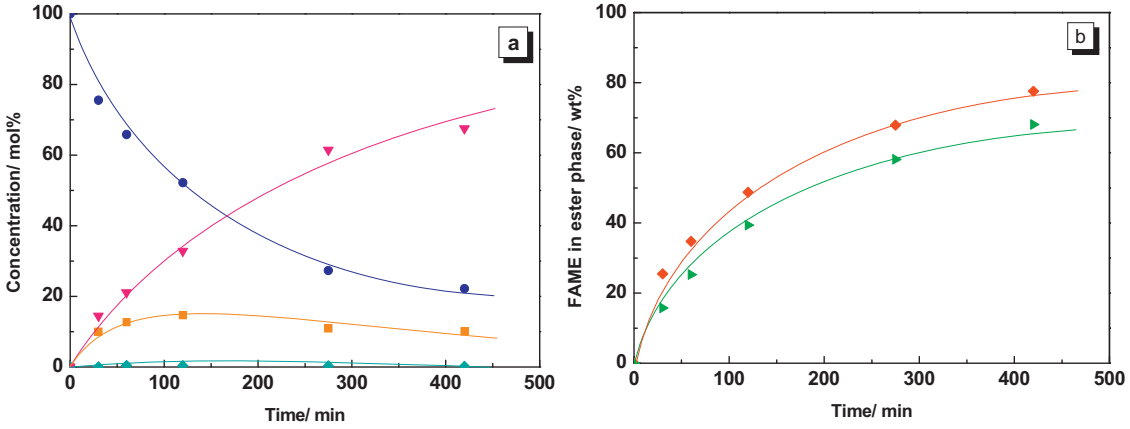

Fig. 2. Kinetics of the transesterification of *Cynara cardunculus* oil with CD-ACET catalyst (403 K, methanol/oil mol ratio = 24, 4 wt% of catalyst referred to the oil weight): (a) (●) TG concentration (mol%), (■) DG concentration (mol%), (▲) MG concentration (mol%), (▼) Glycerol concentration (mol%); (b) (♦) wt% FAME in ester phase and (▶) wt% FAME in ester phase from TG.

solvent [18]. Both catalysts showed to be very active in this reaction. The performance of catalysts was also compared with that of the H_2SO_4 (a homogeneous catalyst). Using the same amounts of acid sites in both cases (ca. 0.11 mmol of $-SO_3H$ groups), quite similar yields to furfural were obtained for all catalysts. It is also remarkable that both WTC-PSSA catalysts (after considering the number of acid sites and water content) displayed quite similar TOF values expressed as μmol of furfural formed·mmol $(SO_3H)^{-1}$ s^{-1} (2.7 for CD-ACET and 2.3 for CD-SUL, respectively). This result contrasts to that observed for TG methanolysis, in that case, ACET samples displayed larger TOF figures than SUL samples. We hypothesized that different molecular topology due to the formation of sulphone bridges was in the origin of the differences in catalyst activity for biodiesel reaction. Considering the smaller size of xylose molecule with respect to triglycerides, it seems likely that topology of the macromolecule is not that critical for xylose conversion. More research is required to fully understand the effect of formation of sulphones in the configuration of the polymer and on the catalytic activity but in any case it is clear that ACET method is preferred due to the lower volume of H_2SO_4 required for the synthesis.

It must be also stressed that both soluble WTC-PSSA catalysts show similar catalytic properties to that of commercial soluble PSSA, both in terms of overall activity (at similar reaction conditions to that used for Fig. 3 results, commercial PSSA xylose conversion after 30 min. of reaction was ca. 30% and furfural yield was ca. 25%) and in terms of μmol of furfural formed·mmol $(SO_3H)^{-1}$ s^{-1} for commercial PSSA TOF value was close to 0.5.

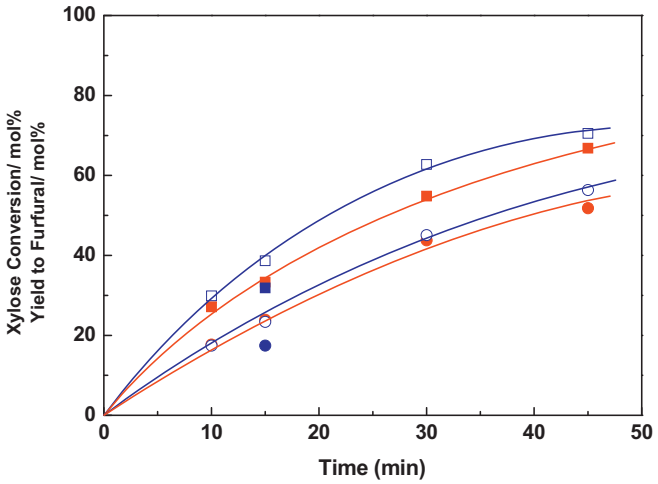

Fig. 3. Kinetics of xylose dehydration to furfural: (■ , ■) xylose conversion (mol%) and (● , ●)yield to furfural (mol%) for CD-ACET and CD-SUL, respectively (xylose/catalyst wt ratio = 6); (□) xylose conversion (mol%) and (○)yield to furfural (mol%) for H_2SO_4 (xylose/catalyst wt ratio = 14). Reaction conditions: 150 mg of D-xylose, 1.5 mL of deionized water and 3.5 g of CPME, 443 K, 1000 rpm.

3.1.2. *Liquid phase oxidation of furfural to C_4 diacids with H_2O_2*

The main products of furfural oxidation by aqueous H_2O_2 are maleic acid (MAc) and succinic acid (SAc). These two C4 diacids are very relevant as they are currently oil-derived chemicals (from butane or benzene oxidation) with important industrial applications. MAc or its derivative maleic anhydride finds applications as agrochemicals, pharmaceuticals, unsaturated polyesters resins, vinyl copolymers, lubricants, etc. [19,20]. On the other hand SAc is used in the synthesis of pharmaceutical, food additives, agrochemicals, cooling and deicing compounds, γ-butyrolactone, butanediol, tetrahydrofuran, pyrrolidones and succinimides [21]. It is worthy to mention that both acids can be readily converted into each other, actually SAc is currently obtained from MAc and the latter, although directly obtained from butane, could be also obtained by dehydrogenation of SAc [21].

Other products as 2(5*H*)-furanone, 2(3*H*)-furanone, 5-hydroxyfuran-2(5*H*)-one and fumaric acid (FAc) are also formed but in a less extent (see Scheme 2). The reaction starts by the Baeyer–Villiger oxidation of the aldehyde to the corresponding formiate ester of 2-hydroxyfuran, which is hydrolyzed in the presence of the acid catalyst to the corresponding formic acid and alcohol (see Scheme SD1 of Supplementary data section). Therefore formic acid is also a major product of the reaction. Moreover malic acid was also detected since it is an oxidation product of either MAc and FAc. Minor amounts of furoic acid was also observed and formed by direct oxidation of aldehydic group of furfural.

A number of acid catalysts have been tested by Ebitani et al. [22–24] who demonstrated that the acids in which a sulphonic group is attached to a tolyl group (*p*-toluensulphonic acid and Amberlyst-15) presented the best yields among those studied. They hypothesized that an interaction between the π-electrons of the furfural ring and the tolyl group are relevant for the reaction. These results encouraged us to test the performance of commercial PSSA in this reaction because tolyl moieties and sulphonic groups are also present in the PSSA.

Fig. 4 shows the catalytic activity results obtained with commercial PSSA at different catalyst loadings (yield is in furfural molar basis). Formic acid is formed by two different routes: Baeyer–Villiger oxidation and deeper oxidation of the organic

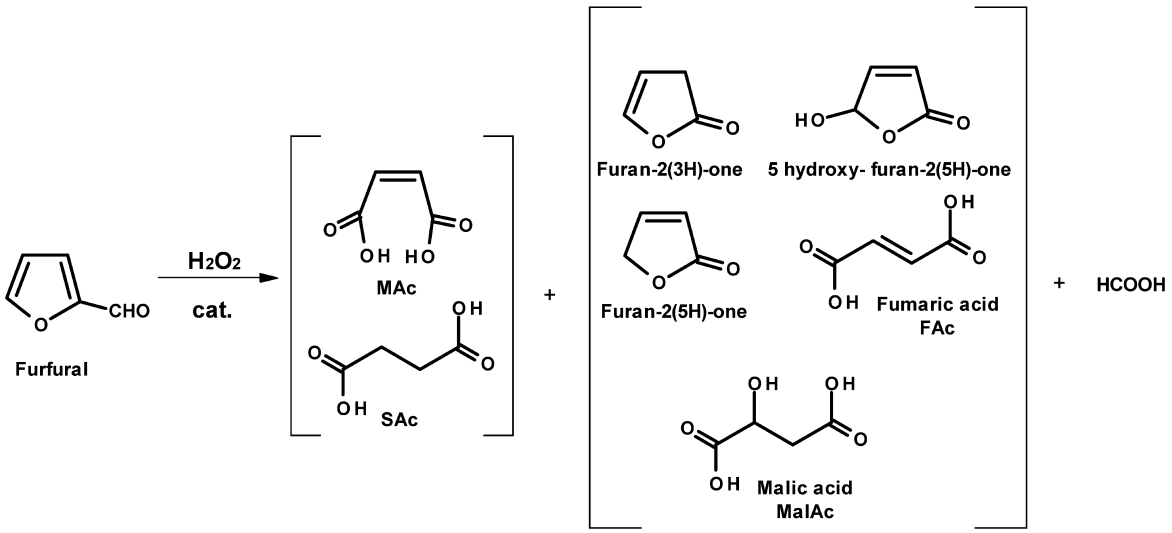

Scheme 2.

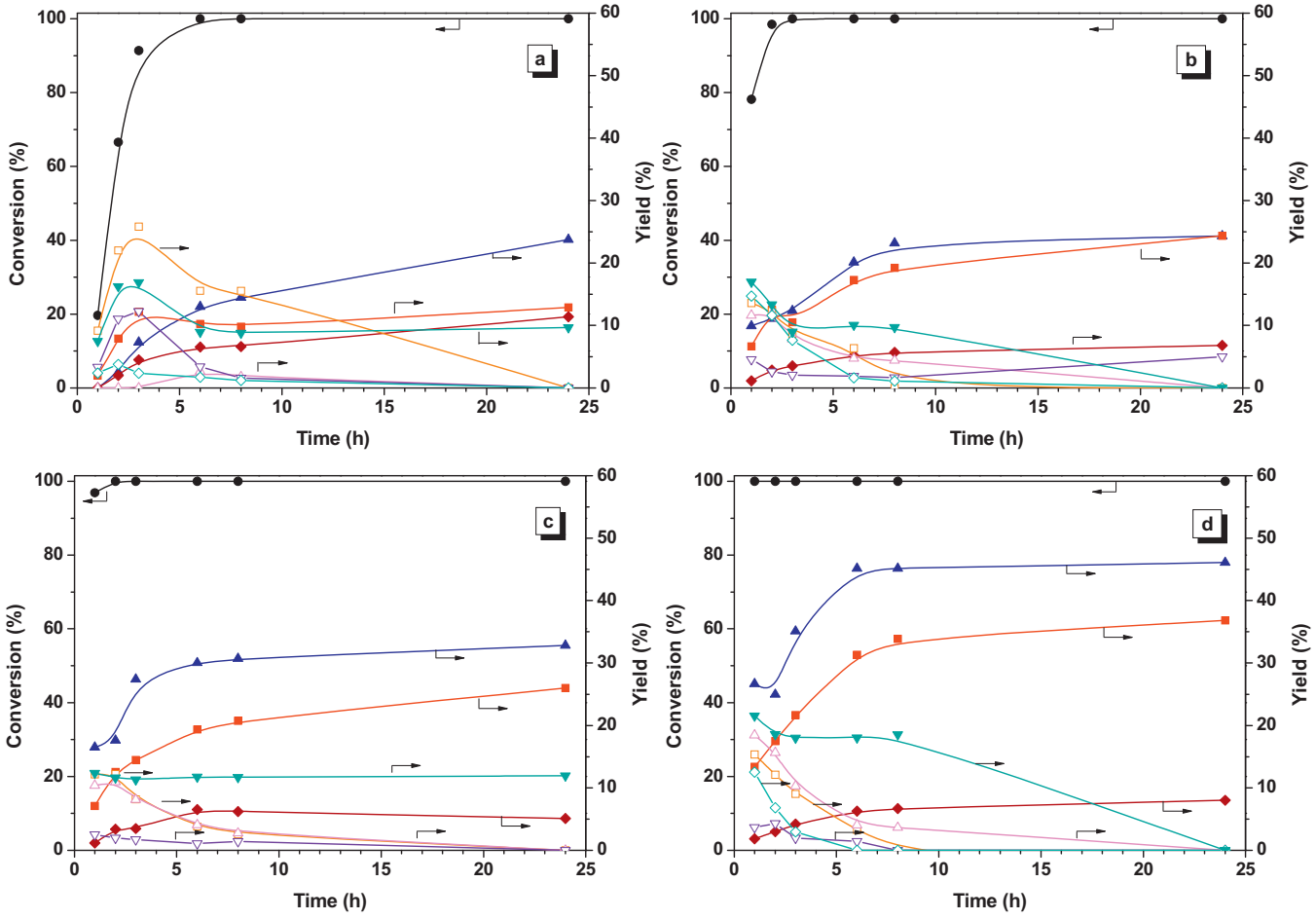

Fig. 4. Catalytic activity of commercial PSSA in aqueous phase oxidation of furfural with H_2O_2: a) no catalyst; b) 1.2 wt.% of catalyst, c) 2.4 wt. % of catalyst; d) 3.6 wt. % of catalyst. Reaction conditions: 4.5% wt. of furfural, 323 K, H_2O_2/furfural molar ratio = 15, 800 rpm. Symbols: (●) furfural conversion; yield to (▲) MAc, (■) SAc, (▼) 5-Furanone, (◆) malic acid, (△) FAc, (○) 5-hydroxyfuranone, (▽) Furoic acid, (□) Formic acid (not derived from Baeyer-Villiger step).

products. The yield to formic acid represented in the figure excludes the formic acid formed in the Baeyer Villager step and therefore indicates that oxidation goes beyond the C4 organic products represented in the figure. Gaseous products like CO_2 and other unknown and undetected products can be also formed and they are evident by the lack of carbon balance. Blank experiments without addition of catalyst are also included: reaction proceeds without the addition of catalysts, but at slower rate, due to the autocatalytic effect provided by the acids formed (formic, furoic, FAc, MAc and SAc) as the reaction progresses. But in the blank run

Table 2
Comparison of the catalytic properties of commercial PSSA with other acid catalysts in the oxidation of furfural with H_2O_2. Reaction conditions: 3.6 wt% catalyst; 4.5 wt% furfural; H_2O_2/F ratio = 15; 323 K; reaction time = 3 h. For H_2SO_4 experiment a 1 wt% is used. (Blank: reaction with H_2O_2 and without catalyst); (H_2O_2 selectivity has been calculated as the fraction used for the formation of C4 organic products with respect to that consumed).

Catal.	Furfural conv. (%)	Yield (%)					C Balance (%)	H_2O_2 conv. and sel[b]. (%)
		MAc	SAc	FAc	2(5*H*)-furanone	Others[a]		
PSSA	100	24.4	12	5.4	12.5	19.2	73.5	19.5 (51.7)
Amberlyst70	100	29.4	13.5	5.6	25	20.7	94.2	46.5 (25.0)
H_2SO_4	100	34.4	9.1	5.8	16.6	31.1	97.0	39.1 (31.0)
Blank	91.4	7.3	12.2	0	16.9	45	89.9	22.8 (30.1)

[a] Malic acid, formic acid, 5-hydroxy-furan-2(5*H*)-one and furoic acid.
[b] Selectivity of H_2O_2 between brackets.

Table 3
Effect of H_2O_2/F ratio on furfural conversion, products yields and carbon balance. Reaction conditions: 3.6 wt% PSSA catalyst; 4.5 wt% furfural; 323 K; reaction time = 24 h. (H_2O_2 selectivity has been calculated as the fraction used for the formation of C4 organic products with respect to that consumed).

H_2O_2/F ratio	Furfural conv. (%)	Yield (%)					C Balance (%)	H_2O_2 conv. and sel[b](%)
		MAc	SAc	FAc	2(5*H*)-furanone	Others[a]		
4	100	19.7	38.0	3.4	26.0	10.6	99.0	67.7 (64.6)
7.5	100	30.3	32.3	0.9	22.3	8	95.0	51.6 (52.1)
15	100	45.8	27.5	0.0	17.5	6.1	96.9	33.7 (45.5)

[a] Malic acid, formic acid, 5-hydroxy-furan-2(5*H*)-one and furoic acid.
[b] Selectivity of H_2O_2 between brackets.

the yields to MAc and SAc are low, so the presence of catalyst is needed for a faster reaction rate. The yields pattern is compatible with the mechanism mentioned above that proposed that MAc and SAc are derived from furanones and hydroxy-furanone as the reaction time progresses. Larger catalyst concentration (3.6 wt%) results in faster reaction rates, especially for SAc formation, and in carbon balance close to 90%. In the 3.6 wt% experiment only 8 h are required to achieve yields to MA and SAc of 45% and 37%, respectively (overall yield to C_4 diacids = 82%).

The catalytic properties of PSSA were compared with those of H_2SO_4 and sulphonic resin (Amberlyst70). Table 2 tabulates the main results. It can be observed that the PSSA catalytic properties are similar to that of Amberlyst regarding the MAc and SAc yields. It is also worth noticing the good behavior of PSSA when compared with H_2SO_4, especially for SAc. For comparison purposes a smaller concentration of H_2SO_4 is employed to compensate the fact that H_2SO_4 possesses ca. 10 mmol H^+ g_{cat}^{-1} whereas PSSA ca. 5.4 mmol H^+ g_{cat}^{-1} maximum. C balance for PSSA is ca. 73.5 but for longer reaction times improves (ca. 90% at 7.5 and 24 h). Regarding H_2O_2 conversion, for PSSA only 20% of H_2O_2 has been consumed for 3 h of reaction whereas consumption is 46.5% for Amberlyst70 and 40% for H_2SO_4. Another relevant feature is that PSSA presents a larger H_2O_2 selectivity. Both results indicate that Amberlyst70 and H_2SO_4 unselectively decompose H_2O_2 at a faster rate than PSSA. Summarizing PSSA compares reasonably well with Amberlyst and H_2SO_4 in the H_2O_2 oxidation of furfural to MAc and SAc.

The effect of the temperature of reaction was also studied and as expected, temperature has a very positive effect in the reaction rate of furfural consumption and of products formation (results not showed). However increasing the temperature is not practical because the temperature also accelerates the autocatalytic reaction and the incorporation of catalyst to obtain reasonable yields to the product of interests is not required when working at higher temperatures. Thus at 343 K without PSSA, full conversion of furfural is already achieved at $t = 3$ h; yields to MAc and SAc after 8 h was 26% and 40%, respectively, and yield to 5-furanone was 22%. We restricted ourselves to conduct the studies at $T = 323$ K.

The effect of H_2O_2/furfural molar ratio was also studied and Table 3 summarizes the results obtained at different ratios after 24 h of reaction (see Fig. SD2 in Supplementary for complete kinetic data). H_2O_2/furfural = 4 results in the formation of more SAc yield than MAc yield. Ebitani et al. [22–24] also obtained a higher SAc yield when using a H_2O_2/furfural = 4 with sulfonic based catalysts. It can be also clearly observed that higher H_2O_2/furfural ratios result in larger yields to MAc at the expenses of 5-furanone and SAc. It seems that the high concentration of H_2O_2 is required to oxidize much faster the 5-furanone to MAc in detriment of the oxidation of 3-furanone to SAc. It must be also noticed that MAc requires three molecules of H_2O_2 and SAc only two and therefore higher H_2O_2 concentration should favor MAc formation.

Selectivity of H_2O_2 utilization decreases as H_2O_2/furfural ratio rises. In all cases ca. 40 mmol of H_2O_2 has been utilized to selectively oxidize organic substrates but H_2O_2 unselectively decomposed upon increasing H_2O_2/furfural ratios (carbon balance were ca. 100% in all cases and therefore this extra consumption of H_2O_2 is not involved in overoxidation of organic substrates to unknown products). At H_2O_2/furfural = 4 only ca. 20 mmol were unselectively consumed whereas at H_2O_2/furfural = 7.5 and 15 H_2O_2, unselective H_2O_2 decomposition affected to 38 and 54 mmol, respectively. The difference must be assigned to a faster decomposition rate of H_2O_2 at larger H_2O_2 concentrations (the blank experiment without addition of acid catalyst showed that a large fraction of H_2O_2 is decomposed without being involved in any oxidation of organic substrates). In any case ca. 26, 75 and 200 mmol of H_2O_2 can be recycled in the case of using a H_2O_2/furfural = 4, 7.5 and 15, respectively.

Fig. 5 represents the catalytic properties of the PSSA catalyst obtained from PS waste (WTC-PSSA) in furfural oxidation at conditions in which commercial PSSA obtained the highest yields to MAc and SAc. Catalytic behavior is quite similar to that obtained from commercial PSSA. In WTC-PSSA case less yield to SAc is obtained apparently at the expenses of 5-furanone. However the overall yield to C_4 diacids is still quite high, ca. 60%.

Recapitulating, the previous results have demonstrated that WTC-PSSA catalyst shows promising catalytic properties in biodiesel reaction, in xylose to furfural dehydration and in oxidation of furfural to MAc and SAc acids. However as mentioned in the Introduction section, reutilization requires ultrafiltration. To circumvent this problem, it is proposed to anchor PSSA on an inorganic solid (SiO_2) to form a solid SiO_2-PSSA nanocomposite that can be filtrated or centrifugated for separation of the reaction medium. Next section will summarize the catalytic results obtained with the

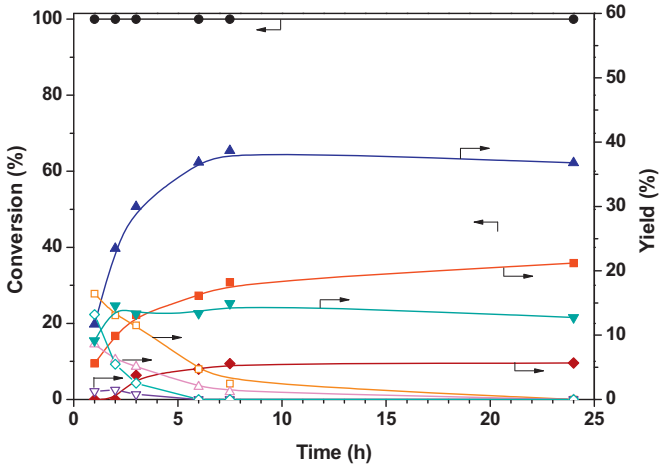

Fig. 5. Catalytic activity of WTC-PSSA in aqueous phase oxidation of furfural with H_2O_2: Reaction conditions: 4.5% wt. of furfural, 3.6% wt. of catalyst, 323 K, H_2O_2/furfural molar ratio = 15, 800 rpm. Symbols: (●) furfural conversion; yield to (▲) MAc, (■) SAc, (▼) 5-Furanone, (◆) malic acid, (△) FAc, (○) 5-hydroxyfuranone, (▽) Furoic acid, (□) Formic acid (not derived from Baeyer-Villiger step).

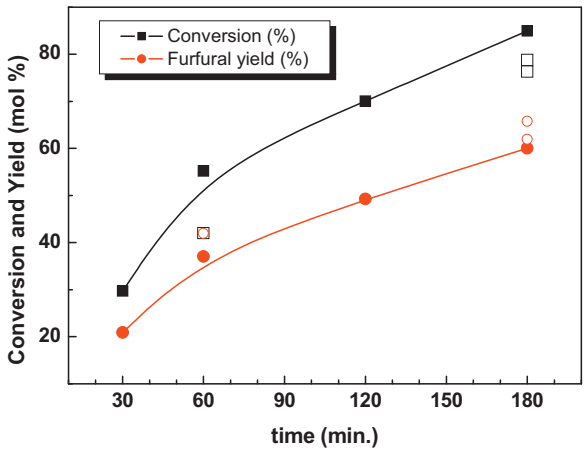

Fig. 6. Comparison of catalytic activity of WTC-SiO_2-PSSA (full symbols) and Amberlyst70 (empty symbols) in xylose dehydration to furfural: (■,□) xylose conversion; (●,○) furfural yield. Reaction conditions: 0.15 g xylose, substrate/catalyst mass ratio = 3, 443 K, 5 mL H_2O/CPME mixture (2.33 wt ratio).

WTC-SiO_2-PSSA nanocomposite in biodiesel, xylose dehydration to furfural and in furfural oxidation to MAc and SAc reactions.

3.2. WTC-SiO_2-PSSA nanocomposite prepared from PSSA waste

Table 4 shows the results of the chemical analysis conducted on the resulting nanocomposite. The actual S and acid sites loading in the fresh solid (that obtained after drying the solid) is 2.3 mmol S g_{cat}^{-1} and the acid sites loading is 1.5 mmol H^+ g_{cat}^{-1}. Both loadings are smaller than those expected considering the amount of PSSA used during the synthesis. However the factual acid site loading is similar to that obtained by considering that part of the sulphonic groups are neutralized by the amino groups (which should be 1.5 mmol H^+ g_{cat}^{-1}).

PSSA-SiO_2 nanocomposites undergo a rearrangement of the texture during the utilization in the reaction mixture and part of the polymer is leached out [2]. Typically, a nanocomposite with this *S*/*N* and Si/N ratio is basically a microporous material with a quite low specific surface area when compared with SiO_2 xerogels prepared by hydrolysis and condensation of organosilanes [2], very likely because the polymer is filling the pores. When the nanocomposite is subjected to the hydrothermal conditions of reaction, the texture of the nanocomposite is remarkably modified: surface area increases because of polymer leaching and the solid becomes essentially mesoporous [2]. To account for the leaching phenomenon, Table 4 also presents the chemical composition of the WTC-SiO_2-PSSA after a hydrothermal treatment in water at 443 K for 10 h. The S and consequently the acid sites loading undertake a remarkable reduction but the resulting solid after the hydrothermal treatment still displays loading values (1.4 mmol S g_{cat}^{-1} and 0.4 mmol H^+ g_{cat}^{-1}, respectively) comparable to other sulphonic silicas (for example 1.1–1.2 mmol H^+ g_{cat}^{-1} [25,26], 0.32–0.67 mmol H^+ g_{cat}^{-1} [27] and 0.44–1.69 mmol H^+ g_{cat}^{-1} [28] for sulphonic-SBA-15 systems or 0.18–0.20 mmol H^+ g_{cat}^{-1} for SBA-15 grafted poly-(styrene sulphonic acid) prepared by surface initiated atom transfer radical polymerization methodologies [29]). Optimization of other synthesis variable is obvioulsy required as it can result in larger values for fresh and treated nanocomposites but these results clearly demonstrate that WTC-SiO_2-PSSA here reported still presents a significant amount of S and acid sites after hydrothermal treatment. The investigation of the catalytic properties of this WTC-SIO_2-PSSA catalyst will be presented next.

3.2.1. Xylose to furfural reaction

First the catalytic activity of WTC-SiO_2-PSSA in biodiesel synthesis was tested. Unfortunately the nanocomposite catalysts fully deactivated in three cycles (results not shown for the sake of simplicity). The deactivation is not related to the stability of the polymer as the sulphur loading remain quite constant along the cycles (results not shown). Very likely deactivation is due to the fouling or poisoning of the active sites by heavy products derived from reactions between reactants and products (TG, DG, MG, FAME and glycerol) [30]. SiO_2-PSSA nanocomposites cannot be used for biodiesel reaction and for this reaction only soluble (non-anchored) PSSA can be used.

We proceed reporting the catalytic activity for xylose dehydration to furfural. Fig. 6 compares the catalytic activity of the waste derived nanocomposite with that of Amberlyst70. Both catalysts present comparable conversion and furfural yields. We have to bear in mind that Amberlyst70 possess an acid loading higher than the nanocomposite (this Amberlyst batch possessed 2.55 mmol H^+ g_{cat}^{-1} in comparison with 1.5 mmol H^+ g_{cat}^{-1} initially present in the nanocomposite), so WTC-SiO_2-PSSA presents promising catalytic properties.

The WTC-SiO_2-PSSA catalyst was also reutilized. Since nanocomposite undertakes a rearrangement of the textural properties and a leaching of polymer when subjected to reaction conditions, prior to the reutilization experiment, the catalyst was exposed to a hydrothermal treatment (443 K in water for 10 h) to conditioning the catalyst. Fig. 7 present the catalytic properties obtained for 5 consecutive runs. Reutilization tests were conducted by separating the used nanocomposite from the reaction mixture by centrifugation (solid was washed until neutral pH so no acid is detected). To compensate the loss of sulphur and acid sites, a larger amount of catalyst was utilized. Catalyst still deactivates during the first run. This deactivation is expected to be due to fouling or poisoning by humins-like products. The solid has been conditioned previously with water at the reaction temperature for 10 h and therefore leaching of polymer should be negligible during this first run. In any case, the catalytic properties for the second and successive were quite similar, indicating that after this initial deactivation process, catalyst maintains relatively high activity.

3.2.2. Liquid phase oxidation of furfural to C_4 diacids with H_2O_2

WTC-SiO2-PSSA was also tested in the oxidation of furfural with H_2O_2. Fig. 8 summarizes its catalytic properties. The catalytic behavior is initially quite promising. In this case, the MAc and

Table 4
Chemical analysis results of the WTC-SiO_2-PSSA catalyst (on dry basis).

Sample	S wt%[a]	N wt%[a]	at. Si/N[b]	at. S/N[a]	mmol g_{cat}^{-1}		
					S[c]	N[c]	H^+[d]
Fresh	7.5 (9.3)[e]	1.1 (0.9)[e]	12.03 (11.0)[e]	3.0 (4.0)[e]	2.3 (2.9)[e]	0.8 (0.7)[e]	1.5 (1.5)[f]
Hydrothermally treated (443 K)	4.5	1.5	not measured	1.3	1.4	1.1	0.4

[a] Obtained by elemental chemical analysis.
[b] Obtained by TXRF and elemental chemical analysis.
[c] Obtained by elemental chemical analysis.
[d] Obtained by acid–base titration.
[e] Value corresponding to nominal values deduced from the TEOS, APTES and WTC-PSSA used for the synthesis.
[f] Deduced by difference between experimental S and N loadings.

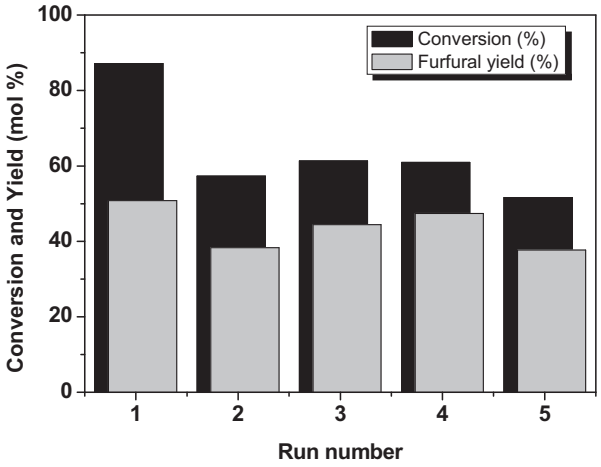

Fig. 7. Reutilization tests of WTC-SiO_2-PSSA in xylose dehydration to furfural (catalyst has been previously conditioned by a hydrothermal treatment with water at 343 K for 10 h). Reaction conditions: 0.15 g xylose, substrate/catalyst mass ratio = 1.5, 443 K, 5 mL H_2O/CPME mixture (2.33 wt ratio, reaction time = 180 min).

SAc yields are smaller than that obtained for soluble PSSA. But it must be taken into account that the factual acid sites concentration present in the reaction mixture with solid nanocomposite is lower than that present when using soluble PSSA (in the nanocomposite the PSSA is "diluted" with SiO_2). As demonstrated in previous section, the acid concentration has a remarkable positive effect on the yield to C_4 acids. This effect can be compensated by using a higher concentration of nanocomposite in the reaction mixture. In any case, for the conditions here used, the overall yield to C_4 diacids is close to 65%.

Fig. 9 shows the reutilization results obtained for (a) the as-synthesized fresh catalyst and (b) the catalyst subjected to a hydrothermal treatment with water at 180 °C overnight. Reutilization tests were conducted by separating the used nanocomposite from the reaction mixture by filtration (filtrate was washed until neutral pH so no acid is detected in the filtrate). Figure also includes the mmol S and mmol H^+ g_{cat}^{-1} loading of the nanocomposite at the beginning of each cycle, as determined by running parallel experiments under the same reaction conditions used for the catalytic experiments of Fig. 8. Concerning the fresh catalysts, the catalytic

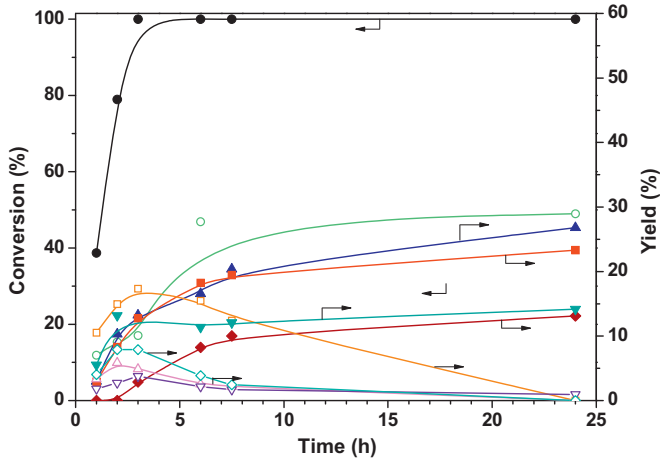

Fig. 8. Catalytic activity of WTC-SiO_2-PSSA in aqueous phase oxidation of furfural with H_2O_2. Reaction conditions: 5% wt. of furfural, 5 wt. % of catalyst, 323 K, H_2O_2/furfural molar ratio = 15, 800 rpm. Symbols: (●) furfural conversion; (○) H_2O_2 consumption; yield to (▲) MAc, (■) SAc, (▼) 5-Furanone, (◆) malic acid, (△) FAc, (○) 5-hydroxyfuranone, (▽) Furoic acid, (□) Formic acid (not derived from Baeyer-Villiger step).

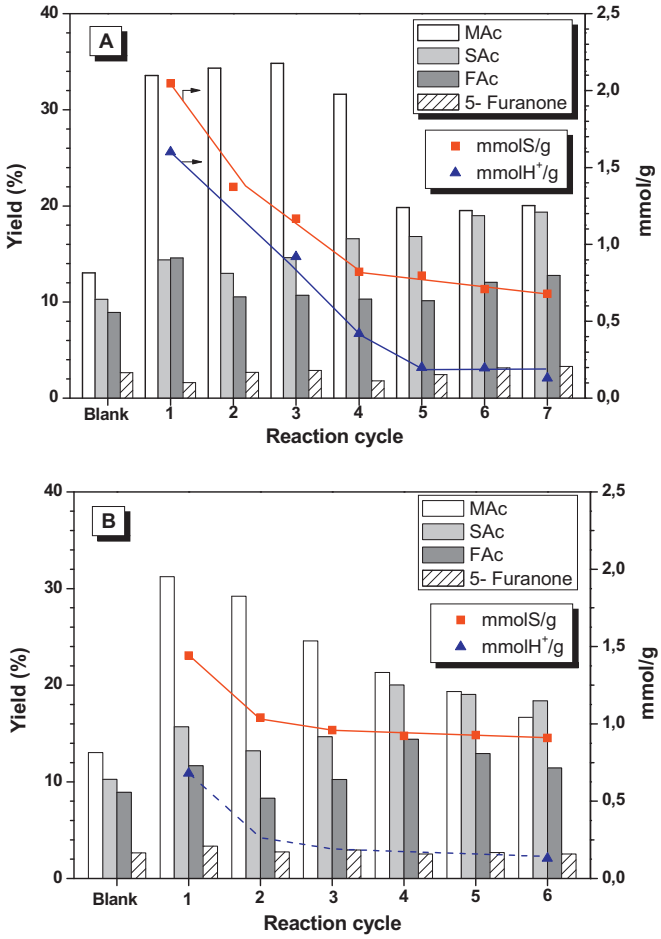

Fig. 9. Reutilization tests for A) Fresh WTC-SiO2-PSSA catalyst; B) hydrothermally treated WTC-SiO2-PSSA with water at 180 °C. Left axis: yield to products, right axis: mmol S g_{cat}^{-1} (■) and mmol H^+ g_{cat}^{-1} (▲). Reaction conditions: 5 wt% of furfural, 5 wt% of catalyst, 323 K, H_2O_2/furfural molar ratio = 15, 800 rpm, 6 h of reaction.

properties remain quite stable for three first runs but deactivation is visible in the fourth run and it reaches a new stable state in the fifth and successive cycles. If attention is paid to the S and acid sites loading, it is clear that polymer is being leached from the first run to the fourth cycle, after this cycle the polymer loading remains constant. Therefore during the first four cycles the polymer leached during the catalytic run must contribute in a large extension to the overall activity (this was also verified by running the reaction with the solutions derived by contacting the catalyst with the water at 323 K; then performing the reaction adding the reactants to the solutions once the nanocomposite was removed by filtration; the results are not shown for the sake of simplicity). The polymer left on the catalyst also participates to the overall activity. Both homogeneous and heterogeneous contributions from leached and supported polymer must become smaller during reusing but it is not noticed for the first three runs as 6 h of reaction time is more than enough to reach the full conversion. However for the fourth run a slight deactivation is visible. No substantial polymer leaching occurs for 5th, 6th and 7th run and their catalytic activity remains quite constant as so does the polymer staying attached to the SiO_2. The sulphur loading is 0.6–0.7 mmol S g_{cat}^{-1} but amino groups responsible for retaining the polymer neutralizes most of the acid sites. Consequently, the effective acid site loading becomes ca. 0.2 mmol H^+ g_{cat}^{-1}. It must be noticed that, notwithstanding that few acid sites are left, the yields to MA and SAc after repetitive utilizations are notably better than those obtained without adding catalyst (represented in the figure in columns labeled as blank).

A similar situation can be observed for the hydrothermally treated nanocomposite but this treatment gives place to a substantially removal of the polymer, so a large fraction of the polymer has been already removed when catalyst is used for the first time and the steady state is achieved earlier. The WTC-SiO_2-PSSA catalyst after hydrothermal conditioning continuously deactivates until 4th run, after that, activity remains quite stable. It must be realized that in both cases, fresh or hydrothermally conditioned, the catalytic properties and the S and acid sites loading once the steady state has been reached are similar. The hydrothermal conditioning only results in the removal of polymer so the steady sate is reached in less number of runs.

Summarizing these preliminary results of WTC-SiO_2-PSSA nanocomposite, it can be said that it presents promising properties in the dehydration of xylose to furfural reaction and oxidation of furfural to MAc and SAc. In the case of biodiesel reaction the catalyst fully deactivates. The synthesis of the nanocomposite must be enhanced: improvements must come from increasing the initial polymer loading (and consequently the acid sites loading) and from the hydrothermal stability of the nanocomposite to prevent the significant leaching.

4. Conclusions

The investigation here reported demonstrates that acid catalysts derived from PS waste by sulphonation can be used in reactions of interest in biomass valorization, namely, biodiesel synthesis, xylose dehydration to furfural and furfural oxidation to maleic and succinic acids. Two types of waste derived catalysts (WTC, Waste To Catalysts) were studied: soluble PSSA (WTC-PSSA) and solid SiO_2-PSSA nanocomposite (WTC-SiO_2-PSSA). The soluble WTC-PSSA shows reasonably good activity for these three reactions but reutilization would require the use of ultrafiltration to separate the polymer from the reaction mixture. The WTC-SiO_2-PSSA nanocomposite represents in principle a better option as this solid can be separated from the reaction mixture by conventional filtration or centrifugation. However for the biodiesel reaction nanocomposite completely deactivates, very likely by extensive deposition of heavy by-products. Utilization of "waste" PSSA for biodiesel reaction must be restricted to the soluble PSSA. In the case of the furfural dehydration and liquid phase oxidation with H_2O_2 reactions, WTC-SiO_2-PSSA deactivates during the first runs, but catalyst remains stable in successive runs. Leaching of polymer is the main cause of deactivation. Hydrothemal stability must be improved in order to reduce the leaching of the polymer and make the nanocomposite more stable and more active through a large number of catalytic runs.

Acknowledgments

This work was funded by the Spanish Ministry of Economy and Competitiveness (Project CTQ2012-38204-C03-01, CARBIOCAT) and the Autonomous Government of Madrid (S2009/ENE-1660, CARDENER-CM partly funded by FSE funds).

References

[1] M. López Granados, A.C. Alba-Rubio, I. Sádaba, R. Mariscal, I. Mateos-Aparicio, A. Heras, Green Chem. 13 (2011) 3203.
[2] I. Sadaba, M. Ojeda, R. Mariscal, M. López Granados, Appl. Catal., B 150-151 (2014) 421.
[3] W. Bajdur, J. Pajczkowska, B. Makarucha, A. Sulkowska, W.W. Sulkowski, Eur. Polym. J. 38 (2002) 299.
[4] W.W. Sulkowski, A. Wolinska, B. Szoltysik, W.M. Bajdur, A. Sulkowska, Polym. Degrad. Stab. 90 (2005) 272.
[5] W.W. Sułkowski, A. Wolińska, D. Pentak, S. Maślanka, A. Sułkowska, Macromol. Symp. 245–246 (2006) 621.
[6] Y. Inagaki, M. Kuromiya, T. Noguchi, H. Watanabe, Langmuir 15 (1999) 4171.
[7] I. Bekri-Abbes, S. Bayoudh, M. Baklouti, Desalination 222 (2008) 81.
[8] I. Bekri-Abbes, S. Bayoudh, M. Baklouti, J. Polym. Environ. 14 (2006) 249.
[9] I. Bekri-Abbes, S. Bayoudh, M. Baklouti, Desalination 204 (2007) 198.
[10] R.M.N. de Assunção, B. Royer, J.S. Oliveira, G. Rodrigues Filho, L.A. de Castro Motta, J. Appl. Polym. Sci. 96 (2005) 1534.
[11] H. Vink, Makromol. Chem. 182 (1981) 279.
[12] D. Baigl, T.A.P. Seery, C.E. Williams, Macromolecules 35 (2002) 2318.
[13] M.J. Cánovas, I. Sobrados, J. Sanz, J.L. Acosta, A. Linares, J. Membr. Sci. 280 (2006) 461.
[14] D.L. VanderHart, Y. Feng, C.C. Han, R.A. Weiss, Macromolecules 33 (2000) 2206.
[15] E.M. Zippi, G.W. Kabalka, Carbon 34 (1996) 1539.
[16] M. Antonietti, D. Radloff, U. Wiesner, H.W. Spiess, Macromol. Chem. Phys. 197 (1996) 2713.
[17] A.K. Sen, S. Roy, V.A. Juvekar, Polym. Int. 56 (2007) 167.
[18] M.J. Campos Molina, R. Mariscal, M. Ojeda, M. López Granados, Bioresour. Technol. 126 (2012) 321.
[19] R.H. Kottke, Furan Derivatives, Kirk-Othmer Encyclopedia of Chemical Technology, vol. 12, John Wiley and Sons, New York, 1998.
[20] H.E. Hoydonckx, W.M. Van Rhijn, W. Van Rhijn, D.E. De Vos, P.A. Jacobs, Furfural and Derivatives, in: Ullmann's Encyclopedia of Industrial Chemistry, Wiley-VCH, Weinheim, Germany, 2007.
[21] A. Cukalovic, C.V. Stevens, Biofuels, Bioprod. Biorefin. 2 (2008) 505.
[22] A. Takagaki, S. Nishimura, K. Ebitani, Catal. Surv. Asia 16 (2012) 164.
[23] H. Choudhary, S. Nishimura, K. Ebitani, Chem. Lett. 41 (2012) 409.
[24] H. Choudhary, S. Nishimura, K. Ebitani, Appl. Catal., A 458 (2013) 55.
[25] J.A. Melero, L.F. Bautista, G. Morales, J. Iglesias, R. Sánchez-Vázquez, Chem. Eng. J. 161 (2010) 323.
[26] J.A. Melero, L.F. Bautista, J. Iglesias, G. Morales, R. Sánchez-Vázquez, I. Suárez-Marcos, Top. Catal. 53 (2010) 795.
[27] C. Pirez, J.M. Caderon, J.P. Dacquin, A.F. Lee, K. Wilson, ACS Catal. 2 (2012) 1607.
[28] I. Agirrezabal-Telleria, J. Requies, M.B. Guemez, P.L. Arias, Appl. Catal., B 115 (2012) 169.
[29] A. Martin, G. Morales, F. Martinez, R. van Grieken, L. Cao, M. Kruk, J. Mater. Chem. 20 (2010) 8026.
[30] A.C. Alba-Rubio, F. Vila, D. Martín Alonso, M. Ojeda, R. Mariscal, M. López Granados, Appl. Catal., B 95 (2010) 279.

PUBLICACIÓN 4:

Título: *"Aqueous-Phase Catalytic Oxidation of Furfural with H_2O_2: High Yield of Maleic Acid by Using Titanium Silicalite-1"*

Autores: *N. Alonso Fagúndez, I. Aguirrezabal Telleria, P.L. Arias, J.L.G. Fierro, R. Mariscal, M. López Granados*

Revista: *RSC Advances*

Año: *2014*

RSC Advances

PAPER

View Article Online
View Journal | View Issue

Cite this: *RSC Adv.*, 2014, **4**, 54960

Aqueous-phase catalytic oxidation of furfural with H_2O_2: high yield of maleic acid by using titanium silicalite-1†

N. Alonso-Fagúndez,[a] I. Agirrezabal-Telleria,[b] P. L. Arias,[b] J. L. G. Fierro,[a] R. Mariscal[a] and M. López Granados*[a]

This investigation explores the selective liquid-phase oxidation of furfural to maleic acid (MA) using hydrogen peroxide as an oxidant and titanium silicalite (TS-1) as a catalyst. The effect of temperature and of the concentration of H_2O_2, furfural and catalyst on the MA yield was studied. The highest yield, 78 mol%, was obtained under the following reaction conditions: 4.6 wt% of furfural, 4.6 wt% of catalyst, a H_2O_2/furfural mol ratio of 7.5, corresponding to 12.3 wt% of H_2O_2, 323 K and 24 hours of reaction. To reduce the amount of H_2O_2 employed, a two-step sequence of reactions was conducted using TS-1 and Amberlyst 70 consecutively as catalysts in the first and second steps, respectively. In this case, a H_2O_2/furfural mol ratio = 4.4 was required, which is quite close to the stoichiometric ratio (3.0), and a maleic acid yield close to 80% was obtained under 4.6 wt% of furfural, 4.6 wt% of catalyst and 28 h of reaction at 323 K; after 52 h of reaction, the MA yield reached 92%. Fresh and used catalysts were characterised by X-ray diffraction (XRD), Raman spectroscopy, total reflection X-ray fluorescence (TXRF), X-ray photoelectron spectroscopy (XPS), N_2 adsorption–desorption isotherms and thermogravimetric analysis. Ti was largely incorporated within the silicalite framework, but the presence of some TiO_2 anatase was also confirmed. Ti leaching was observed, especially during the first run but became much less important in successive cycles. Leaching affects both anatase and Ti species within the silicalite framework. Notwithstanding the leaching, when using pure furfural, TS-1 could be reused for six runs without noticeable deactivation, whereas when using furfural directly derived from biomass, weak but visible deactivation occurred upon reutilisation; this deterioration must be related to the presence of some organic products other than furfural.

Received 31st July 2014
Accepted 13th October 2014

DOI: 10.1039/c4ra11563e

www.rsc.org/advances

Introduction

Maleic anhydride (MAN) and its hydrated form, maleic acid (MA), are important C_4 chemical intermediates with applications in multiple fields of the chemical industry. They are important raw materials used in the manufacture of unsaturated polyester resins, vinyl copolymers, tetra- and hexahydrophthalic anhydride (curing agents in epoxy resins), surface coatings, lubricant additives, plasticisers, copolymers, agrochemicals, and pharmaceuticals, as well as in the production of γ-butyrolactone, butanediol and tetrahydrofuran. Succinic acid and fumaric acid, both of which have multiple additional applications, are also synthesised from MA and/or MAN.[1,2] Currently, maleic anhydride is industrially produced primarily by selective oxidation of *n*-butane (it can also be produced from benzene, but this obsolete route has been almost fully displaced for environmental and economic reasons by butane technology).[3] Both MA and MAN are interconverted into one other by hydration–dehydration processes.[1,2]

Alternative routes based on the oxidation of furfural to MAN and MA, either in gas or liquid phase, have been reported by different research groups. Furfural is a chemical currently obtained from the pentoses contained in lignocellulosic agroresidues; approximately 250–400 ktons of furfural are synthesised annually from this carbohydrate feedstock.[4–6] Therefore, these routes from furfural constitute renewable pathways for the manufacture from biomass of MA, MAN and their derived products. Thus, a renewable route for phthalic anhydride formation by Diels–Alder condensation with furan has very recently been demonstrated.[7]

Gas-phase oxidation of furfural to maleic anhydride is a well-known route, and yields up to 75% can be achieved by using

[a]*Group of Sustainable Energy and Chemistry (EQS), Institute of Catalysis and Petrochemistry (ICP-CSIC), C/ Marie Curie 2, Campus de Cantoblanco, 28049 Madrid, Spain*

[b]*Department of Chemical and Environmental Engineering, Engineering School of The University of The Basque Country (UPV/EHU), Alameda Urquijo s/n, Bilbao 48013, Spain. E-mail: mlgranados@icp.csic.es*

† Electronic supplementary information (ESI) available: Additional information on experimental details, catalytic activity, other proposals of mechanism of reaction and characterisation of catalysts by TG analyses, XRD, and N_2 adsorption. See DOI: 10.1039/c4ra11563e

vanadium-oxide-based catalysts; cheap air O_2 is used as an oxidising agent.[8–12] However, dilute furfural streams (below 1% v/v) are required to achieve high MAN selectivity. The reaction is conducted at high temperatures (higher than 523 K), and the vaporisation of furfural is required. Both of these features have a negative impact on the energy balance and consequently the economic viability of this process.

Liquid oxidation with O_2 at milder temperatures has also been explored using homogeneous catalysts like phosphomolybdic acid in a water/tetrachloroethane biphasic system, achieving MA yields not larger than 50%.[13,14] Moreover, although milder temperatures are required (383 K), high O_2 pressure (2 MPa) is needed. The reusability of these catalysts has not been proved, which is crucial to evaluate the feasibility of possible industrial applications.

Another liquid-phase alternative that has recently been investigated is furfural oxidation with hydrogen peroxide. So far, the best results using this strategy have been achieved by using either a soluble acid catalyst like H_2SO_4 and *p*-toluensulphonic acid or by using solid sulphonic-based catalysts such as sulphonic resins or poly-(styrene sulphonic acid).[15–19] Oxidation with H_2O_2 seems attractive for industrial application, first because the reaction proceeds under very mild conditions (low temperatures and atmospheric pressure), and second because aqueous furfural solutions can be processed, which is a key advantage. When pure furfural is produced from lignocellulosic agroresidues, the primary raw product is an aqueous furfural solution that must be further purified by an energy-intensive double distillation. Processing primary raw aqueous furfural solutions would imply that distillation steps are not required, which positively impacts the energy and economic balance of the overall process.

However, the main drawback for oxidation with hydrogen peroxide using acid catalysts is the control of selectivity. A wide distribution of products such as MA, succinic acid (SA), fumaric acid (FumA), β-formylacrylic acid or 2(5*H*)-furanone is obtained. This lack of selectivity is a consequence of the very complex reaction network that starts with the Baeyer–Villiger oxidation of furfural to the corresponding ester.[15,16,19] Large H_2O_2/furfural ratios (much larger than 7) are required to improve the MA yield, whereas for lower ratios succinic acid is the main product. Maleic acid could be obtained by dehydrogenation of succinic acid,[20] but this would mean an additional step. The identification of a robust solid catalyst that can selectively oxidise furfural to MA in one step and that can be easily recovered from the reaction mixture and reutilised for a large number of runs is still a challenge.

The selective oxidation of furan with aqueous H_2O_2 using TS-1 has been already investigated.[21,22] The furan ring possesses a similar chemical structure to furfural, except for the absence of the aldehydic functional group. Maleic dialdehyde and 5-hydroxy-furan-2(5*H*)-one were obtained selectively by the oxidation of furan using H_2O_2/furan with approximate mol ratios of 1 and 2, respectively. These products are closely related to maleic acid, as the latter can be obtained from them by further oxidation. Titanium silicalite 1 (TS-1) is frequently used in the epoxidation of numerous alkenes.[23–25] The ability of TS-1 to activate hydrogen peroxide is linked to the particular environment of Ti(IV) cations incorporated into the silicalite framework and located within the hydrophobic pores of the zeolite. This allows simultaneous adsorption of the hydrophobic substrate and the oxidant.[21,26,27]

The latter results using furan encouraged us to explore the utilisation of TS-1 in the selective oxidation of furfural to MA by using H_2O_2. Because the oxidation of furfural (a C_5 aldehyde) to maleic acid (a C_4 diacid) implies the loss of a carbon atom, the key question is whether, besides the epoxidation and oxidation steps, the TS-1 catalyst can also promote in practice the removal of a C atom.

In principle the oxidation of furfural with H_2O_2 is more advantageous than the furan oxidizing route previously demonstrated.[21,22] Furan is currently produced by decarbonylation of furfural[1,2] and therefore the production of MA from furan would imply two steps: first decarbonylation and subsequently the oxidation of furan. A first drawback of this furan route is that the decarbonylation of furfural is conducted at relatively high temperatures (423–453 K) and in the presence of noble metal catalysts that unavoidably deactivate. Reactivation periods are required to regenerate the initial activity that complicates the viability of the furan route. On the contrary the route here proposed implies the direct conversion of furfural in one-step and at mild temperatures.

In this work, we demonstrate for the first time that TS-1 is an excellent catalyst for the transformation of furfural to MA. We have also conducted the necessary study examining the effect of operating variables like temperature, H_2O_2/furfural ratio and catalyst and furfural concentration on the catalytic properties of TS-1. Specific attention was paid to the deactivation of catalyst and the reutilisation behaviour of TS-1 under the optimum reaction conditions, using both pure furfural provided by a commercial supplier and aqueous solutions of furfural obtained directly from corncob residues. A commercial TS-1 with a Ti/Si at. ratio above the threshold required to fully saturate the silicalite framework with Ti cations was used in this investigation. This means that a TS-1 with the largest possible incorporation of Ti within silicalite (active sites) was used.

Experimental

Materials

Titanium silicalite 1 was purchased from Tricat Zeolites, H-ZSM-5 (Si/Al = 19) was purchased from Akzo Nobel, anatase catalyst support was purchased from Alfa Aesar and Amberlyst-70 was purchased from The Dow Chemical Company. Furfural (99 wt%), hydrogen peroxide (30 wt%), furan (99 wt%) and furan-2(5*H*)-one (98 wt%) were supplied by Sigma-Aldrich. Furoic acid (98 wt%) was provided by Fluka, and oxalic acid (99.5 wt%), used as internal standard, was purchased from Alfa Aesar. 5-Hydroxy-furan-2(5*H*)-one, which was used as a starting reactant, was synthesised according to the findings of Kumar *et al.*,[22] comprising the oxidation of furan with H_2O_2 using TS-1 as catalyst. Further details of the preparation are given in the ESI section.†

Catalytic activity measurements

The oxidation of furfural was carried out in a glass flask reactor with three necks: one for the thermocouple, one for the addition of reactants through an addition funnel and the third for sampling through a septum. The required amounts of TS-1 and of H_2O_2 solution were loaded into the reactor and heated up to the reaction temperature by immersion in an oil bath. After the reaction mixture reached the selected temperature, the reaction started when a known amount of aqueous furfural solution was added to the reactor. To prevent the mixture from cooling down because of the incorporation of the aqueous furfural, the latter solution was preheated to the reaction temperature and rapidly added to the reactor. The resulting reaction mixture (approximately 40 mL) was vigorously stirred by a magnetic bar at 800 rpm.

A known amount of reaction mixture (*ca.* 0.5 g) was sampled at different reaction times and was analysed by HPLC, using a known amount of a 30 mg g^{-1} aqueous solution of oxalic acid as an internal standard (*ca.* 15 mg of oxalic acid was added to each aliquot). Subsequently, the aliquot was diluted 10–20 times with water. This diluted aliquot, after being filtered through a 0.22 μm syringe filter, was then analysed in an Agilent 1200 HPLC chromatograph equipped with a refraction index detector and a Bio-Rad Aminex HPX-87H column (300 mm × 7.8 mm). A 0.005 M H_2SO_4 mobile phase was employed as the eluent at 328 K and a 0.4 mL min^{-1} flow rate. In addition to oxalic acid and furfural, the following products were detected by HPLC: MA, malic acid, SA, formic acid (FA), fumaric acid (FumA), 5-hydroxy-furan-2(5*H*)-one (hydroxyfuranone), furan-2(5*H*)-one (furanone) and furoic acid (FurA). Deeper details of the analyses are given in Fig. SI1 of ESI section.†

Furfural conversion and product yields were calculated according to the following formulas:

$$\text{Furfural conversion (mol\%)} = \frac{m^0_{\text{furf}} - m_{\text{furf}}}{m^0_{\text{furf}}} \times 100$$

$$\text{Product yield (mol\%)} = \frac{m_{\text{prod}}}{m^0_{\text{furf}}} \times 100$$

where m^0_{furf} refers to the mole quantity initially loaded into the reactor, and m_{furf} and m_{prod} refer to the number of moles of the furfural and products, respectively, in the reaction mixture at a given time. The HPLC chromatographic factor of the organic products was calculated by analysing solutions with known concentrations of the different organic products.

The hydrogen peroxide concentration at a given reaction time was determined by iodometric titration. Approximately 0.5 g of reaction sample was diluted 10–20 times with water. Then, 0.5 g of this diluted solution was poured into an Erlenmeyer flask containing 20 mL of water. After adding 2 mL of potassium iodide solution (10%) and 2.5 mL of an acid mixture consisting of a solution of ammonium molybdate and H_2SO_4, the flask was closed, gently agitated and allowed to rest for five minutes to form triiodide species by oxidation of the iodide with H_2O_2, which gives a brown colour to the solution. The mixture was then titrated with a *ca.* 0.1 M sodium thiosulfate solution until the brown triiodide colour was reduced to a light straw colour. A few drops of starch solution (10 g L^{-1}) were added, and the solution became dark blue. Titration was continued until the colour of the solution changed sharply from blue to colourless. A titration of a blank solution (pure water) was also carried out following the same procedure. The actual titer of the sodium thiosulfate solution was determined by titration with potassium iodate solution (0.1 N).

The amount of H_2O_2 present in solution was calculated as follows:

$$\begin{aligned}&\text{H_2O_2 present in reaction mixture (mol)}\\ &= (A-B)(M)\frac{1\ \text{mol}\ H_2O_2}{2\ \text{mol}\ Na_2S_2O_3}\frac{34}{1\ \text{mol}\ H_2O_2}\end{aligned}$$

where A is the titration volume of $Na_2S_2O_3$ for the sample, B is the titration volume of $Na_2S_2O_3$ consumed for the blank and M is the molarity of the $Na_2S_2O_3$ solution.

For the reutilisation tests, catalyst was filtered out of the reaction medium by using a filtration cell and a ceramic membrane. The catalyst was washed twice with water (*ca.* 200 mL) to remove reaction products that could interfere in successive analysis, carefully removed from the membrane to prevent losses during handling, and dried at 333 K overnight before performing a new reaction run. The filtered solution from the catalyst wash steps (including the filtrate from the reaction medium) was analysed by TXRF for the quantitative determination of Ti and Si.

Catalyst characterisation

Powder X-ray diffraction (XRD) measurements were performed at room temperature in the 5–50° range in scan mode (0.02°, 1 s) with a Siemens D5000 automated diffractometer, over a 2θ Bragg–Brentano geometry using Cu Kα radiation and a graphite monochromator.

Nitrogen adsorption–desorption isotherms were recorded at the temperature of liquid nitrogen (77 K) using a Micromeritics TriStar 3000 apparatus. The sample was previously outgassed at 140 °C for several hours. The specific area was calculated by applying the BET method to the range of relative pressures (P/P^0) of the isotherms between 0.03 and 0.3 and by assuming a value of 0.162 nm^2 for the cross-section of adsorbed nitrogen molecules at 77 K.

TXRF (total reflection X-ray fluorescence) analysis was performed in a S2 PICOFOX instrument equipped with two X-ray fine focus lines, Mo and W anodes, and a Co(Li) detector with an active area of 80 mm^2 and a resolution of 157 eV at 5.9 keV (Mn Kα). The acquisition time was 300 s and 500 s for qualitative and quantitative analysis, respectively. To carry out the TXRF analysis, a Mo X-ray source was used for Si and Ti determination. For the analysis of solid samples, 10–15 mg of sample was ground in an agate mortar to a powder with a particle size less than 10 μm. Subsequently, 10 mL of high-purity water was added to the powder. The sample was homogenised for 15–20 min by ultrasonic desegregation in order to disperse any possible agglomeration of particles. A 5 μl aliquot of the

suspension was removed and placed on a flat carrier of plastic after which the water was evaporated by vacuum.

Raman spectra were recorded on a single-monochromator Renishaw 1000 spectrophotometer equipped with a CCD cool detector (200 K), with an argon laser as the exciting source ($\lambda = 532$ nm), a supernotch filter, and an *in situ* cell that enables sample treatment under a flow of gas. Raman spectra were recorded at room temperature with a laser power of 2 mW after an *in situ* calcination of the samples in synthetic air with a heating rate of 10 K min^{-1} up to 833 K for 30 min.

X-ray photoelectron spectra (XPS) were acquired with a VG Escalab 200 R spectrometer equipped with a hemispherical electron analyser and a Mg Kα (1253.6 eV) X-ray source. The solids were outgassed at 393 K for 1 h at 10^{-5} mbar to remove water before transfer to the ion-pumped analysis chamber. Ti 2p, C 1 s, O 1 s and Si 2p core level were scanned a sufficient number of times to obtain high signal-to-noise ratios. The static charge of the samples was corrected by referencing all binding energies (BEs) to the Si 2p peak (103.4 eV). The accuracy of the BE was $\pm$0.1 eV. The areas of the peaks were computed by fitting the experimental spectra to Gaussian/Lorentzian curves after removing the background (using the Shirley function). Surface atom ratios were calculated from peak area ratios normalised by using the corresponding atomic sensitivity factors.[28]

Thermogravimetric analysis (TGA) under a controlled atmosphere was carried out on a Mettler Toledo TGA/SDTA 851^e, using a heating rate of 10 K min^{-1} up to a maximum temperature of 973 K under a synthetic air atmosphere.

Results and discussion

Parametric study of the reaction conditions

A study of the effect of different operating variables on catalytic behaviour was performed first. The aim was to find the best reaction conditions to obtain the highest MA yield. The following operation variables were modified: reaction temperature, H_2O_2 and furfural concentrations and catalyst loading.

Reaction temperature effect. The effect of reaction temperature on the catalytic properties was examined first. Temperatures in the range used for other catalysts were explored.[15–19] Fig. 1 compares the catalytic activity of commercial TS-1 at three different temperatures (323, 333 and 343 K) while keeping the rest of the reaction conditions constant (4.6 wt% of furfural, 2.3 wt% of catalyst and 12.3 wt% H_2O_2, equivalent to an H_2O_2/furfural mol ratio of 7.5). Yields are based on the initial amount of furfural loaded into the reactor.

5-Hydroxy-furan-2(5*H*)-one (hydroxyfuranone), MA and FA were the main reaction products, malic acid was also detected but with a yield less than 5%. The yield for the remaining possible reaction products (SA, furanones, FumA, furoic acid) was well below 2.4%. The low yield of these products, especially SA and furanones, was rather unexpected: previous results obtained in the liquid phase oxidation of furfural with H_2O_2 yielded a wider variety of products including SA and furanones.[15–19] It is concluded that the reaction mechanism when using TS-1 is different to that of the conventional acid catalysts used previously to conduct this reaction. When acid catalysts

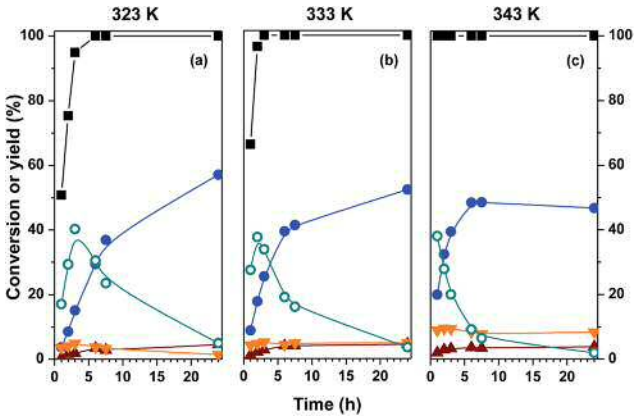

Fig. 1 Effect of reaction temperature on the catalytic properties of TS-1 at three different temperatures: (a) 323 K, (b) 333 K and (c) 343 K. Reaction conditions: 4.6 wt% of furfural, 2.3 wt% of catalyst, 12.3 wt% of H_2O_2, equivalent to a H_2O_2/F mol ratio = 7.5. Symbols: furfural conversion (■); 5-hydroxy-furan-2(5*H*)-one yield (○); maleic acid yield (●); formic acid yield (▼); and malic acid yield (▲).

are used, the reaction initiates with a Bayer–Villiger step to form 2-hydroxyfuran, which is in equilibrium with furan-2(5*H*)-one and furan-2(3*H*)-one (see Scheme SI1†). The eventual oxidation of these furanones gives rise to SA, hydroxyfuranone and MA. Therefore, it appears that when reaction initiates with a Baeyer–Villiger oxidation, a wider distribution of products is obtained.[15–19] This is not the case with TS-1. We will return to these points when discussing the reaction mechanism below.

It was also assumed that formic acid arises both from the deep oxidation of the organics and from the loss of formic acid required to convert a C_5 chemical into a C_4 compound.[19] Accordingly, the FA yield was calculated by subtracting the FA supposedly released by the formation of C_4 products (1 mol of FA per mol of C_4 product) from the total molar quantity of FA detected (the molar quantity of FA formed by deep oxidation was divided by 5 to express the value on a furfural basis). As shown in further figures, the carbon balance can approach 100% under optimum reaction conditions, but for the reaction conditions used in Fig. 1, the carbon balance was always below 100%. In principle, this incomplete carbon balance may be due to the total oxidation to CO_2 (not quantifiable by HPLC analysis). However, this is not the only possibility, and the formation of HPLC-silent products can also contribute to the incomplete carbon balance. The carbon balance improved as the reaction progressed, suggesting that these unidentified HPLC products may be (partially oxidised) intermediates of the reaction.

As expected, the rate of furfural conversion increased upon raising the reaction temperature. Thus, at 323 K, full furfural conversion was reached after 6 h, whereas only 3 h was required for 333 K and 1 h was enough at 343 K. A rapid perusal of the figures also indicates that at short reaction times, hydroxyfuranone predominates among the detected products, but for longer periods, MA is the major product. It has been previously suggested that MA is formed at the expense of hydroxyfuranone oxidation; in our experiments at 323, 333 and 343 K, the hydroxyfuranone yield reached a maximum (close to 40%) at 3,

2 and 1 h, respectively, while MA yield continuously rose, indicating that the latter is not a primary product.[19] A remarkable result is that the maximum yield of MA (57%) was achieved at 323 K after 24 h of reaction, whereas at higher reaction temperatures, the yield decreased. Thus, the maximum yield at 333 K was 52% (for 24 h), and the maximum at 343 K was 49% (for 6 h). For longer reaction times at 343 K, the MA yield visibly decreased.

In a reaction pathway compatible with the results of Fig. 1, furfural is rapidly oxidised through unknown intermediates to hydroxyfuranone: a C_1 species (formic acid) is released to form the C_4 product. Hydroxyfuranone is subsequently oxidised to MA. In addition, furfural and all the other organic products can undergo deep oxidation to formic acid and to CO_2.

In summary, for the reaction temperatures tested, 323 K results in the maximum MA yield. This was the reaction temperature selected for further studies. We discarded lower temperatures because the reaction rates would be very slow. Similar conclusions can be reached by working at lower H_2O_2 concentrations at the three different temperatures tested (results included in Fig. SI2 of the ESI†).

H_2O_2 concentration effect. Fig. 2 shows the effect of hydrogen peroxide concentration on the catalytic properties. Three different H_2O_2 concentrations were tested (6.6, 12.3 and 24.6 wt%), equivalent to H_2O_2/furfural mol ratio of 4, 7.5 and 15, respectively. The remaining reaction parameters were kept constant (4.6 wt% of furfural, 2.3 wt% of catalyst and 323 K). The hydrogen peroxide concentration was in excess of the stoichiometric amount required for the oxidation of furfural to MA, which is H_2O_2/MA (mol mol^{-1}) = 3. The larger the H_2O_2 concentration, the faster the furfural conversion rate. For the highest H_2O_2/furfural mol ratio tested, which was 15, full furfural conversion was attained in just 2 hours of reaction, whereas 3 h was needed for H_2O_2/furfural mol ratio = 4.

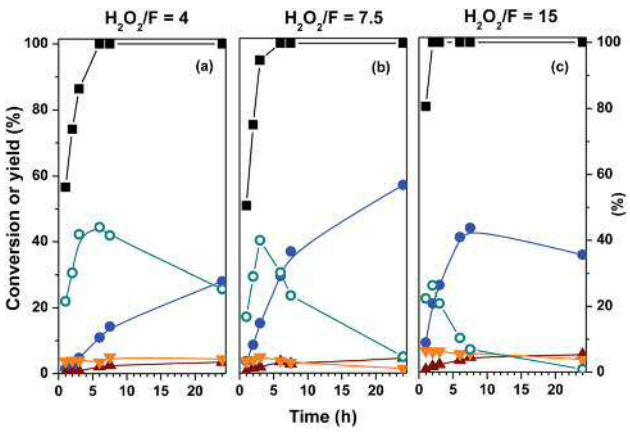

Fig. 2 Effect of H_2O_2 concentration on the catalytic properties of TS-1 for three different H_2O_2/furfural mol ratios (4, 7.5 and 15), corresponding to (a) 6.6, (b) 12.3 and (c) 24.6 wt% of H_2O_2. Reaction conditions: 4.6 wt% furfural, 323 K, 2.3 wt% catalyst. Symbols: furfural conversion (■); 5-hydroxy-furan-2(5*H*)-one yield (○); maleic acid yield (●); formic acid yield (▼); and malic acid yield (▲).

As regards the transformation to oxidised C_4 compounds, the major detected products were hydroxyfuranone and maleic acid; the combined yield of FA and malic acid was smaller than 9%. The yields of the remaining products was smaller than 2%. For H_2O_2/furfural mol ratio = 4, the MA formation rate was slower than that at 7.5; thus, after 24 h of reaction, only a 28% MA yield was reached, whereas for a ratio of 7.5, the yield was 57%. In principle, one might assume that a H_2O_2/furfural mol ratio > 7.5 would result in a better MA yield, and at short reaction times (time < 7.5 h) in these conditions, the formation rate of MA is substantially faster (at the expense of a faster disappearance of hydroxyfuranone). However, the MA yield attains a maximum yield of 44% at 7.5 h of reaction, and after 24 h of reaction it decreases to 36%. The high hydrogen peroxide concentration results in an overoxidation of MA.

In summary, an excess of H_2O_2 with respect to the stoichiometric amount for furfural oxidation to MA is needed to improve the MA yield. The optimum H_2O_2/furfural mol ratio is approximately 7.5; lower ratios result in lower reaction rate, and larger ratios result in overoxidation. Similar conclusions were obtained when conducting similar experiments to those presented in Fig. 2, but with a larger catalyst concentration (4.6 wt%). The results are presented in Fig. SI3 of the ESI section.†

Catalyst loading effect. The effect of catalyst loading on catalytic properties is depicted in Fig. 3: experiments were conducted by changing the catalyst concentration and keeping constant the reaction temperature (323 K), the furfural concentration (4.6 wt%), and the H_2O_2 concentration (12.3 wt%, H_2O_2/furfural mol ratio = 7.5). When no catalyst was incorporated, the furfural conversion rate was lower than when catalysed with TS-1; SA and furan-2(5*H*)-one were the major products detected; FumA and FurA were also observed but with a yield lower than 4 and 6%, respectively; and the MA yield was negligible except at 24 h of reaction. This behaviour is compatible with a self-catalysed reaction, following a reaction mechanism in which the first step is the Baeyer–Villiger oxidation of furfural to 2-hydroxyfuran. A similar situation was found for other experiments conducted without TS-1 catalyst but with lower and higher H_2O_2 concentrations: SA and furan-2(5*H*)-one were the major products (see Fig. SI4 in the ESI†). The addition of 1.2 wt% of catalyst substantially accelerated the furfural conversion rate and, more importantly, remarkably modified the yield pattern of the obtained products: the yields of SA and furanone significantly decreased and became negligible, whereas MA and hydroxyfuranone were the major products.

The incorporation of more catalyst intensifies this effect, and thus, for a catalyst concentration of 4.6 wt% (TS-1/furfural wt. ratio = 1), a MA selectivity close to 80% was attained for 24 h of reaction, with residual formation of malic and formic acids. It must be stressed that, for the latter specific reaction conditions, the carbon balance was close to 100% for all aliquots analysed throughout the kinetic experiments. The latter suggests that for a catalyst concentration lower than 4.6% a carbon balance smaller than 100% would be very likely due to the formation of undetectable intermediates. On the other hand, a larger catalyst concentration (9.2 wt%) resulted in the overoxidation of MA,

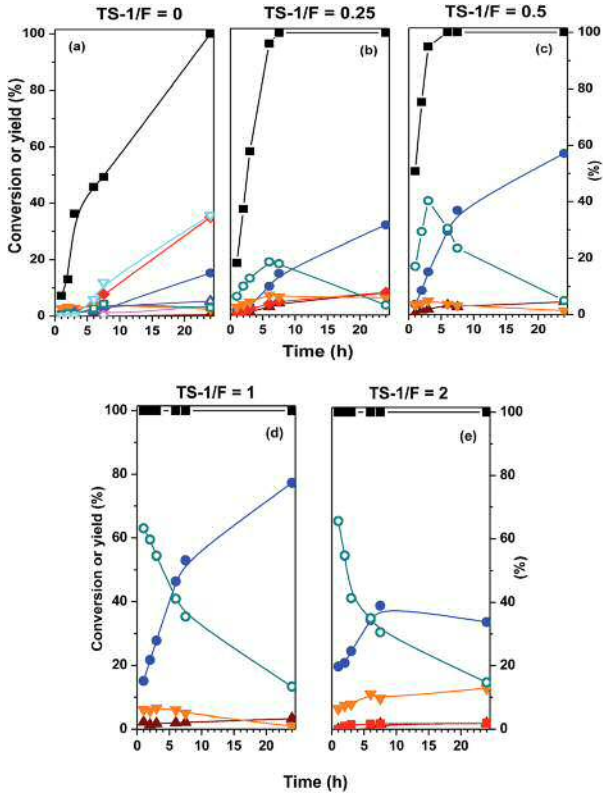

Fig. 3 Effect of catalyst loading (wt%) on the catalytic properties of TS-1: (a) 0 wt%; (b) 1.2 wt%; (c) 2.3 wt%; (d) 4.6 wt%; (e) 9.2 wt%. Reaction conditions: 4.6 wt% furfural, 323 K and H_2O_2/F = 7.5, which correspond to 12.3 wt% H_2O_2. Symbols: furfural conversion (■); 5-hydroxy-furan-2(5*H*)-one yield (○); maleic acid yield (●); formic acid yield (▼); malic acid yield (▲); furan-2(5*H*)-one yield (▽); succinic acid yield (◆).

very likely to CO_2, as can be deduced from the lower MA yield, larger FA yield and incomplete carbon balance.

Effect of concentration of furfural in aqueous solution. Fig. 4 shows the effect of furfural concentration on conversion and yields; the reaction temperature, H_2O_2/furfural mol ratio and TS-1/furfural wt ratio were kept constant at 323 K, 7.5 and 1, respectively. In this figure, the conversion and selectivity of H_2O_2 during the course of the reaction is also included. H_2O_2 conversion % indicates the ratio of the total H_2O_2 consumed to the initial H_2O_2 loaded, whereas the selectivity is the ratio of the mol% of H_2O_2 consumed to produce the C_4 organic compounds detected by HPLC analysis to the mol% of H_2O_2 actually consumed (the amount theoretically consumed to produce FA is not included in this quantity). Except for the experiment conducted with 9.2 wt% of furfural, the carbon balance was essentially well above 90% in all experiments. This indicates that most of the organic products were detected by HPLC in this series of experiments, and consequently, the deviation of the H_2O_2 selectivity from 100% is an indication of the unselective conversion (decomposition) of H_2O_2.

H_2O_2 consumption is very selective at the beginning of the reaction when hydroxyfuranone predominates. However, as the reaction proceeds, selectivity worsens, indicating that a large fraction of H_2O_2 is consumed in unselective transformations.

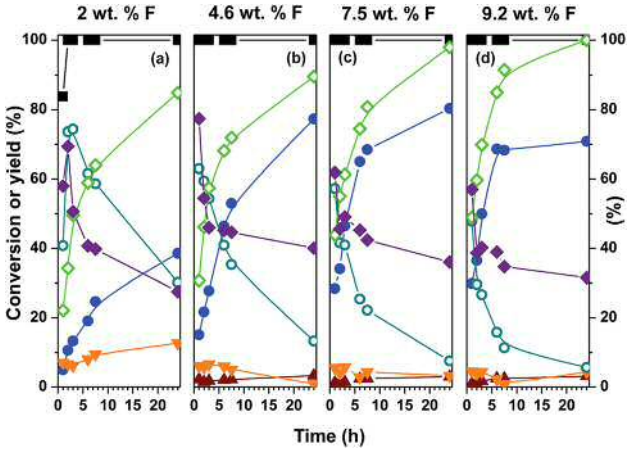

Fig. 4 Effect of furfural concentration (wt%) on the catalytic behaviour of TS-1: (a) 2 wt%; (b) 4.6 wt%; (c) 7.5 wt%; and (d) 9.2 wt% of furfural. Reaction conditions: 323 K, TS-1/F wt ratio = 1; H_2O_2/F mol ratio = 7.5. Symbols: furfural conversion (■); 5-hydroxy-furan-2(5*H*)-one yield (○); maleic acid yield (●); formic acid yield (▼); malic acid yield (▲); H_2O_2 conversion (◇); H_2O_2 selectivity (◆).

Thus, when 4.6 wt% of furfural is used (Fig. 4b), for 1 h of reaction, the selectivity of the H_2O_2 devoted to produce C_4 compounds is close to 80%, and as the reaction progresses, the selectivity continuously decreases down to a value of 40% after 24 h of reaction. Similar trends can be observed for the remaining experiments in Fig. 4. Formic acid formation partly explains the unselective transformation of H_2O_2, but there are other unselective routes; we will address this point in Section 3.3.

Regarding MA selectivity, a very remarkable result is that for reaction times shorter than 7.5 h, the furfural concentration clearly has a very positive effect on the MA yield. Thus, the MA yield after 7.5 h of reaction is 25, 53, 68 and 69% for 2, 4.6, 7.5 and 9.2 wt% of furfural, respectively. The intrinsic MA formation rate was calculated after 1 h of reaction to take into account the fact that the catalyst concentration also increases throughout the series of experiments (furfural/TS-1 ratio was kept constant). The intrinsic rate was found to be 0.14, 0.44, 0.82 and 0.87 μmol of furfural g_{cat}^{-1} s^{-1} for 2, 4.6, 7.5 and 9.2 wt% of catalyst, respectively. Therefore, the intrinsic MA reaction rate also rises with furfural concentration, which means that the effect is due to the increase of furfural concentration. An explanation could be that as the furfural concentration rises, so does the relative surface furfural coverage with respect to other reactants. In any case, the increase in both the MA yield and formation rate levels off for furfural concentrations larger than 7.5 wt%. Moreover, when 9.2 wt% of furfural is used, overoxidation of MA is evident for longer reaction times; thus, for 24 h of reaction, the MA yield (71% yield) is smaller than that for the 4.6 and 7.5 wt% experiments (78 and 80% yields, respectively). The overoxidation of products in the 9.2 wt% experiment is also evident by the stronger deviation of the carbon balance, to a value notably lower than 100%.

In summary, we can conclude that among all the reaction conditions tested, the optimum reaction conditions to obtain

the highest MA yield (80%) are those used in Fig. 4b and c: 323 K, between 4.6–7.5 wt% of TS-1, TS-1/furfural wt ratio = 1; H_2O_2/furfural mol ratio = 7.5 and 24 h of reaction.

Comparison with other solid catalysts and reaction mechanisms

Fig. 5 compares the catalytic behaviour of TS-1 with other selected catalysts. Reaction conditions, indicated in the caption, were selected to obtain a high MA yield with TS-1. Ambelyst 70, a sulphonic resin, was chosen because of its proven capacity to catalyse furfural oxidation to C_4 diacids.[15,16,19] ZSM-5, a Ti-free zeolite with acid sites, was tested because it presents the same MFI-like silica framework as TS-1. Finally, anatase, which has also been detected to be present in the TS-1 as a result of deficient insertion of Ti within the MFI-like framework, was also investigated.

Amberlyst 70 displayed an oxidation activity pattern typically catalysed by strong acids and a wide number of products can be obtained.[15,16,19] Succinic acid, furan-2(5*H*)-one and maleic acid are mainly formed, hydroxyfuranone, and malic, fumaric and formic acids are also detected at non-negligible yields, especially at shorter reaction times. After 24 h of reaction, the yield of SA, furan-2(5*H*)-one and MA was approximately 50, 30 and 20%, respectively. Although the ZSM-5 zeolite presents acid sites on its surface, these sites are not as active as those of TS-1 or as the sulphonic sites of Amberlyst 70. The latter presents a comparatively large strong-acid-site concentration (2.55 mmol g_{cat}^{-1}),[19] which explains its relatively high activity. ZSM-5 displays an activity pattern resembling that of a catalyst-free run (see Fig. 3a). After 24 h of reaction, an MA yield of 15% and SA yield of 30% was observed for ZSM-5. Accordingly, the catalytic activity of TS-1 cannot be associated to acid sites present in the MFI-framework of TS-1, but rather to the presence of Ti(IV) sites in the TS-1. Anatase presents very active sites, but the Ti sites in anatase are not as selective as framework Ti in TS-1: the H_2O_2 efficiency is lower, the carbon balance is incomplete and the MA yield is lower (MA yield of 31% was observed after 24 h of reaction). These latter results suggest that Ti sites in anatase are not responsible for the good behavior of TS-1. In summary, among the family of catalysts tested, TS-1 features a high activity and selectivity to MA.

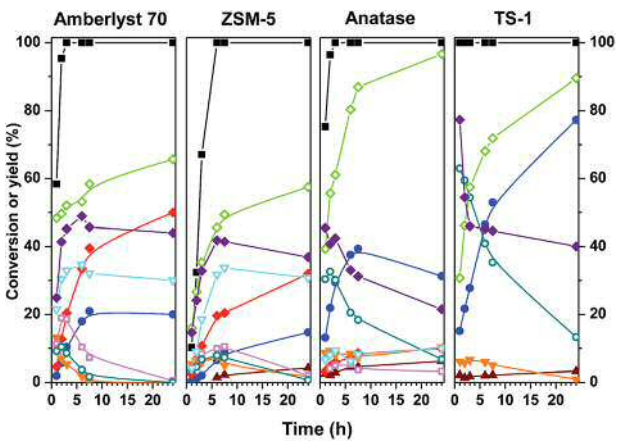

Fig. 5 Catalytic activity of the different catalysts tested: (a) Amberlyst 70; (b) ZSM-5; (c) Anatase; and (d) TS-1. Reaction conditions: 4.6 wt% furfural, 4.6 wt% catalyst, 323 K, H_2O_2/F = 7.5, which corresponds to 12.3 wt% H_2O_2. Symbols: (■) furfural conversion; 5-hydroxy-furan-2(5*H*)-one yield (○); maleic acid yield (●); formic acid yield (▼); malic acid yield (▲); furan-2(5*H*)-one yield (▽); succinic acid yield (◆); fumaric acid yield (□); H_2O_2 conversion (◇); H_2O_2 selectivity (◆).

A proposal of the reaction mechanism for oxidation using TS-1 catalyst. The first characteristic of the performance of TS-1 is the low selectivity for succinic acid and furan-2(3*H*)-one with respect to values obtained with sulphuric acid, sulphonic resins or poly(-styrene sulphonic acid).[15–18,29] This strongly suggests that the reaction with TS-1 goes through a different mechanism. It is accepted that, when using catalysts possessing sulphonic acid sites, the reaction starts with a Baeyer–Villiger step (see Scheme SI1†). Fig. SI6† and the discussion therein demonstrate that, when using TS-1, furfural oxidation does not start with a Baeyer–Villiger oxidation.

It has been reported that furan can be oxidised very selectively with hydrogen peroxide to maleic dialdehyde[21] or to hydroxyfuranone[22] by using a H_2O_2/furfural mol ratio of 1 and 2, respectively. The latter can eventually be oxidised to MA. Therefore, if furan could be formed from furfural, the oxidation of furan would yield MA, provided that a H_2O_2/furfural ratio > 2 is used.

One possibility is that the reaction starts with the oxidation of furfural to furoic acid, which can subsequently be transformed to furan by releasing formic acid (see Scheme SI2 in the ESI† for a description of this mechanism proposal). However, this possibility can be discarded because when the oxidation of furoic acid with H_2O_2 was conducted by using TS-1 (at 323 K, 4.6 wt% of furoic acid, 4.6 wt% of TS-1 and a H_2O_2/furoic acid mol ratio of 7.5, equivalent to 12.3 wt%) the MA yield was much lower than that obtained with furfural (see Fig. SI7 in the ESI† for further details).

Another plausible possibility is that furan can be formed by the decarbonylation of furfural. However, the decarbonylation of furfural requires different catalysts and reaction conditions to proceed,[30–32] and therefore this route can also be discarded.

We propose a different mechanism based on the results and on the proposal of Jacobs *et al.* when oxidising furan to maleic dialdehyde.[21] They proposed that one of the double bonds in the furan ring is epoxidised and the thus-formed epoxide then rapidly rearranges, yielding unsaturated 1,4-dicarbonyl compounds. The same epoxidation and rearrangement steps can be applied to furfural (see Scheme 1): the double bond with less steric hindrance is selectively epoxidised, and the furfural-epoxide rapidly undergoes a rearrangement to yield the *Z*-4-oxopent-2-enedial. The loss of a carbon atom is still needed for the formation of the corresponding C_4 derivative. We propose that the formation of a C_4 intermediate occurs *via* Baeyer–Villiger oxidation of the aldehyde functionality at 1-position of the *Z*-4-oxopent-2-enedial. An ester is formed, which is rapidly hydrolysed to form β-formylacrylic acid ((*Z*)-4-oxobuten-2-enoic acid), releasing formic acid. The electron withdrawing nature of the acyl group directly bonded to the reacting aldehyde at C1 strongly increases its electrophilicity favoring the Baeyer–

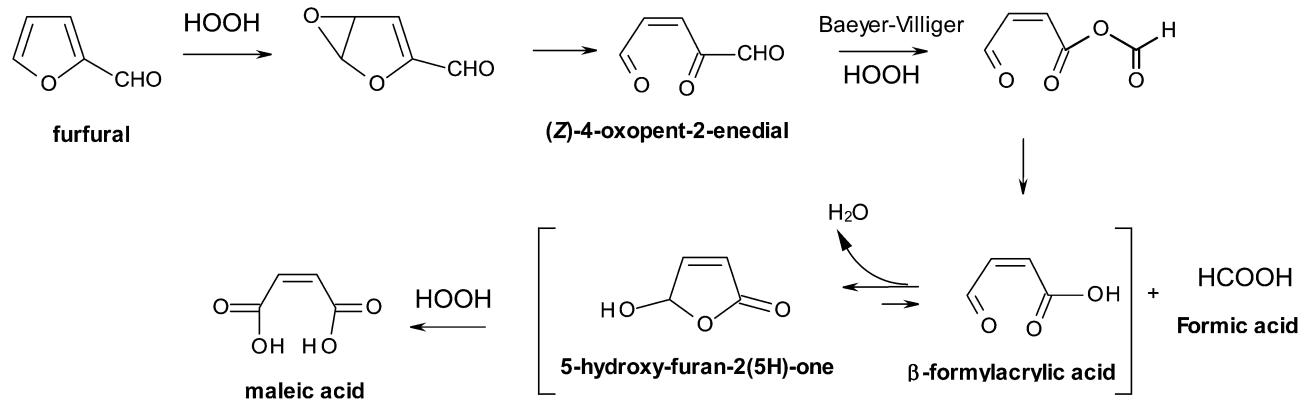

Scheme 1 Proposal of mechanism via epoxidation of the furan ring and subsequent release of formic acid.

Villiger reaction and justifying the regioselecctivity of the process. Formylacrylic acid is in equilibrium with the hydroxyfuranone. Experimentally, the formation of MA parallels the consumption of hydroxyfuranone. This suggests that hydroxyfuranone can be directly oxidised to MA. However, it cannot be excluded that MA is formed by the oxidation of β-formylacrylic, in equilibrium with hydroxyfuranone. We could not identify any HPLC peak as β-formylacrylic, very likely because the equilibrium is strongly shifted to hydroxyfuranone. It is also possible that the former is present at very low concentration, and therefore difficult to detect by HPLC, but still involved as an intermediate of the reaction. If so, whereas β-formylacrylic is consumed by oxidation to MA, so must be hydroxyfuranone.

Improvement in selective utilisation of H_2O_2 using a two-step process

In principle, there are three routes to convert H_2O_2: conversion to organic products (including formic acid), catalytic decomposition and uncatalysed thermal decomposition. Blank experiments (see Fig. SI5 in the ESI† and discussion therein) allowed us to conclude that (i) although TS-1 catalytically decomposes H_2O_2, the decomposition is remarkably inhibited by the presence of furfural, especially at short reaction times and (ii) thermal decomposition is less than 20% after 24 h of reaction. This has practical implications when searching for further improvements in the selective utilisation of hydrogen peroxide: first, catalytic decomposition is very low at short reaction times, and second, the thermal decomposition of H_2O_2 is as important as catalytic decomposition.

The stoichiometric H_2O_2/furfural mol ratio required to selectively oxidise furfural to MA is 3. The maximum yield to MA was achieved by using a mol ratio = 7.5, which is more than double the stoichiometric ratio. The unselective utilisation of H_2O_2 comes from thermal and catalytic decomposition. Interestingly, the results presented in Fig. SI5† indicate that the catalytic decomposition is seriously inhibited by the presence of furfural. At the beginning of the reaction, decomposition is practically negligible: only after 5 hours is the catalytic decomposition detectable.

On the other hand, when TS-1 is used as catalyst and at short reaction times, hydroxyfuranone is primarily produced, with a relatively selective utilisation of H_2O_2. Kinetic data show that furfural oxidation to hydroxyfuranone is very rapid and selective, even when lower H_2O_2/furfural mol ratios are used (see Fig. SI3a†). Therefore, a good strategy would be to conduct the oxidation in two steps; in the first step, to oxidise rapidly furfural to hydroxyfuranone using TS-1 and a H_2O_2/furfural mol ratio close to stoichiometry. For short reaction times, the unselective catalytic decomposition of H_2O_2 is prevented. In a subsequent step, the oxidation of hydroxyfuranone to MA will be conducted with another catalyst because TS-1 unselectively decomposes H_2O_2. Sulphonic-based catalysts have demonstrated a capacity to transform hydroxyfuranone to MA.[15,16,19]

In practice, we proceeded as follows: first, the oxidation of furfural to hydroxyfuranone was conducted by using TS-1 as catalyst with a H_2O_2/furfural mol ratio of 2.4 (2 mol of H_2O_2 are needed for the stoichiometric oxidation of furfural to hydroxyfuranone). Previous reactions with a low H_2O_2 concentration (Fig. SI3a† (H_2O_2/F mol ratio = 2.15)) showed that after 4 hours of reaction, the hydroxyfuranone concentration did not increase, most likely because of the total consumption of the H_2O_2. For that reason, this first reaction step was carried out for 4 h. After that, the TS-1 catalyst was filtered off and the second oxidation step was conducted by using an Amberlyst 70 sulphonic resin as a catalyst. Further addition of H_2O_2 was performed to obtain a H_2O_2/furfural mol ratio of 2 with respect to the initial furfural concentration. One mol of H_2O_2 is needed for the stoichiometric oxidation of hydroxyfuranone to maleic acid, so a small excess of H_2O_2 was incorporated to account for non-selective decomposition. To prevent the dilution of the reaction media, a 70 wt% H_2O_2 solution was used to incorporate H_2O_2 in this second step. Fig. 6 displays the results obtained by taking samples at different reaction times. Products yields are calculated with respect to the initially loaded furfural.

After 4 h, the oxidation of furfural with TS-1 resulted in a 70% hydroxyfuranone yield, while the yield of maleic acid was less than 10%. However, once the TS-1 was filtered off and Amberlyst 70 and further H_2O_2 were incorporated, the selective

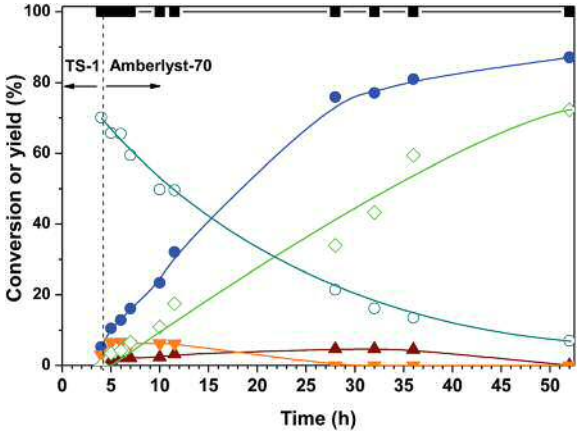

Fig. 6 Consecutive two-step oxidation of furfural with TS-1 and Amberlyst 70. Reaction conditions: 4.6 wt% furfural, 323 K and 4.6 wt% of catalyst for each step. Symbols: furfural conversion (■); 5-hydroxyfuran-2(5*H*)-one yield (○); maleic acid yield (●); formic acid yield (▼); malic acid yield (▲); and H_2O_2 conversion (◇).

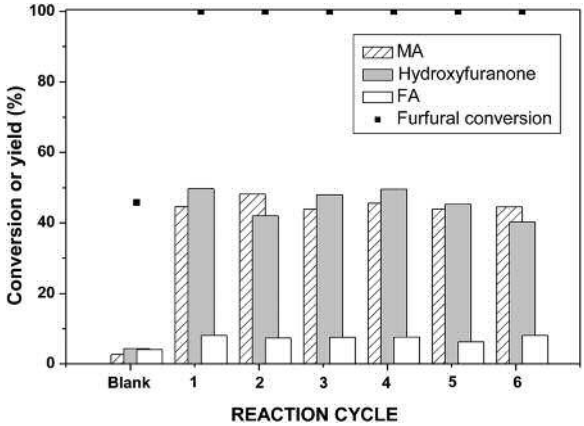

Fig. 7 TS-1 catalyst reutilisation tests for aqueous solution of furfural (4.6 wt%), 323 K, H_2O_2/F mol ratio = 7.5, corresponding to 6.6 wt% of H_2O_2, 4.6 wt% catalyst and 7 h reaction.

oxidation of hydroxyfuranone to maleic proceeded continuously, and after 24 h of reaction with Amberlyst (equivalent to 28 h of total reaction time), the MA yield was close to 76%, very close to that obtained after 24 h with TS-1 (78%). The MA yield reached almost 90% after 2 days with Amberlyst. These results therefore demonstrate that MA can be produced from furfural by a two-step catalyst process with high selective utilisation of both furfural and H_2O_2. The overall H_2O_2/furfural mol ratio was 4.4.

Stability of the TS-1 catalyst

To evaluate the stability of the TS-1 catalyst in the oxidation of furfural, two different experiments were conducted. First, successive reutilisation runs were performed with aqueous solutions of pure furfural distributed by laboratory chemical suppliers. In another set of experiments, the stability of the catalysts was tested with furfural aqueous solutions obtained from biomass (corncobs).

Regarding the aqueous solution of pure furfural, successive reutilisation runs were carried out after 7 h of reaction, with a catalyst and furfural content of 4.6 wt% and a H_2O_2/furfural molar ratio of 7.5, corresponding to 12.3 wt% H_2O_2. The catalyst was filtered off and dried before each new run (see Experimental section for details). Medium-term reaction times (7 h) are more sensitive to detect the deactivation processes. Longer reaction times may miss the deactivation if the deactivation is not very intense. Fig. 7 shows the results obtained after 6 reutilisation cycles. The conversion and the yields of the main products are represented (MA, 5-hydroxyfuranone and FA). The results of a blank experiment without TS-1 catalyst are also included (first column): much lower values for the conversion and yields to selective oxidation products were obtained in this blank test.

When TS-1 was reused, the conversion values remained at 100% throughout all the runs. Moreover, the yields of MA, hydroxyfuranone and formic acid remained quite similar for all the runs investigated; MA yields were between 43–48% and hydroxyfuranone between 40–50%. Attending to these results, we can conclude that when commercial furfural is used, TS-1 is quite stable, and no sign of deactivation could be observed for at least 6 cycles.

Reutilisation runs were also conducted by using aqueous furfural solutions obtained from lignocellulosic biomass. Briefly, furfural was obtained from corncobs by using Amberlyst 70 as catalyst, at 453 K, 19 bar and by using a N_2 flow of 150 mL min^{-1} (STP) to strip the water-furfural vapour stream. Stripping of furfural by N_2 results in the rapid extraction of furfural from the reaction mixture, which prevents furfural from being consumed in further secondary reactions in the liquid phase. This furfural stream is condensed to separate gases from the aqueous furfural solution. Further details of the procedure can be found elsewhere.[33,34] The furfural concentration of this aqueous solution was determined to be 2.5% (GC analysis). Other impurities like acetic acid and 5-methyl-furfural were also detected by GC-MS. The results obtained after successive reutilisation runs at 323 K, 24 h of reaction, H_2O_2/furfural mol. ratio = 7.5 and catalyst/furfural wt ratio = 1 are displayed in Fig. 8. The actual furfural concentration in the reaction media was 2 wt%, and at this relatively low concentration of furfural, the rates of furfural conversion and MA formation are lower than those found when the optimum reaction conditions are set (see Fig. SI8 in the ESI† for the kinetics of oxidation when this biomass furfural solution was used, and see also Fig. 4a for the kinetic curve of commercial furfural at similar reaction conditions to those in Fig. 8). To obtain a measurable and relatively high MA yield (larger than 30%), a long reaction time is needed (24 h).

When aqueous furfural obtained directly from biomass is used, a slight but continuous deactivation of TS-1 can be observed. The deactivation is more visible in the MA yield, as the hydroxyfuranone yield remained above 40% for the first six runs (in the seventh run the yield dropped to 31%). It is also noteworthy that the formic acid yield slightly but inexorably increased upon reutilisation runs, which confirms that the selective oxidation sites of TS-1 are being deteriorated by the

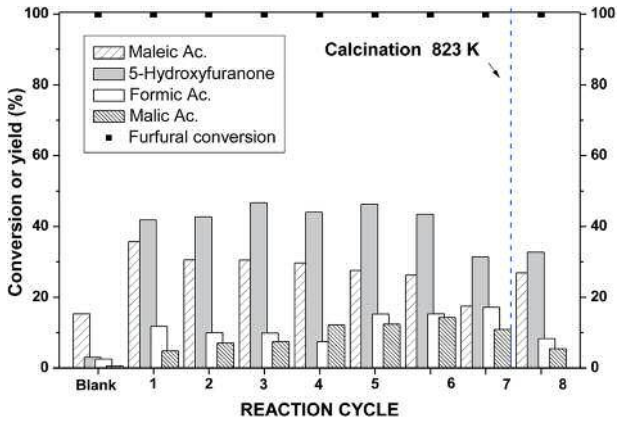

Fig. 8 Reutilisation experiments for aqueous furfural solution obtained from biomass. Reaction conditions: 2 wt% furfural, 323 K, $H_2O_2/F = 7.5$, which corresponds to 5.3 wt% H_2O_2, and 2 wt% catalyst, 24 h.

utilisation of real furfural. All these results strongly suggest that the impurities present in the real aqueous furfural derived from biomass have a detrimental effect on the deterioration of TS-1. The removal of these impurities from biomass-derived furfural aqueous solutions is recommended to prevent the deterioration of TS-1.

After the 7th run, the used TS-1 was filtered off, dried at 323 K overnight and finally calcined at 823 K in an oven under air for 3 hours. This calcined catalyst was again used for an additional 8th run, and the MA yield was partially restored. This indicates that the deactivation of TS-1 is partially due to the deposition of organic products derived from these impurities, which are removed by calcination. Other sources of deactivation will be discussed below.

These contaminants must be removed when considering an industrial application. As indicated in the Introduction, a double distillation is required to purify furfural.[1] The first distillation removes impurities and an azeotrope with 35% of furfural is yielded. The second distillation column further removes water and results in pure and very concentrated furfural.

The double distillation may compromise seriously the economic viability of the process here described. Possible solutions to reduce the cost and energy consumption can be the following. The azeotrope free of contaminants can be used for the oxidation to MA, preventing the use of the second distillation column. In practice the furfural–water azeotrope is condensed before entering the second vacuum distillation column and two phases are formed: a rich furfural phase (which is that readily further distilled) and a poorer aqueous furfural stream. Another solution could be that the latter diluted stream, free of contaminants, could be withdrawn and used in the oxidation to MA, leaving the concentrated furfural for processes requiring very concentrated and free of contaminants furfural.

Characterisation of fresh and used catalyst

Fresh and used catalysts after several reaction cycles were characterised by different techniques with the intention of identifying the possible physico-chemical changes occurring during utilisation. Laser Raman spectra of fresh and used catalyst samples using a 523 nm laser are represented in Fig. 9. The used catalyst after 6 runs with pure furfural is represented in Fig. 7. Samples were previously calcined *in situ* in the cell by flowing synthetic air at 823 K for 30 min. This treatment is required because hydrocarbonaceous species remain adsorbed on the catalyst after utilisation, which precludes the recording of good quality Raman spectra due to the fluorescence phenomenon associated with these C-containing residues (see Fig. SI9 in the ESI†).

Raman bands at 290, 380, 437, 469, 815, 837, 960 and 1125 cm^{-1} that have been previously reported for TS-1 are clearly observed in the Raman spectra of Fig. 9; the features at 960 and 1125 cm^{-1} demonstrate the substitutional Ti(IV) insertion within the silica framework: they have been assigned to the stretching Ti–O–Si vibrations of inserted TiO_4 tetrahedra (respectively, in-phase and out of phase antisymmetric stretching of the four connected Ti–O–Si bridges).[35–38] The bands detected at 144, 515 and 637 cm^{-1} correspond to Raman features of anatase (TiO_2); there must be another anatase-derived band at 390 cm^{-1}, but it is overshadowed by the most intense band of TS-1 at 380 cm^{-1}. Visible Raman spectroscopy is very sensitive to extraframework titanium oxide species and therefore is an excellent probe for the detection of very small TiO_2 domains. Therefore, these bands demonstrate the presence of extraframework Ti and that not all the Ti cations are inserted within the zeolite framework.

No large differences can be detected between the spectra from fresh and used catalysts, which suggests that TS-1 is essentially unaltered by the utilisation of the catalyst in the reaction medium. Nevertheless, a closer examination (see inset in the figure) indicates that the TiO_2 band at 144 cm^{-1} is apparently less intense, which could suggest that there may be some leaching during the utilisation as catalyst.

Chemical analyses by TXRF were conducted to confirm the leaching. Ti and Si were analysed in both the fresh and used solids and in the liquid phase after each reaction run, the latter

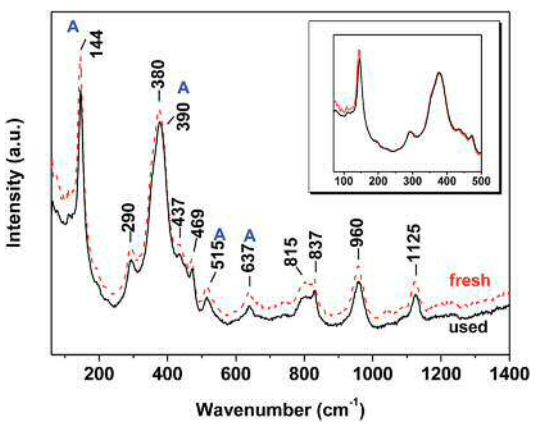

Fig. 9 Visible laser Raman spectra of fresh (dashed) and used (continuous) catalysts after *in situ* calcination at 823 K for 30 min in synthetic air. A denotes Raman bands from the anatase phase.

Table 1 Summary of TXRF results of fresh and used catalysts and in the liquid reaction mixtures after successive reaction cycles

Catalyst	Si/Ti at. ratio in solid		Amount of metal leached to the reaction mixture (mg) Run 1[b]	Run 2[b]	Run 3[b]	Run 4[b]	Run 5[b]	Run 6[b]	Run 7[b]
Used with comm. furfural	31 (25.5)[a]	Ti	3.51 (11.2%)	0.96 (3%)	0.41 (1.3%)	0.47 (1.5%)	0.56 (1.8%)	0.36 (1.1%)	—
		Si	0.31 (0.03%)	0	0	0	0	0.27 (0.03%)	—
Used with biomass-derived furfural	29.4 (25.5)[a]	Ti	2.29 (15.4%)	0.46 (3.1%)	0.28 (1.9%)	0.28 (1.9%)	0.21 (1.4%)	0.24 (1.6%)	0.20 (1.3%)
		Si	0.48 (0.13%)	0.52 (0.14%)	0	0.31 (0.81%)	0.16 (0.04%)	0	0

[a] Si/Ti at. ratio of fresh sample. [b] Values between brackets represent the metal leached during the run cycle with respect to the total amount of metal initially present in the solid (expressed as wt%).

case for runs conducted with commercial and biomass-derived furfural. Table 1 summarises the results of TXRF.

The Si/Ti at. ratio of the catalyst used with the commercial furfural is clearly higher than that of fresh catalyst, which indicates that Ti was leached during the six utilisation runs. The same conclusion may be reached by examining the Ti concentration in the liquid reaction mixture. Most of the Ti is leached during the first run (*ca.* 56% of the total Ti leached), and the impact of lixiviation seems to decline upon reutilisation. Si leaching also takes place, although to a much smaller degree, and in some cases below the detection limit of the technique: Ti leaching represents *ca.* 20% of the initial Ti content, whereas Si leaching accounts for less than 0.1% of the initial Si.

The former TXRF analyses also suggest that the contribution of the leached species to the overall activity is not relevant. In the first run 3.5 mg of Ti was leached to the reaction medium, whereas for the 3rd and successive runs the amount of Ti leached was much smaller (around 0.4–0.6 mg). If the leached homogeneous Ti species would have a significant contribution to the overall activity, the total activity of the latter runs would have been appreciably smaller than that of the first run, and not similar.

The same analyses were carried out with furfural from biomass. As with commercial furfural, Ti is leached in all reaction cycles, especially after the first one. When considering the relative amount of Ti losses in successive runs, we have to take into account that the loading of catalyst for the experiments with biomass-derived furfural was smaller (2 wt%) than that used with commercial furfural (4.6 wt%). In this case, the aggregate loss of Ti represents *ca.* 27% of the total Ti. This slight increase in the leached Ti may be due either to the longer contact time between the furfural and catalyst (when using furfural from biomass, each run takes 24 hours) or to some of the products detected with the furfural from biomass (dihydroxyacetone, acetic acid, and 5-methyl-2-furancarboxaldehyde) that could promote Ti leaching. As for pure furfural, most of the Ti is leached (*ca.* 58%) during the first run. Si leaching also takes place to a slightly higher extent than with "commercial" furfural: Ti leaching represents *ca.* 27% of the initial Ti content, whereas the leached Si accounts for less than 0.4% of the initial Si.

The leaching of Ti is also evidenced by the comparison of the XPS spectra of fresh and used TS-1 catalyst. Fig. 10 compares the Ti 2p core level of both samples, and Table 2 summarises the main chemical parameters deduced from the XPS analyses. The Ti 2p core level was deconvoluted into two contributions; one is represented by the Ti $2p_{3/2}$ peak at 459.8 ± 0.1 eV, and other is represented by the Ti $2p_{3/2}$ contribution at 458.6 ± 0.2 eV (the corresponding Ti $2p_{1/2}$ levels are at located at 5.7 eV higher BE). The first contribution was assigned to tetrahedral Ti(IV) incorporated in the silicalite framework (Ti_t), whereas that represented by the peak at 458.6 was assigned to octahedral Ti(IV) in anatase TiO_2 (Ti_o).[39–41] For very good fitting, a small contribution represented by the Ti $2p_{3/2}$ contribution at *ca.* 457.2 eV was required; this has been assigned to Ti(III) produced by the photoreduction of Ti(IV) within the XPS chamber, driven by the X-ray impact and the ultrahigh vacuum required to record the spectra.[40,41]

The first evidence of leaching arises from the comparison between the XPS Ti/Si ratios of fresh and used samples. The XPS Ti/Si ratio of used samples is 0.027, half the value of the fresh samples (0.052). Moreover, a comparison between the XPS and TXRF Ti/Si ratios of fresh and used samples indicates that the leaching process is very intense at the surface of the TS-1 crystallites. Thus, the XPS value of the fresh sample (0.052) is larger

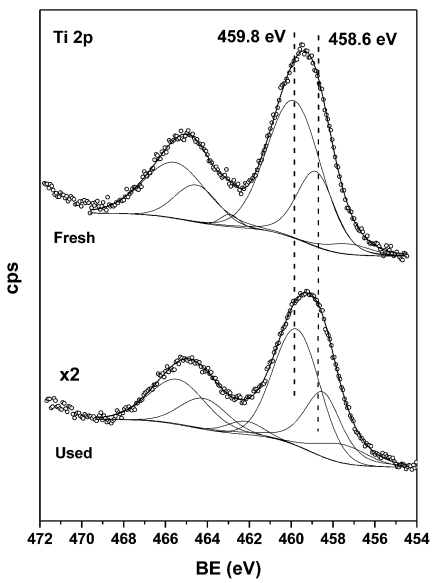

Fig. 10 Ti 2p core level of fresh and used TS-1 (with commercial furfural).

Table 2 Summary of XPS results in the fresh and used catalysts

	Ti 2p 3/2	Ti/Si	Ti_t/Si	Ti_o/Si
Fresh	459.9 (67.4%) 458.8 (28.5%) 457.2 (4.1%)	0.052 (0.039)[a]	0.035	0.015
Used	459.8 (57.0%) 458.5 (29.3%) 457.2 (13.7%)	0.027 (0.032)[a]	0.015	0.008

[a] Ti/Si determined from TXRF analysis.

than that determined by TXRF analysis (0.039), perhaps because anatase-like domains are present at the external surface of TS-1. However, the XPS Ti/Si value of the used sample (0.027) is smaller than that determined by TXRF (0.032), indicating the surface is no longer enriched in Ti and therefore that Ti leaching at the surface is very intense. Finally, the Ti leaching process affects both anatase Ti (Ti_o) and Ti inserted in the silicalite (Ti_t). Thus, the XPS Ti_o/Si ratio of the used sample is 0.008, *vs.* 0.015 for the fresh sample, and the XPS Ti_t/Si ratio of the used sample is 0.015, *vs.* 0.035 for the fresh sample.

Taking into account that 20% of Ti was leached upon reutilization, it is quite remarkable that no deactivation was observed when pure furfural is used for the reutilization experiments. A likely hypothesis is that outermost Ti is being leached and innermost active Ti sites remain to conduct the reaction. In this sense, the decrease observed upon reutilization of the surface at. Ti/Si by XPS (from 0.052 to 0.027, *ca.* 50% decrease) is larger than that observed for the bulk TXRF ratio (from 0.039 to 0.032, 18% decrease) indicating that leaching affects mainly to Ti cations located at the surface.

The leaching of Ti also seems to result in slight modifications of the long range order in the framework and in the textural properties of the TS-1: slight but visible modifications of the XRD reflections and of N_2 isotherms are evident when comparing the patterns of the fresh and used samples (see Fig. S10 and SI11 in the ESI† and the discussion therein for further details).

Conclusions

Titanium silicalite 1 (TS-1) selectively catalyses the aqueous phase oxidation of furfural to maleic acid by using H_2O_2 as an oxidant agent. A MA yield as high as 78 mol% was obtained under the identified optimum conditions: 4.6 wt% of furfural, 4.6 wt% of catalyst, a H_2O_2/furfural mol ratio of 7.5, corresponding to a 12.3 wt% of H_2O_2 and 24 hours of reaction at 323 K.

All the characterisation data confirm the existence of Ti leaching, which is also associated with a slight leaching of Si. This leaching is very intense during the first run but much less important in successive cycles and affects Ti both in anatase and within the silicalite framework.

Notwithstanding the leaching, when using pure commercial furfural, TS-1 could be reused for six runs without noticeable deactivation. When using furfural directly derived from biomass, weak but visible deactivation occurs upon reutilisation; this deterioration must be related to the presence of other organic products than furfural.

The amount of H_2O_2 required when using TS-1 is 2.5 times the value that is stoichiometrically needed. A very selective two-step process has also been demonstrated, which needs a H_2O_2/furfural mol ratio of 4.4, an amount of H_2O_2 much closer to the stoichiometric value (which is 3). This process involves the consecutive utilisation of TS-1 to selectively oxidise furfural to hydroxyfuranone, and consequently, once TS-1 is removed, Amberlyst 70 to catalyse the selective oxidation of hydroxyfuranone to MA.

Acronym list

FA	Formic acid
FumA	Fumaric acid
Hydroxyfuranone	5-Hydroxy-furan-2(5*H*)-one
MA	Maleic acid
MAN	Maleic anhydride
SA	Succinic acid

Acknowledgements

Financial support from Spanish Ministry of Economy and Competitiveness (CTQ2012-38204-C03-01) is gratefully acknowledged.

Notes and references

1 H. H. K. Lohbeck, W. Fuhrmann and N. Fedtke, in *Ullmann's Encyclopedia of Industrial Chemistry*, Weinheim, Germany, 2000, vol. 20, p. 463.
2 T. R. Felthouse, J. C. Burnett, B. Horrell, M. J. Mummey and Y.-J. Kuo, Maleic Anhydride, Maleic Acid, and Fumaric Acid, in *Kirk-Othmer Encyclopedia of Chemical Technology Online*, 2001.
3 S. Albonetti, F. Cavani and F. Trifirò, *Catal. Rev.: Sci. Eng.*, 1996, **38**, 413.
4 D. M. Alonso, S. Wettstein, M. A. Mellmer, E. I. Gurbuz and J. A. Dumesic, *Energy Environ. Sci.*, 2013, **6**, 76.
5 A. S. Mamman, J. M. Lee, Y. C. Kim, I. T. Hwang, N. J. Park, Y. K. Hwang, J. S. Chang and J. S. Hwang, *Biofuels, Bioprod. Biorefin.*, 2008, **2**, 438.
6 R. Karinen, K. Vilonen and M. Niemela, *ChemSusChem*, **2011**, **4**, 1002.
7 E. Mahmoud, D. A. Watson and R. F. Lobo, *Green Chem.*, 2014, **16**, 167.
8 E. R. Nielsen, *Ind. Eng. Chem.*, 1949, **41**, 365.
9 K. Rajamani, P. Subramanian and M. S. Murthy, *Ind. Eng. Chem. Prod. Res. Dev.*, 1976, **15**, 232.
10 M. S. Murthy and K. Rajamani, *Chem. Eng. Sci.*, 1974, **29**, 601.
11 D. R. Kreile, V. A. Slavinskaya, M. V. Shimanskaya and E. Y. Lukevits, *Chem. Heterocycl. Compd.*, 1972, **5**, 429.
12 N. Alonso-Fagúndez, M. López Granados, R. Mariscal and M. Ojeda, *ChemSusChem*, 1984, **5**, 1984.

13 H. Guo and G. Yin, *J. Phys. Chem. C*, 2011, **115**, 17516.
14 S. Shi, H. Guo and G. Yin, *Catal. Commun.*, 2011, **12**, 731.
15 H. Choudhary, S. Nishimura and K. Ebitani, *Appl. Catal., A*, 2013, **458**, 55.
16 H. Choudhary, S. Nishimura and K. Ebitani, *Chem. Lett.*, 2012, **41**, 409.
17 L. A. Badovskaya, V. M. Latashko, V. V. Poskonin, E. P. Grunskaya, Z. I. Tyukhteneva, S. G. Rudakova, S. A. Pestunova and A. V. Sarkisyan, *Chem. Heterocycl. Compd.*, 2002, **38**, 1040.
18 G. F. Muzychenko, L. A. Badovskaya and V. G. Kul'nevich, *Chem. Heterocycl. Compd.*, 1972, **8**, 1311.
19 N. Alonso-Fagúndez, V. Laserna, A. C. Alba-Rubio, M. Mengibar, A. Heras, R. Mariscal and M. López Granados, *Catal. Today*, 2014, **234**, 285.
20 A. Cukalovic and C. V. Stevens, *Biofuels, Bioprod. Biorefin.*, 2008, **2**, 505.
21 J. Wahlen, B. Moens, D. E. De Vos, P. L. Alsters and P. A. Jacobs, *Adv. Synth. Catal.*, 2004, **346**, 333.
22 P. Kumar and R. K. Pandey, *Green Chem.*, 2000, **2**, 29.
23 M. G. Clerici, G. Bellussi and U. Romano, *J. Catal.*, 1991, **129**, 159.
24 S. B. Kumar, S. P. Mirajkar, G. C. G. Pais, P. Kumar and R. Kumar, *J. Catal.*, 1995, **156**, 163.
25 M. A. Uguina, D. P. Serrano, R. Sanz, J. L. G. Fierro, M. López Granados and R. Mariscal, *Catal. Today*, 2000, **61**, 263.
26 E. Astorino, J. B. Peri, R. J. Willey and G. Busca, *J. Catal.*, 1995, **157**, 482.
27 F. Bonino, A. Damin, G. Ricchiardi, M. Ricci, G. Spanò, R. D'Aloisio, A. Zecchina, C. Lamberti, C. Prestipino and S. Bordiga, *J. Phys. Chem. B*, 2004, **108**, 3573.
28 C. D. Wagner, *J. Electron Spectrosc. Relat. Phenom.*, 1983, **32**, 99.
29 A. Takagaki, S. Nishimura and K. Ebitani, *Catal. Surv. Asia*, 2012, **16**, 164.
30 H. E. Hoydonckx, W. M. Van Rhijn, W. Van Rhijn, D. E. De Vos and P. A. Jacobs, Furfural and Derivatives, in *Ullmann's Encyclopedia of Industrial Chemistry*, Wiley-VCH Verlag GmbH & Co. KGaA, 2000.
31 K. J. Jung, A. Gaset and J. Molinier, *Biomass*, 1988, **16**, 89.
32 W. Zhang, Y. Zhu, S. Niu and Y. Li, *J. Mol. Catal. A: Chem.*, 2011, **335**, 71.
33 I. Agirrezabal-Telleria, A. Larreategui, J. Requies, M. B. Güemez and P. L. Arias, *Bioresour. Technol.*, 2011, **102**, 7478.
34 I. Agirrezabal-Telleria, I. Gandarias and P. L. Arias, *Bioresour. Technol.*, 2013, **143**, 258.
35 C. Li, G. Xiong, J. Liu, P. Ying, Q. Xin and Z. Feng, *J. Phys. Chem. B*, 2001, **105**, 2993.
36 L. Wang, G. Xiong, J. Su, P. Li and H. Guo, *J. Phys. Chem. C*, 2012, **116**, 9122.
37 G. Ricchiardi, A. Damin, S. Bordiga, C. Lamberti, G. Spanò, F. Rivetti and A. Zecchina, *J. Am. Chem. Soc.*, 2001, **123**, 11409.
38 S. Bordiga, A. Damin, F. Bonino, G. Ricchiardi, A. Zecchina, R. Tagliapietra and C. Lamberti, *PCCP Phys. Chem. Chem. Phys.*, 2003, **5**, 4390.
39 X. Gao and I. E. Wachs, *Catal. Today*, 1999, **51**, 233.
40 G. Moretti, A. M. Salvi, M. R. Guascito and F. Langerame, *Surf. Interface Anal.*, 2004, **36**, 1402.
41 F. Langerame, A. M. Salvi, M. Silletti and G. Moretti, *Surf. Interface Anal.*, 2008, **40**, 695.

Supplementary Information

1. Experimental

1.1. Materials

5-hydroxy-furan-2(5H)-one was synthesised by a procedure adapted from P. Kumar et al.[1] consisting in the oxidation of furan with H_2O_2, using TS-1 as catalyst. Furan (2 g, 29 mmol) was added into a round-bottom flask with a magnetic stirrer containing 10 ml of acetonitrile, 0.4 g of TS-1 and 8 g of 30 wt.% H_2O_2 (70 mmol). The reaction was carried out for 8 h at 273 K and then at room temperature overnight. The catalyst was filtered off, and a sample of the filtrate was analysed by HPLC. The presence of 5-hydroxy-furan-2(5H)-one was confirmed, in addition to furan's total conversion. The filtrate was concentrated, and a white solid and an oily phase were formed. This mixture was filtered off and washed with diethyl ether. The solid was identified as MA, whereas HPLC analysis of the oily phase determined the presence of 5-hydroxy-furan-2(5H)-one and only traces of MA and FumA. The oily phase was dried and concentrated by vacuum and used for the determination of the chromatographic factor.

1.2. Catalytic activity measurements

Figure SI1 shows a typical chromatogram from the HPLC analysis of the reaction media. The retention times were 12.4 min for oxalic acid, 15.6 min for maleic acid, 17.6 min for malic acid, 21.3 min for succinic acid, 24.4 min for formic acid, 26.1 min for fumaric acid, 29.8 min for 5-hydroxy-furan-2(5H)-one, 48.7 min for furan-2(5H)-one, 53.6 min for furoic acid and 78.2 min for furfural (not shown in the figure because the chromatogram corresponds to a aliquot with full furfural conversion).

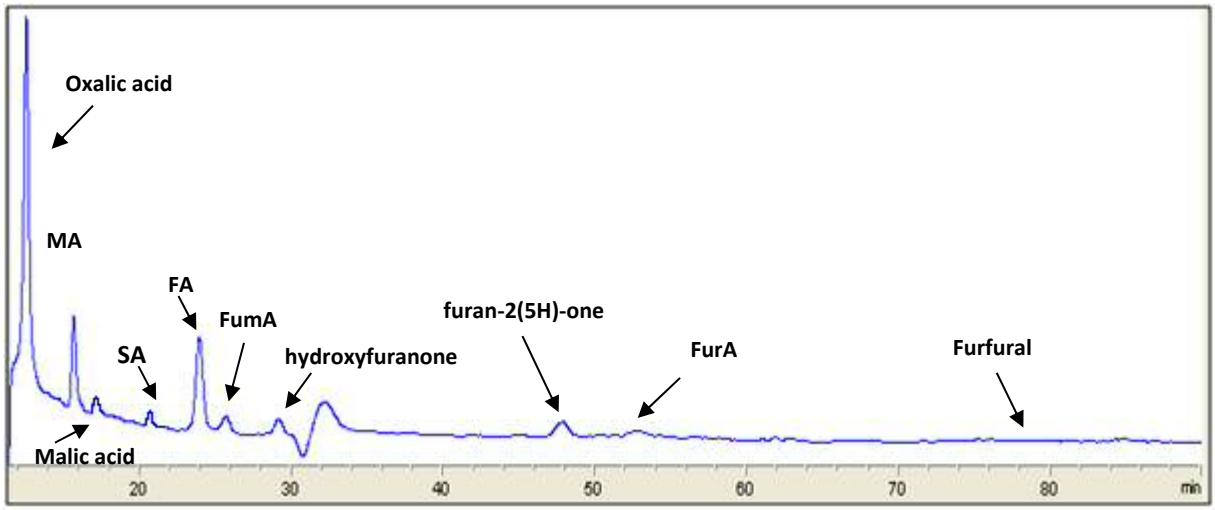

Figure SI1. Typical reaction chromatogram

2. Results and discussion

2.1 Parametric study

Temperature effect on catalytic activity

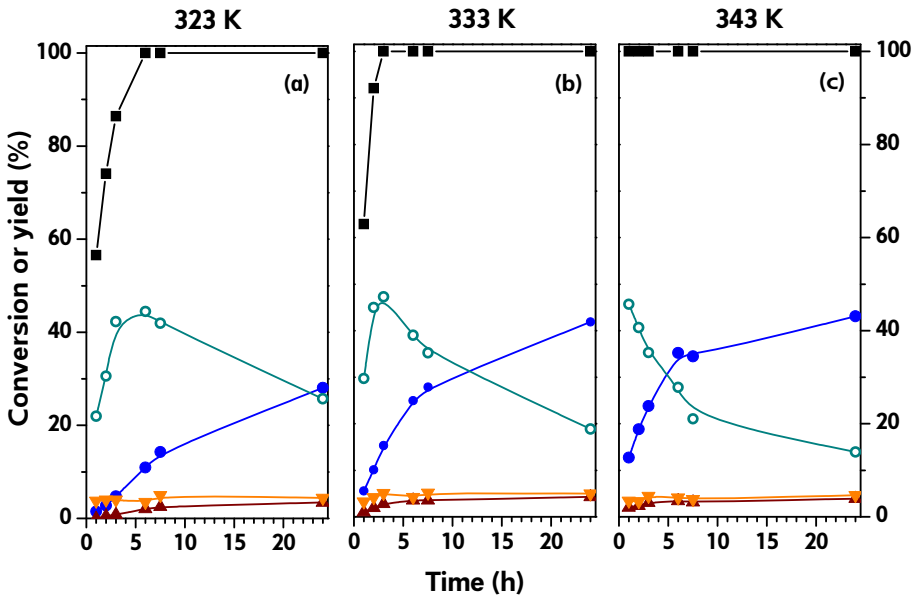

Figure SI2. Effect of reaction temperature on the catalytic properties of TS-1 at three different temperatures: (a) 323 K, (b) 333 K and (c) 343 K. Reaction conditions: 4.6 wt. % of furfural, 2.3 wt. % of catalyst, 6.6 wt. % of H_2O_2, equivalent to a H_2O_2/F mol ratio = 4. Symbols: (■) furfural conversion; 5-hydroxy-furan-2(5H)-one yield (○); maleic acid yield (●); formic acid yield (▼); and malic acid yield (▲).

The effect of reaction temperature on catalytic properties was also examined for a H_2O_2/furfural mol ratio of 4, equivalent to 6.6 wt. % of H_2O_2, and as shown in the results in Figure 1 of the main article, hydroxyfuranone, MA and FA were the main reaction products. Furfural conversion is also enhanced by temperature, and total furfural conversion was reached after 1 h when the reaction was carried out at 343 K. At short reaction times, hydroxyfuranone was the main product, and the MA yield increased for longer reaction times at the expense of the former. A notable positive effect was observed when the temperature increased from 323 to 333 K, and the MA yield after 24 h enhanced from 28 to 42 %. However, this positive effect is not evident for longer reaction times when the reaction is carried out at 343 K. Therefore, for low H_2O_2 concentrations, 333 K is the optimum temperature for the oxidation of furfural to MA.

Effect of H_2O_2 concentration on catalytic activity

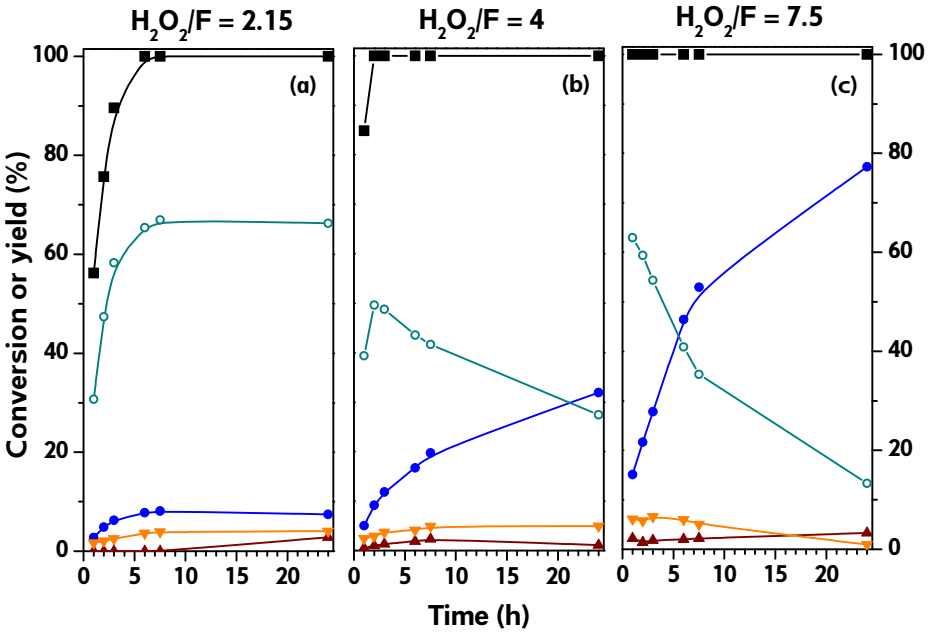

Figure SI3. Effect of H_2O_2 concentration on the catalytic properties of TS–1 for three different H_2O_2/furfural mol ratios (2.15, 4 and 7.5), corresponding to (a) 3.5, (b) 6.6 and (c) 12.3 wt. % of H_2O_2. Reaction conditions: 4.6 wt. % furfural, 323 K, 4.6 wt. % catalyst. Symbols: (■) furfural conversion; 5-hydroxy-furan-2(5H)-one yield (○); maleic acid yield (●); formic acid yield (▼); and malic acid yield (▲).

H_2O_2 concentration had a remarkable positive effect on both the furfural conversion rate and MA yield. As shown in the above figure, three different H_2O_2/furfural mol ratios (2.15, 4 and 7.5) were studied for 4.6 wt. % of furfural and TS–1. When a low H_2O_2 concentration was used (H_2O_2/furfural mol ratio = 2.15), close to that needed for the

oxidation of furfural to hydroxyfuranone, the latter is the main product, with a yield close to 70 %. MA yield was negligible. The product yield remained constant after 6 h of reaction, most likely because after that reaction time, the H_2O_2 is fully consumed, and no more H_2O_2 is available for the oxidation of hydroxyfuranone to MA. In fact, with a larger H_2O_2/furfural mol. ratio, furfural conversion is faster and MA yield is higher.

Autocatalytic reaction

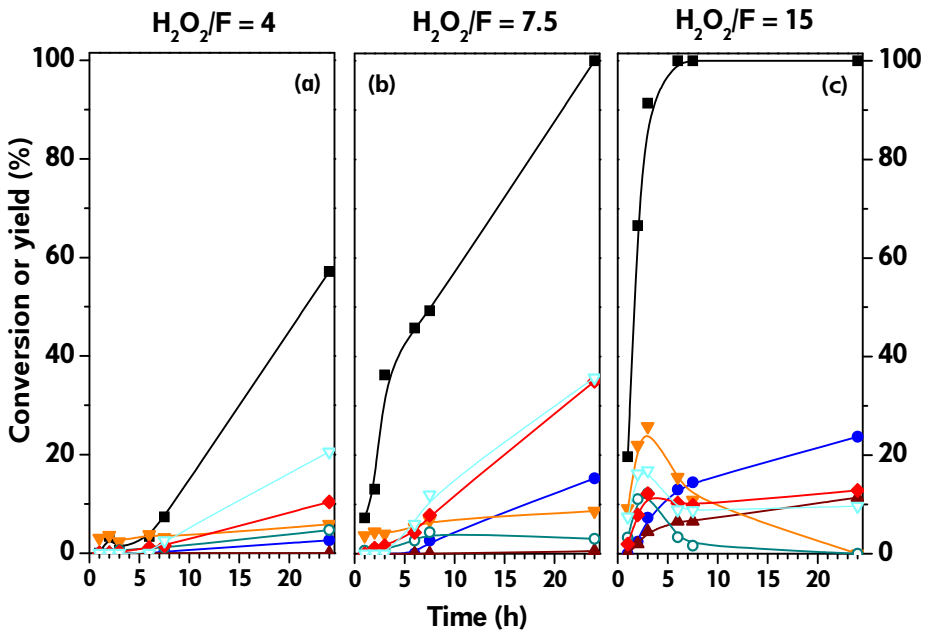

Figure SI4. Auto-catalysed reactions with no catalyst for three different H_2O_2/furfural mol ratios (4, 7.5 and 15), which corresponds to (a) 6.6, (b) 12.3 and (c) 24.6 wt. % of H_2O_2. Reaction conditions: 4.6 wt. % furfural and 323 K. Symbols: (■) furfural conversion; 5-hydroxy-furan–2(5H)-one yield (○); maleic acid yield (●); formic acid yield (▼); malic acid yield (▲); furan–2(5H)-one yield (▽); succinic acid yield (◆).

Reactions without catalyst (autocatalytic reaction) and with different H_2O_2 concentrations were also carried out, and the results are plotted in Figure SI4. The furfural conversion rate is slower than in catalysed reactions, and for a H_2O_2/furfural mol ratio of 4, a reaction time of 24 h is needed to reach a conversion of ca. 60 %. The product distribution is also different to that when catalysed by TS–1, and now furan–2(5H)-one and succinic acid are the major products. The MA yield increases with H_2O_2 concentration, but only a maximum of 25 % is achieved after 24 h reaction when a H_2O_2/furfural mol ratio of 15 is used. For this highest H_2O_2 concentration, high yields of formic acid are obtained for short reaction times, but the yield starts to decrease after 3

h of reaction, most likely because overoxidation to CO_2 takes place due to the excess H_2O_2.

2.2. Selective vs. unselective conversion of H_2O_2 (thermal and catalytic decomposition of H_2O_2)

In principle, there are three routes to convert H_2O_2: conversion to organic products (including formic acid), catalytic decomposition and uncatalysed thermal decomposition. In an attempt to quantify these contributions, two blank experiments were conducted using 12.3 wt % H_2O_2 (the same as used for Figure 4b) in the absence of furfural: one in the absence of TS–1 (Figure 5a) and other in the presence of TS–1 (Figure 5b). Trace *a* accounts for uncatalysed thermal decomposition, and the difference between trace *b* and trace *a* (trace *c*) corresponds to catalysed decomposition in the absence of furfural. Apparently the catalysed decomposition in the absence of furfural is very intense and after 24 h is close to 65 %.

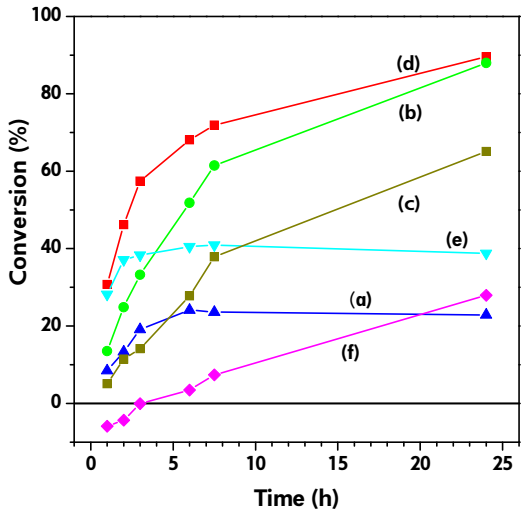

Figure SI5. Decomposition of H_2O_2. Symbols: (a) thermal decomposition of H_2O_2 in the absence of furfural and TS–1 (◆); (b) decomposition of H_2O_2 by TS–1 (thermal plus catalytic) in the absence of furfural (●); (c) difference between curve b and curve a, corresponding to catalytic decomposition of H_2O_2 in the absence of furfural (■); (d) H_2O_2 converted when both furfural and TS–1 are present (■); (e) H_2O_2 consumed to produce organic compounds, including FA, calculated from experimental results of Figure 4b (▼); (f) H_2O_2 catalytically decomposed by TS–1 in the presence of furfural (◆) (curve f = curve d – curve e – curve a).

Figure SI5 also includes the experimental total conversion of H_2O_2 obtained when both TS–1 and furfural were present (trace *d*) and the H_2O_2 utilised to transform selectively furfural to all organic products, including formic acid (trace *e*); the latter was calculated from the yields of Figure 4b and the stoichiometry of the corresponding

reactions. The sum of trace *b* plus trace *e* (consumed in selective transformation in the presence of furfural) should result in trace *d* (overall H_2O_2 consumption), and a visual examination indicates that this hypothetical trace would be well above trace *d*. This imbalance strongly indicates that the catalytic decomposition of H_2O_2 is inhibited in the presence of furfural. The actual catalytic decomposition of H_2O_2 driven by TS–1 in the presence of furfural can in practice be estimated by subtracting both traces *a* and *e* from trace *d*. This is represented by trace *f*. It is evident that trace *f* is well below trace *c*. Even negative values are obtained for reaction times shorter than 3 h. After 24 h, the catalytic decomposition in the presence of furfural affects less than 30 % of the H_2O_2 (in comparison to 65 % when furfural is absent). Therefore, although TS–1 catalytically decomposes H_2O_2, the decomposition is remarkably inhibited by the presence of furfural.

2.3. Proposed reaction mechanisms

– *Reaction mechanism involving Baeyer-Villiger oxidation of furfural as first step.*

When using sulphonic-acid-based catalysts, it is accepted that the reaction starts with a Baeyer–Villiger oxidation of furfural to furanol formate ester, which is rapidly hydrolysed into the corresponding carboxylic acid and alcohol (formic acid and 2–hydroxyfuran, see scheme SI1). This first step explains the large concentration of formic acid that is always detected in the reaction mixture as the reaction progresses and fulfils the C atom loss required to go from a C_5 to a C_4 compound. 2–hydroxyfyuran is in equilibrium with the other two tautomeric isomers: furan-2(3H)-one and furan-2(5H)-one; the former yields SA and the latter MA after the corresponding oxidation steps. The presence of these tautomeric species explains why SA and MA are always simultaneously formed with acid catalysts and why the selectivity of SA (lower ratio) or MA (higher ratio) can be tuned by changing the H_2O_2/furfural ratio. MA requires more H_2O_2 to be formed (3 mol of H_2O_2 per mol of furfural).[2–5]

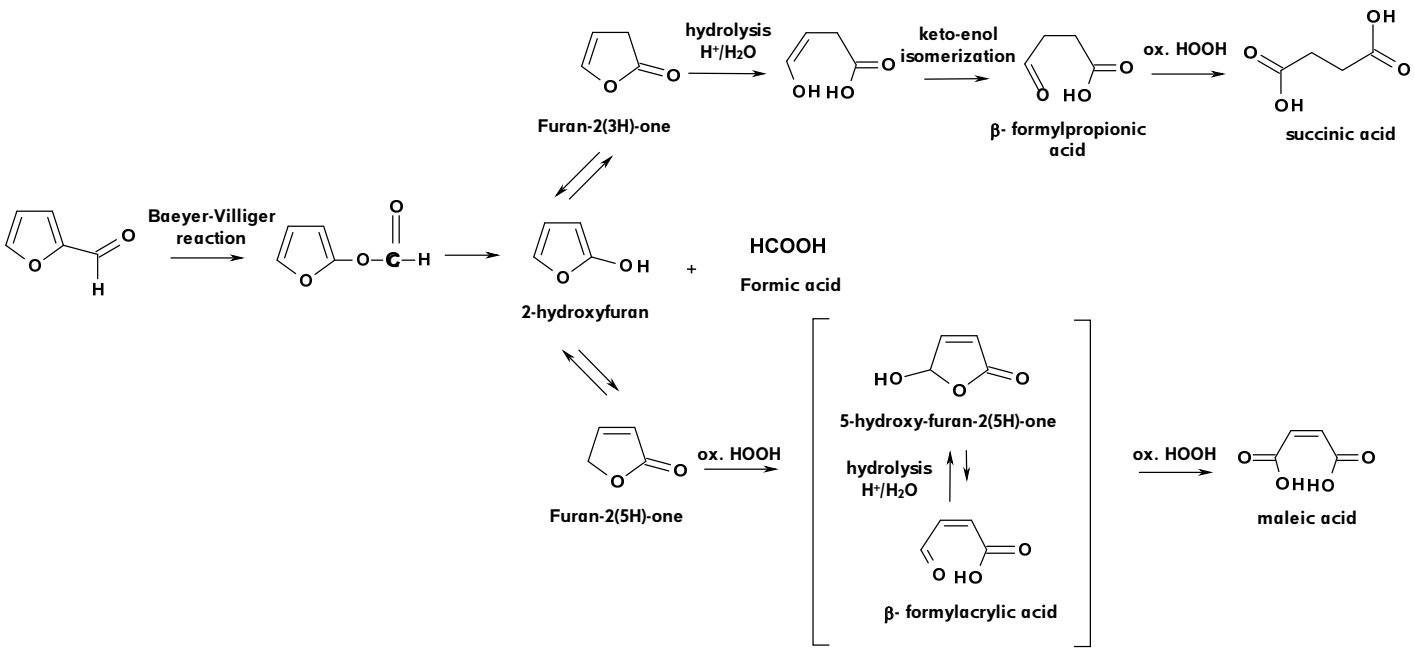

Scheme SI1. Reaction mechanism proposed for sulphonic-based catalysts starting with a Baeyer–Villiger oxidation of the aldehyde group of furfural [2-4, 6]

Furan-2(5H)-one is the compound initially produced by Baeyer–Villiger oxidation of furfural with H_2O_2. Furan-2(5H)-one is in tautomeric equilibrium with furan-2(3H)-one. Therefore, if the TS-1 oxidation of furfural utilised this mechanism, furan-2(5H)-one would be rapidly oxidised to either MA or SA. The oxidation of furan-2(5H)-one is plotted in Figure SI6 for a concentration of 4.6 wt. % of furanone and TS-1, a H_2O_2/furanone mol ratio of 7.5 and at 323 K. The oxidation of 5-furanone is very slow, the MA yield is very low and the yields of hydroxyfuranone and SA are negligible. Therefore, furan-2(5H)-one is not an intermediate when TS-1 is used as catalyst, so the first stage in the oxidation of furfural is not a Baeyer–Villiger reaction.

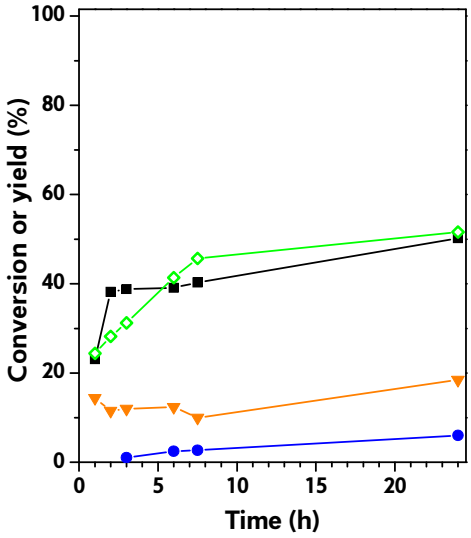

Figure SI6. Oxidation of furan-2(5H)-one with TS-1. Reaction conditions: 4.6 wt. % of furan-2(5H)-one, 4.6 wt. % of catalyst, 6.6 wt. % of H_2O_2, equivalent to a H_2O_2/furanone mol ratio = 7.5, and 323 K. Symbols: (■) furan-2(5H)-one conversion; maleic acid yield (●)formic acid yield (▼); H_2O_2 conversion (◇)

- *Mechanism of reaction involving the oxidation of furfural to furoic acid as the first step.*

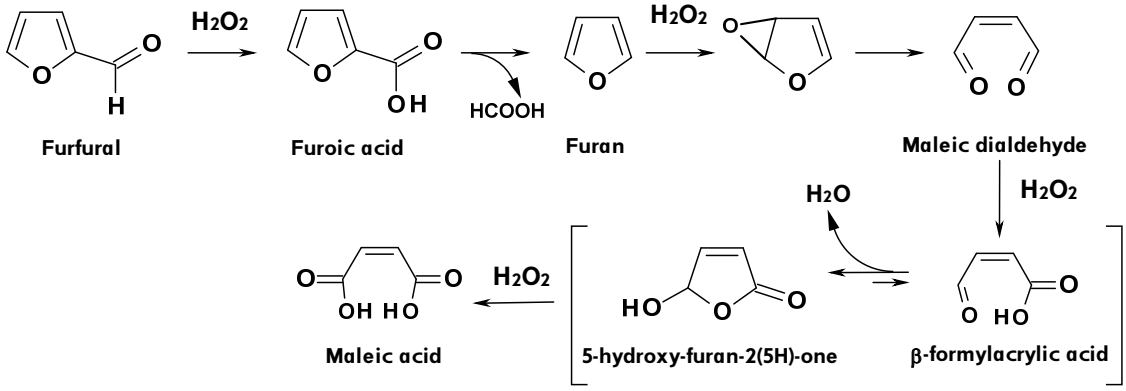

Scheme SI2. Reaction mechanism through epoxidation of furoic acid and decarboxylation

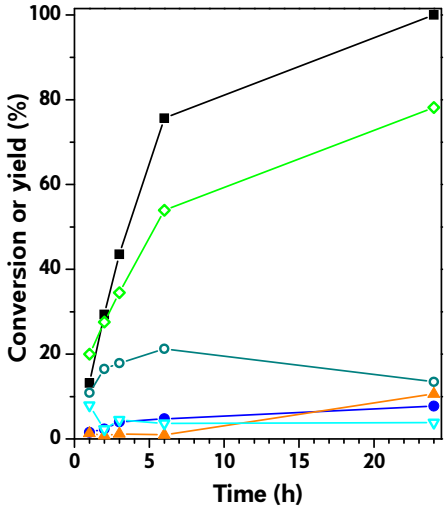

Figure SI7. Oxidation of furoic acid. Reaction conditions: 2.3 wt. % furoic acid, 2.3 wt. TS–1, H_2O_2/FurA = 7.5, which corresponds to 5.4 wt. % H_2O_2, and 323 K. Symbols: (■) furoic acid conversion; 5-hydroxy-furan-2(5H)-one yield (○); maleic acid yield (●); formic acid yield (▼); furan-2(5H)-one yield (▽); H_2O_2 conversion (◇)

Taking into account Scheme SI2, it is proposed that furfural is initially oxidised to FurA and then the reaction proceeds to the subsequent epoxidation of furoic acid, the formation of maleic dialdehyde and hydroxyfuranone and finally MA. The results of Figure SI7 show that the oxidation of furoic acid with TS–1 is slow and not very selective. Thus, although hydroxyfuranone is the main reaction product, only a maximum of 20 % yield is achieved after 6 h reaction, and after that it starts to decrease (most likely because oxidation to formic acid takes place). Furan-2(5H)-one and MA are also detected, but in low concentration. Therefore, the conversion and yield patterns are not in agreement with those expected for the involvement of furoic acid in the reaction mechanism.

2.4. Stability of the catalysts

Oxidation of furfural obtained from biomass

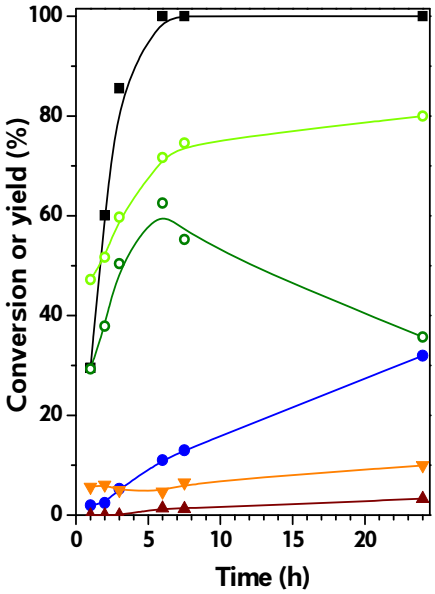

Figure SI8. Oxidation of furfural obtained from biomass. Reaction conditions: 2 wt. % furfural from biomass, 2 wt. % catalyst, 323 K, H_2O_2/F = 7.5. Symbols: (■) furfural conversion; maleic acid yield (●); malic acid yield (▲); formic acid yield (▼); 5-hydroxy-furan-2(5H)-one yield (○); H_2O_2 conversion (◇)

An aqueous solution of furfural obtained from lignocellulosic biomass was used as raw material. The concentration of furfural in this solution was 2.5 wt %, so the final concentration of furfural in the reaction media was 2 wt. %. Comparing the results in Figure SI7 with those in Figure 4a, where a reaction with 2 wt. % of commercial furfural was performed, it can be seen that the reaction rate is slower when furfural from biomass is used: a 6-h reaction time is needed to achieve the total conversion of furfural from biomass, while 2 h is enough when commercial furfural is used. As regards product yield, the values are lower when furfural from biomass is oxidised, though after 24 h reaction, the MA and FA yields are very similar. These results suggest that the impurities associated with furfural in the aqueous solution from biomass may interfere in the oxidation of furfural.

2.5. Catalyst characterisation

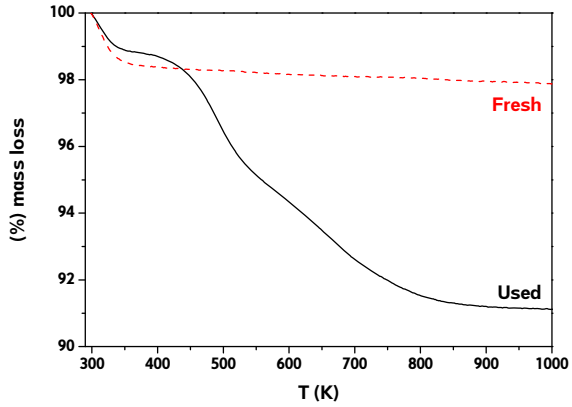

Figure SI9. Thermogravimetric analysis of fresh and used catalyst after 6 runs with commercial furfural

Thermogravimetric analyses of fresh and used catalyst are plotted in Figure SI8. For fresh TS–1, there is a main mass loss up to 373 K due to physisorbed water on the surface of the zeolite, but it is only 2 wt. % of the total. For higher temperatures, no great mass loss is observed. For used catalyst, in addition to the mass loss of physisorbed water, further mass losses are observed up to 800 K, most likely due to reaction product residues that are on the surface of the catalyst and that are burnt in the air atmosphere with increasing temperature. The total mass loss in the used catalyst is approximately 9 wt. %.

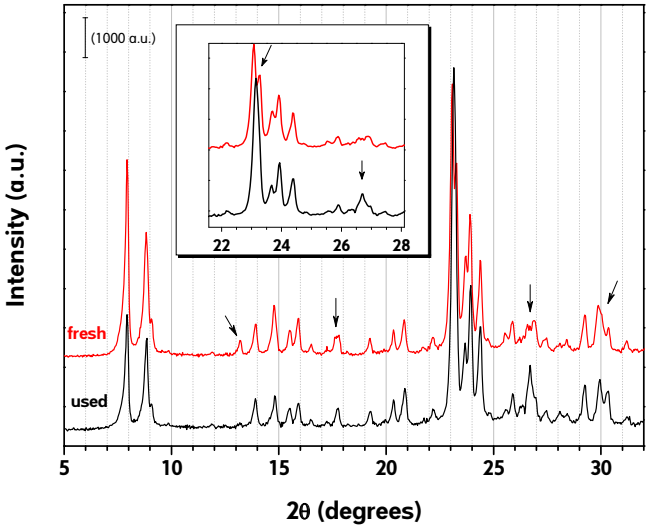

Figure SI10. XRD patterns of titanium silicalite 1, fresh and used 6 times

Analysis of X-ray diffraction patterns shows the presence of TS–1, with the main diffraction peaks of titanium silicalite. The use of the catalyst induces slight though significant changes to the crystal structure of titanium silicalite. Some of the differences are indicated in figure above with arrows. Peaks at 23.1° and 23.3° in fresh catalyst become only one diffraction peak at 23.2°, which has greater intensity. In addition, new peaks at approximately 27° and 13° appear after catalyst utilisation.

BET area and N_2 adsorption and desorption isotherms of fresh and use catalyst after six reaction cycles with commercial furfural were also measured. The results are summarized in Figure SI10 and in Table SI1. Fresh and used catalyst present a reversible type I isotherm, typical of microporous solids having relatively small external surfaces. Rouquerol methodology[7] was employed for the determination of BET surface area and t-plot method was used to estimate micropore area.[8] A loss of specific surface is observed which can be explained by the leaching, the modification of the framework, and the deposition of organics in the pore structure.

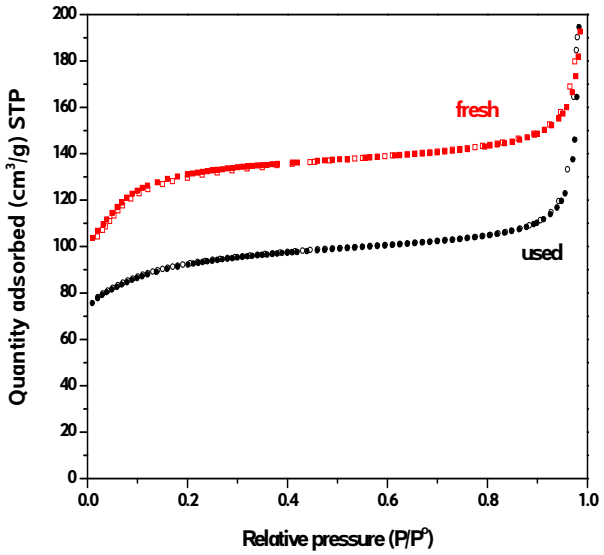

Figure SI11. N_2 adsorption-desorption isotherms of TS–1 catalyst, fresh and used (after six reaction cycles) (full symbols refer to N_2 adsorption and empty symbols to N_2 desorption isotherms)

Table SI1. Textural properties of fresh and used catalyst

Catalyst	BET area (m^2/g)	Micropore area (m^2/g)	Pore volume (cm^3/g)	Micropore volume (cm^3/g)	Micropores/total[a]
Fresh	494	419	0,27	0,17	0,85
Used	341	318	0,16	0,14	0,93

[a] Calculated as the ratio between micropores and total BET area

References

1. P. Kumar and R. K. Pandey, *Green Chem.*, 2000, **2**, 29.
2. H. Choudhary, S. Nishimura and K. Ebitani, *Appl. Catal. A*, 2013, **458**, 55.
3. A. Takagaki, S. Nishimura and K. Ebitani, *Catal. Surv. Asia*, 2012, **16**, 164.
4. H. Choudhary, S. Nishimura and K. Ebitani, *Chem. Lett.*, 2012, **41**, 409.
5. N. Alonso-Fagúndez, M. L. Granados, R. Mariscal and M. Ojeda, *ChemSusChem*, **5**, 1984.
6. L. A. Badovskaya, V. M. Latashko, V. V. Poskonin, E. P. Grunskaya, Z. I. Tyukhteneva, S. G. Rudakova, S. A. Pestunova and A. V. Sarkisyan, *Chem. Heterocycl. Compd.*, 2002, **38**, 1040.
7. J. Rouquerol, P. Llewellyn and F. Rouquerol, in *St. Surf. Sci. Catal.*, 2006, vol. 160, pp. 49.
8. B. C. Lippens and J. H. de Boer, *J. Catal.*, 1965, **4**, 319.